University of Stavanger

FACULTY OF SCIENCE AND TECHNOLOGY

MASTER'S THESIS

Study programme/specialisation: Petroleum Engineering / Well Engineering	Spring semester, 2018 Open
Author: Budi Wachyu Ramadhani	…… (signature of author)
Programme coordinator: Supervisor(s): Dr. Mesfin Belayneh	
Title of master's thesis: **FEM Modelling and Simulation of Production Casing with Local Wear Damage**	
Credits: 30 ECTS	
Keywords: Wear Burst Collapse FEM API Burst/Barlow Triaxial Collapse Crescent Wedge Production Casing	Number of pages: 111 + supplemental material/other: 27 Stavanger, 15.06.2018

Abstract

Field data show that casing and production tubing experiences wear on both the internal and external parts of the tubular. The main mechanisms of the wear are the mechanical friction between drill string and casing, hydraulics, erosion, and corrosion. The occurrence of wear on the production casing results in reduced burst and collapse strength.

The API Burst/Barlow and triaxial collapse models are commonly used to estimate the de-rated burst and collapse strength of the production casing. These analytical models are applied by removing the damaged part of the tubular.

The applicability of the API Burst/Barlow and triaxial collapse models in the case of local wear on the production casing is examined in this thesis by employing Finite Element Method (FEM) analysis. Several local wear model scenarios are simulated. The results of these simulations show that the API Burst/Barlow and triaxial collapse models are not suitable for locally worn production casing. Specifically, the results from FEM analysis are significantly lower than the API Burst/Barlow and triaxial collapse model results. For instance, the results of the FEM analysis show that

- For undamaged and uniform wall cylinder, the analytical models are nearly the same as the FEM simulation result.
- For single crescent-shaped local damage, as the wear depth varies from 0% to 45% of the wall thickness, the API Burst/Barlow model over-predicts the de-rated burst pressure by 0% to 52% as compared with the FEM model.
- For double crescent local damage, as the wear depth varies from 0% to 45% of the wall thickness, the API Burst/Barlow model over-predicts the de-rated burst pressure by 0% to 55% as compared with the FEM model.
- The size, shape, and number of damages effect the magnitude of the de-rated pressure.

This page intentionally left blank.

Acknowledgments

This master's thesis was written in spring 2018 to fulfill the requirement of the Master of Science program in petroleum engineering at the University of Stavanger.

I want to thank various individuals who have supported me throughout the thesis writing process. I would especially like to thank Dr. Ove Mikkelsen and Dr. Adugna Deressa Akassa for giving me access and tips related to Abaqus CAE software.

I would like to express my sincere gratitude and appreciation to Dr. Mesfin Agonafir Belayneh, my thesis supervisor for his unlimited support, help, discussion and academic guidance. He has always patiently guided and encouraged me to stay consistent during the whole process of thesis writing.

This page intentionally left blank.

Table of Contents

List of Figures

List of Tables

Nomenclature

a = *Crack length*

a = *Inside radius*

b = *Outside radius*

C_{wt} = *Tripping wear coefficient*

C_{ww} = *Wireline wear coefficient*

D = *Wireline tool diameter*

D_t = *Total depth of well at time of interest*

D_w = *Depth of wear*

D_δ = *Depth of wear point*

DF = *Design factor*

E = *Young's modulus*

E_f = *Drill pipe joint that contact wear point fraction*

F_a, F_a = *Axial force*

H = *Brinell hardness*

ID,d_i = *Inner diameter*

N_t = *Number of round trips per day*

N_w = *Number of wireline runs*

OD,d_o,D = *Outer diameter*

P_E = *Elastic collapse pressure*

P_P = *Plastic collapse pressure*

P_T = *Transitional collapse pressure*

P_Y = *Yield collapse pressure*

p_a,P_i = *Internal pressure*

p_b,P_o = *External pressure*

R, r = Any radial distance between r_1 *and* r_2

r_b = *Radius of the bend*

r_i,r_a,r_1 = *Inner radius*

r_o,r_b,r_2 = *Outer radius*

SF = Safety factor

T = Buoyed weight of drill string below wear point

t = Nominal wall thickness

T_s = *Maximum wireline tension on surface*

U^* = *Strain energy per volume of stressed material*

V_t = *Volume worn caused by tripping*

V_w = *Volume worn caused by wireline*

x,y,z = Dimensionless parameter

Y_p = *Minimum yield strength*

β = *Geometry factor*

ϵ = *Strain*

ν = *Poisson' ratio*

τ = *Torque*

σ_θ = *Hoop stress (tangential stress)*

σ_a = *Axial stress*

σ_b,σ_{DL} = *Bending stress*

σ_h = *Hoop stress*

σ_r = *Radial stress*

σ_y = *Yield stress*

σ_z = *Total axial stress*

σ_{ds} = *Drill string tension*

σ_{max} = *Maximum stress*

σ_{min} = *Minimum stress*

σ_{VME} = *Von Mises stress*

Abbreviations

API = American Petroleum Institute

CO_2 = Carbon Dioxide

COPNO = ConocoPhillips Norway

DLS =Dogleg Severity, deg/100 ft

DOF =Degrees of Freedom

FEM = Finite Element Method

H_2S = Hydrogen Sulfide

MD = Measured Depth

NACE = National Association of Corrosion Engineers

NCS = Norwegian Continental Shelf

O_2 = Oxygen

PSA = Petroleum Safety Authority

SCC = Stress Corrosion Cracking

SF = Safety Factor

TVD = True Vertical Depth

ZRA = Zero Resistance Ammetry

1. Introduction

Casing and tubing wear are common problems in the petroleum industry. Casing and tubing are exposed to high risk of wear, especially in deep and high inclination wells, where the doglegs are high, and there is a large amount of tension load. Casing wear often results from contact forces between the drill string and casing wall, while production tubing wear occurs due to intervention work on the well, such as coiled tubing, wireline, and snubbing. These problems can cause loss of well integrity and lead to production loss [1, 2].

According to NORSOK standard D-010, there shall always be two barriers between the hydrocarbon zone and the surface to avoid any accidents related to the risk of uncontrolled formation fluid release into the environment during the lifetime of the well [3]. This standard requires the production tubing to serve as the primary barrier and production casing as the secondary barrier on a typical production well during its production phase. Both production tubing and production casing are exposed to high pressures, temperatures, chemical injection, mechanical loading due to well intervention, produced fluids, and borehole environments which affect the integrity of the production and casing. Previous studies showed that local wears occurs on the production tubing and production casing due to corrosion and mechanical load during the drilling phase and well intervention activity [1, 4, 5]. These studies investigate in depth the effect of local wear on the maximum burst and collapse capacity of production tubing by using the Finite Element Method (FEM) approach [1, 5]. Building on these studies, in this thesis, production casing with local wear will be simulated by using Finite Element Method (FEM) approach under various loading scenarios. The applicability of the currently used analytical modelling approaches for locally worn production casing will be investigated and will be compared with FEM result.

1.1 Background

According to a Petroleum Safety Authority (PSA) survey in 2006, 75 of 406 wells at 12 offshore facilities had well integrity problem. About 39% of well integrity problems were associated with tubing integrity [6]. In another study, 4.6% of wells in Alberta, Canada were found to have leak problems [7]. Casing integrity problems contributed to 8 of 75 well integrity issues in the Norwegian Continental Shelf (NCS) as shown in Figure 1 [6].

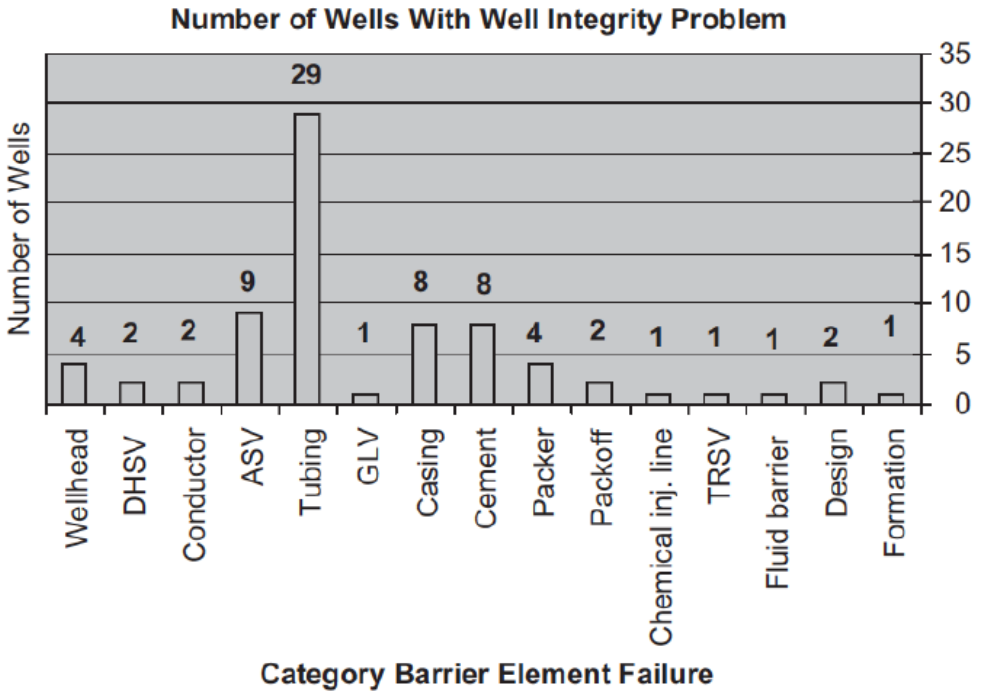

Figure 1. Barrier element failure categories [6]

A considerable amount of time and cost are needed to repair well integrity issues. These issues may also accelerate the lifecycle of the well if they lead to early permanent abandonment due [1]. To avoid unnecessary spending of time and cost, measure should be taken to these well integrity issues.

Casing and production tubing integrity is a paramount element of well integrity. Particularly, based on NORSOK D-010 standard, production tubing is the primary barrier element [3]. However, production tubing is exposed to high pressure and temperature, corrosive gases, chemicals, mechanical loading during production and intervention [1]. This thesis focuses on the tubular integrity of casing and production tubing by simulating locally damaged tubular under different loading scenarios to estimate the de-rated burst and collapse pressure of tubing FEM.

1.2 Problem Statement

During the lifetime of a well, production casing is exposed to various mechanical load and corrosion circumstances which lead to the occurrence of local wear that has non-uniform characteristics. This characteristic creates a concern regarding the production casing integrity because, it can be concluded that the reduction in the wall thickness around the circumference of the production casing is not uniform. However, the existing models which are used

practically by the industry to estimate burst and collapse strength of the production casing assume uniform wear [8]. Therefore, the compatibility and applicability of the existing analytical models which are the API Burst/Barlow model and triaxial collapse model for local wear production casing are being investigated.

This thesis simulates the different types of local wear at various depths and locations on the production tubing by employing FEM (using Abaqus CAE software) under specific conditions based on the casing wear data from the Gullfaks Field [2] and hypothetical data. From the FEM simulation results, the maximum de-rated burst and collapse strength of the production casing are estimated. Because the simulation is based on specific conditions, the simulation result are only valid under these particular circumstances.

This thesis addresses issues such as:

- Effect of local wear on the burst and collapse strength of the production casing when compared to uniform wear type.
- Effect of local wear position (internal and external part of the casing) on the burst and collapse strength of the casing.
- Applicability and limitations of the API Burst/Barlow and triaxial collapse models for predicting burst and collapse strength for production casing with local wear.
- Effect of single and combined wear shape of the same and different geometry and sizes on the de-rated burst and collapse strength of production casing.

1.3 Thesis Objective

The objective of this thesis is to model and analyse the effect of wear on the burst and collapse strength of the production casing. The following activities were performed as part of this study:

1. Literature review of studies on production tubing and production casing wear
2. Review of the tubular stress theory and burst/collapse analytical models
3. Modelling wear including tubular with analytical models by removing the damaged part to predict de-rated burst and collapse pressures
4. FEM modelling of various shapes and sizes of local wear (from 0% to 45% wear) on the production casing to predict de-rated burst and collapse pressures
5. Generating FEM-based de-rated burst and collapse pressure empirical models as a function of wear percentage

2. Literature Review

Casing wear is a common problem in the petroleum industry. This problem can occur during drilling operation. In deep wells drilling where the tension loads and doglegs are high, there is the possibility of casing wear due to contact forces between the drill string and the casing wall. Well intervention activity, such as coiled tubing can also pose the risk of casing wear. Contact force between the rotated coiled tubing and the casing wall during operation may also result in damage to the casing and lead to casing wear. Loss of well integrity such as blowout may occur as a consequence of casing wear and lead to production loss which will impact the economic condition of the company [1].

Corrosion is another common problem in the petroleum industry. Corrosion occurs during most of the lifetime of the well, especially in the operation phase. Production wells have a risk of corrosion due to environmental conditions, exposure to corrosive substances such as carbon dioxide (CO_2) and hydrogen sulfide (H_2S), potential differences between metal types of the downhole equipment, rapid fluid stream and geometrical pipe conditions. Most of the wear that results from corrosion is non-uniform wear type or local wear.

In the current oil industry practice, the most common analytical method to calculate burst pressure of the casing is by implementing API Burst/Barlow model which is based on uniform thin-walled cylinder theory [8]. Therefore, the burst strength of the casing decreases linearly as the casing wear is uniformly removed. However, there are many cases in the industry where the wear on the casing is non-uniform, such as local wear due to contact between the casing wall and drill string that results in crescent-shaped wear or conditions resulting from pitting corrosion. The API Burst/Barlow model cannot be implemented on non-uniform wear casing.

It is critical to investigate the effect of non-uniform wear or local wear on the load capacity of the casing. Various types of non-uniform wear or local wear can appear due to drilling and coiled tubing activity and corrosion processes. The following section presents a review of studies of non-uniform wear and local wear on the casing.

2.1 Mechanisms of String Damage

The continuous contact between the casing and tool joint or the casing and borehole environment lead to the risk of casing wear. One example of this is the mechanical force which occurs due to contact between the tool joint or drill string and the casing wall during drilling activity. Another example is scratching on the casing due to contact with other casing or the

wellbore during the running into hole (RIH) process that leads to the occurrence of external casing wear. Yet another cause is the contact between coiled tubing and the casing wall during well intervention activity [1, 5, 9, 10]. The following section discusses the possibility of drilling and coiled tubing activities as the cause of casing wear.

Casing wear due to contact with the drill string is a common problem during drilling deep wells and extended reach wells [2]. Figure 3 illustrates casing wear development due to long-term contact of the casing with the rotating drill string during the drilling operation. High contact forces occur between the casing and drill string when the casing is bent. This forces result from setting the casing in a dogleg section of the well or due to buckling of the casing under a large axial compressive load [2]. The burst and collapse strength of the casing is reduced due to wear on the casing and this reduction worsens as the wear percentage of the casing. Total casing failure might occur due to holes that are created by wear on the casing [1].

2.1.1 Coiled Tubing Operation

Studies conducted by ConocoPhillips Norway suggest that contact between coiled tubing equipment and the casing wall during well intervention contributes to the wear on the inside part of the tubing or casing [1]. In this study, the wear generated by coiled tubing is assumed to be a crescent-shaped wear type due to the similarity of the coiled tubing equipment geometry. However, there is no proof that coiled tubing operation has the primary role in the occurrence of wear on the tubing and casing [1].

Figure 2 shows findings of an investigation conducted by ConocoPhillips on a production well in the Ekofisk Field, North Sea. Before the investigation, there were 16 coiled tubing operations from 2009 to 2010. The majority of coiled tubing operations were intended for acid stimulation. The graph presents the joint number to damage profile percentage of production tubing and shows significant damage to the tubing in the deep section where dogleg severity is high. This investigation indicates that the deviated section of a well is very crucial to well integrity since it shows the highest damage profile compared to other section deep of the well [1].

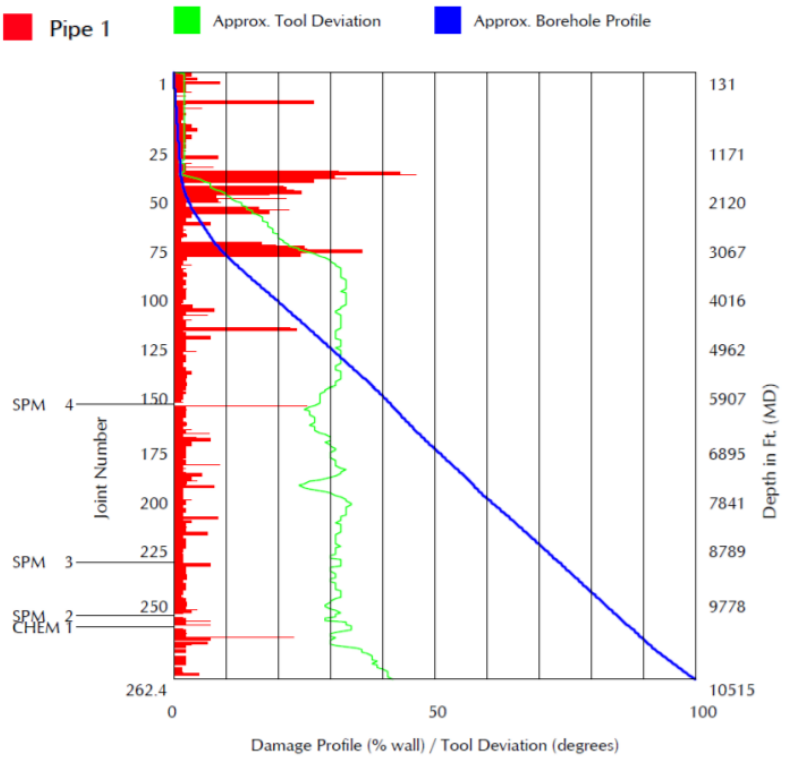

Figure 2. Correlation of recorded tubing wear to depth [1]

2.1.2 Drilling Operation

During drilling operation, there is a risk of casing wear due to contact between the casing wall and the tool joint. The casing also has a risk of non-uniform crescent-shaped wear in the internal part of the casing wall due to drill string rotation, resulting in the decreased thickness of the casing wall. In a study conducted by Shen, Beck, and Ling [4], casing wear due to tool joint contact is more severe than casing wear caused by the drill pipe.

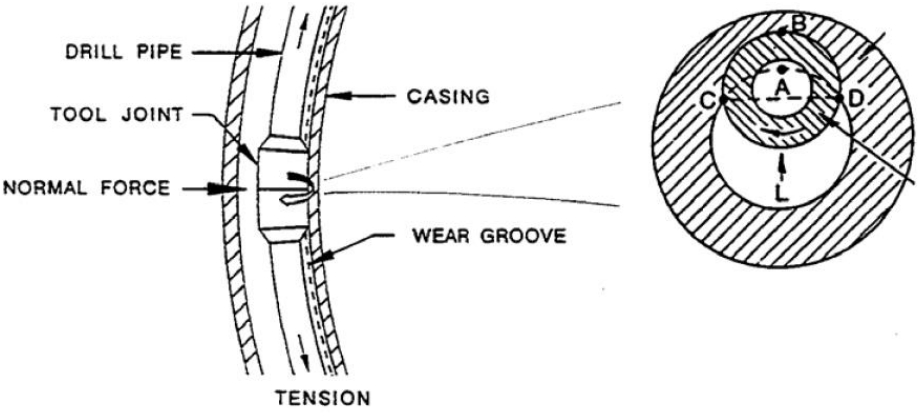

Figure 3. Casing wear caused by drill string rotation [2]

The contact forces between the drill string and casing wall can result in casing wear. Wu and Zhang [2] studied the "crescent-wear" type damage on the casing and developed an equation to explain the relation between wear of casing, burst strength of casing, and hoop stress. They also showed that when the bending effect is neglected, the burst strength of "crescent-worn" casing is similar to the "uniform worn" casing model. By considering tolerance on the API burst strength (87.5% minimum wall), a safe prediction of the burst strength of "crescent-worn" casing is obtained [2].

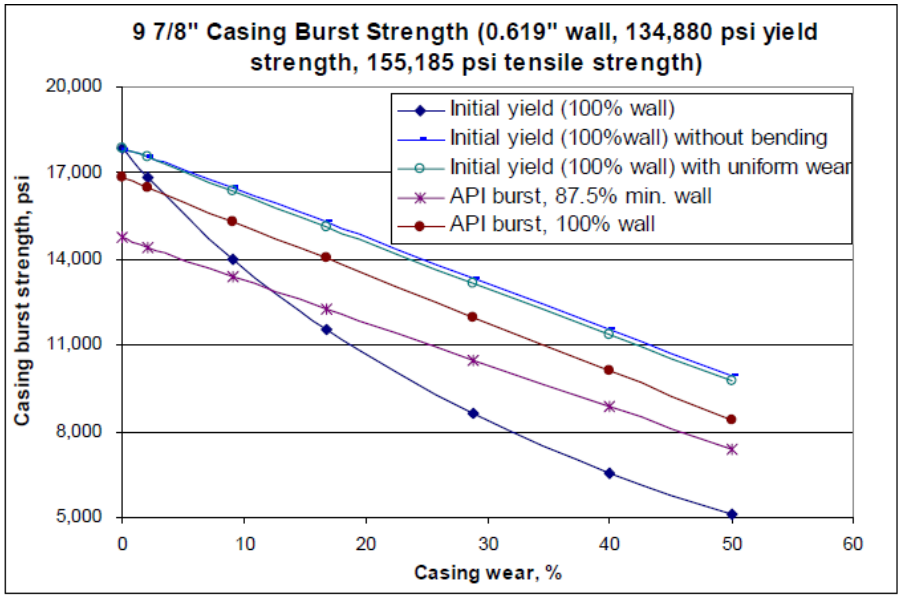

Figure 4. Burst strength comparison of worn casing [2]

Nagy [10] evaluated wear on the casing and stated that crescent-shaped wear occurs as a result of friction force between the casing and the rotating tool joint. The wear on the casing occurs because the contact pressure between the casing and the drill string is high. The area where the contact occurs is changed slowly from line-shaped to crescent-wear shaped [10].

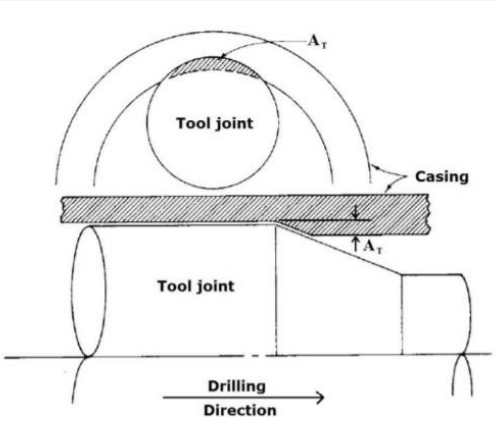

Figure 5. Tool joint casing wear [11]

An investigation was conducted to assess and predict the casing wear in Gullfaks Well A-42 in the North Sea. Measurement by using an ultrasonic imager log, showed a maximum of about 35% wear of the nominal wall thickness of the casing at 480 meters MD. The known cause of the casing wear on this well was from the drilling operation and back-reaming the subsequent hole section [2]. Figure 6 presents the result and prediction of casing wear at 2508 meters MD in 13 3/8 in casing at Gullfaks Field [2].

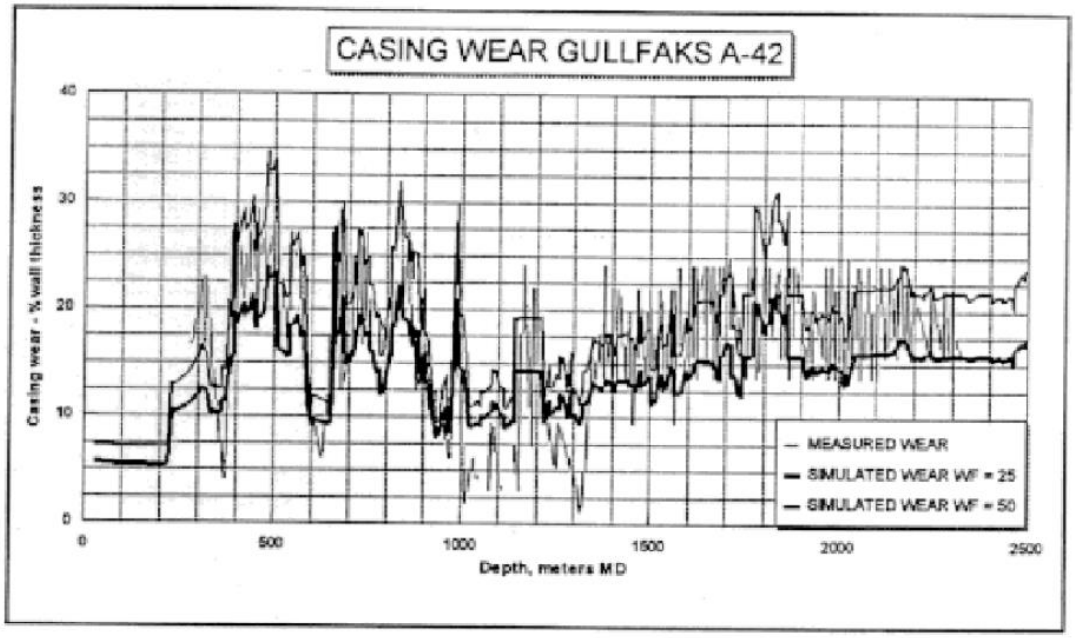

Figure 6. Casing wear measurement and prediction in Gulfaks Field [2]

A previous study [4] showed that contact pressure between the casing wall and the tool joint resulted in local wear on the intermediate casing. Crescent-shaped wear is generated after the casing wall thickness is reduced due to contact with the tool joint in the particular area as shown in Figure 7. When the wall thickness of the casing decreases, the stress concentration due to wellbore fluid pressure and in-situ stresses of formation on the worn part of the casing is expected to be higher. The study also showed that casing wear from tool joint contact is influenced by several factors such as drill string rotation time and the speed, drilling mud characteristics and properties, casing grades, and dogleg severity of the well [4].

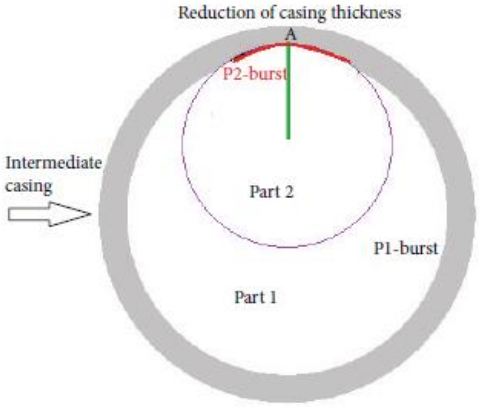

Figure 7. Crescent-shaped wear from tool joint contact [4]

Internal wear on the casing is not the only concern as a result of drilling activity. When the casing is running into hole (RIH), there is a risk of external casing wear due to scratching on the casing while it is running into the wellbore. The protective layer of the casing is removed due to scratching on the casing and local wear is generated on the external part of the casing [9].

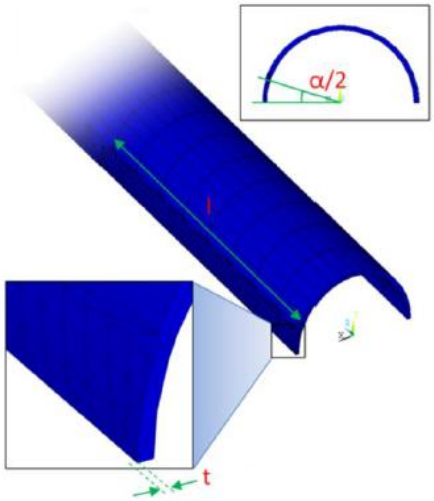

Figure 8. Scratching on the external part of casing [9]

Several finite element analysis (FEA) studies have been conducted to investigate the effect of non-uniform wear on the strength capacity of the casing. Haning, Doherty and House [12] build an eccentrically worn casing model to investigate the burst strength of the casing and analyse the results with several burst strength equations such as, API Burst/Barlow equation, rupture burst strength equation, and Klever Stewart's burst equation. API Burst/Barlow equation gives the most conservative result [12].

Various geometry models of local wear on the inner part of the casing have been built to accommodate the irregular shape of local wear in real condition. To idealize the local wear shape, three shape models are built based on regular geometric shapes, rectangular-shaped wear, crescent-shaped wear, and multiple-shaped wear (two rectangular-shaped wear occurrences with various lengths). Models of these shapes are shown on Figure 9 [13].

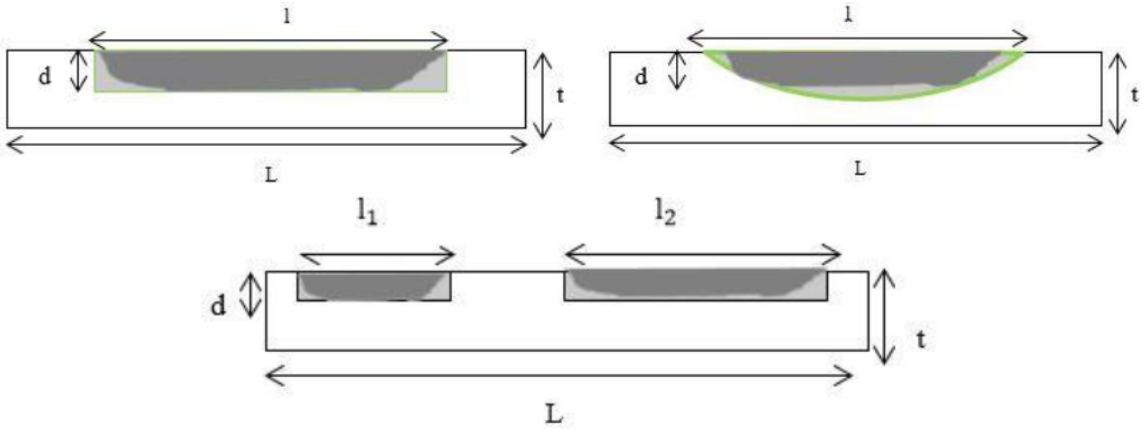

Figure 9. Various geometrical approximations of local wear shape [13]

2.1.3 Wear Depth

Several casing wear coefficients have been developed from experimental studies conducted by Fontenot and McEver [11]. The coefficients are categorized into two types: wear coefficients caused by drill pipe tripping activity and wear coefficients caused by wireline activity. The parameters of these wear coefficients are mud type, contact load, and casing grade [11].

2.1.3.1 Wear Caused by Drill Pipe Tripping

Casing wear estimation due to drill pipe tripping activity can be made when the wear coefficient of tripping and hole condition are known [11]. The coefficient values of wear caused by drill pipe tripping are shown in Table 1.

Table 1. Wear Coefficients from Drill Pipe Wear Test [11]

Type of Mud	Contact Load (lb/ft)	Wear Coefficient (C_{wt} (in.^{3}/lb-ft))	
		K-55	P-110
Water	500	2.9×10^{-8}	2.6×10^{-8}
	1000	8.5×10^{-8}	4.2×10^{-8}
	2000	5.9×10^{-8}	3.7×10^{-8}
Unweighted water-base mud + 3 percent sand	500	7.9×10^{-8}	9.3×10^{-8}
	1000	2.9×10^{-8}	5.7×10^{-8}
	2000	4.4×10^{-8}	5.0×10^{-8}
Weighted water-base mud without drill solids	1000	1.4×10^{-9}	3.6×10^{-9}
	2000	0.7×10^{-9}	1.4×10^{-9}
Weighted water-base mud with 2 to 8 percents drill solids	1000	1.4×10^{-9}	2.9×10^{-9}
	2000	1.0×10^{-9}	0.7×10^{-9}
Weighted water-base mud with drill solids and 3 percent sand	500	3.6×10^{-9}	
	1000	1.4×10^{-9}	4.3×10^{-8}
	2000	0.7×10^{-9}	0.7×10^{-9}

The volume of wear caused by drill pipe tripping is computed by Equation (1) [11]:

$$V_t = 2C_{wt}TN_tE_f(D_t - D_\delta)sin(\frac{\delta}{2}) \quad (1)$$

where V_t is defined as the volume of wear caused by tripping, C_{wt} is defined as the tripping wear coefficient (the values of C_{wt} are shown in Table 1), T is the buoyed weight of the drill string below the wear points, N_t is the number of round trips per day, E_f is the fraction of drill pipe per joints that contacts wear point, D_t is the total depth of the well at time of interest, D_δ is the wear point depth and δ is the dogleg severity. The wear depth caused by drill pipe tripping is acquired from the wear volume and wear depth correlation graph as shown in Figure 10.

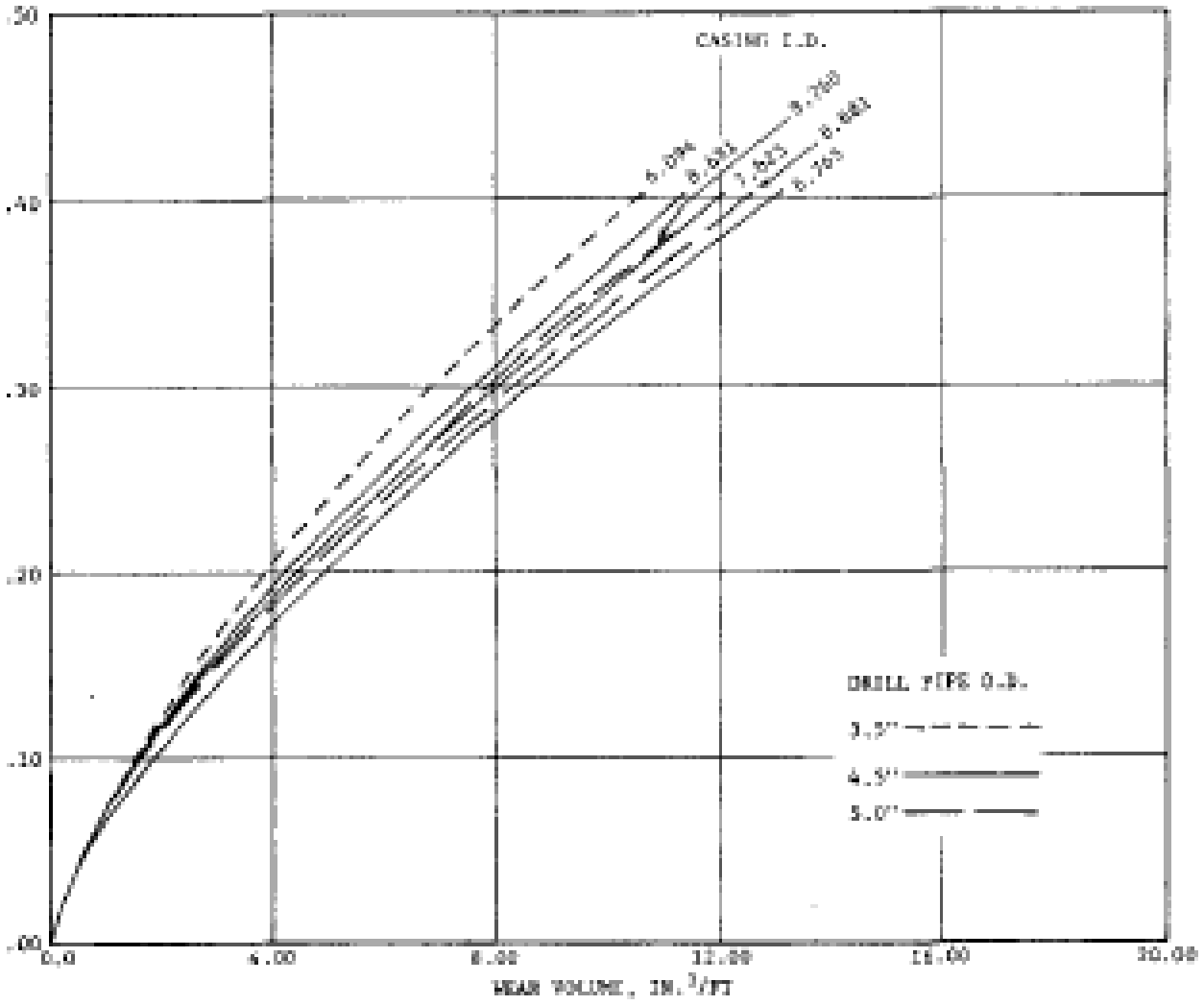

Figure 10. Wear depth and wear volume correlation [11]

2.1.3.2 Wear Caused by Wireline

The experimental study conducted by Fontenot and McEver also developed wear coefficient caused by wireline activity. The parameters these wear coefficients are the same as the parameters of the wear coefficients caused by the drill pipe tripping [11]. The values of the wear coefficients are shown in Table 2.

Table 2. Wear Coefficients from Wireline Wear Test [11]

Type of Mud	Contact Load (lb/ft)	Wear Coefficient (C_{ww} (in^3./lb-ft))	
		K-55	P-110
Water	09.08	1.1×10^{-8}	1.2×10^{-8}
	19.06	2.0×10^{-8}	0.8×10^{-8}
Unweighted water-base mud + 3 percent sand	4.9	15×10^{-8}	11.0×10^{-8}
	9.8	8.6×10^{-8}	8.0×10^{-8}
	19.6	7.1×10^{-8}	7.2×10^{-8}
Weighted water-base mud without drill solids	9.8	3.9×10^{-8}	3.9×10^{-8}
	19.6	1.9×10^{-8}	2.2×10^{-8}
Weighted water-base mud with 2 to 8 percents drill solids	9.8	5.2×10^{-8}	3.5×10^{-8}
	19.6	2.1×10^{-8}	2.2×10^{-8}
Weighted water-base mud with 8 percent drill solids + 3 percent sand	9.8	12×10^{-8}	13×10^{-8}
	19.6	5.2×10^{-8}	4.3×10^{-8}
Weighted water-base mud without drill solids + 3 percent sand	19.6	6.1×10^{-8}	5.9×10^{-8}

The wear volume caused by the wireline activity is computed by Equation (2) [11]:

$$V_w = 2C_{ww}T_sN_w\left(\frac{D_t - D_\delta}{D_t}\right)sin(\frac{\delta}{2}) \quad (2)$$

where V_w is defined as the volume of wear caused by the wireline, C_{ww} is defined as the wireline wear coefficient (the values of C_{ww} are shown in Table 2), T is the maximum wireline tension at the surface, N_w is the number of wireline runs, D_t is the total depth of the well at the time of interest, and D_δ is the wear point depth.

Bradley and Fontenot use the following equation from the *Handbook of Chemistry and Physics* to obtain wear depth caused by the wireline [11]:

$$V_{wireline}\left(\frac{in^3}{ft}\right) = \frac{\pi D^2}{8} - [(\frac{D}{2} - D_W\sqrt{D_w(D - D_w} + \frac{D^4}{4} sin^{-1}\left(1 - \frac{D_w}{D}\right)] \quad (3)$$

where D is the wireline tool diameter and D_w is wear depth.

2.2 Corrosion

2.2.1 Theory

Corrosion is a natural phenomenon by which a material (usually a metal) experiences deterioration due to an electrochemical reaction with the surrounding environment. The electrochemical reaction involves two-half cell reactions and a flow of electrical charge [14, 15]. The reaction requires four essential parts [14]:

1. Anode
2. Cathode
3. Electrolyte
4. The flow of electrical charge

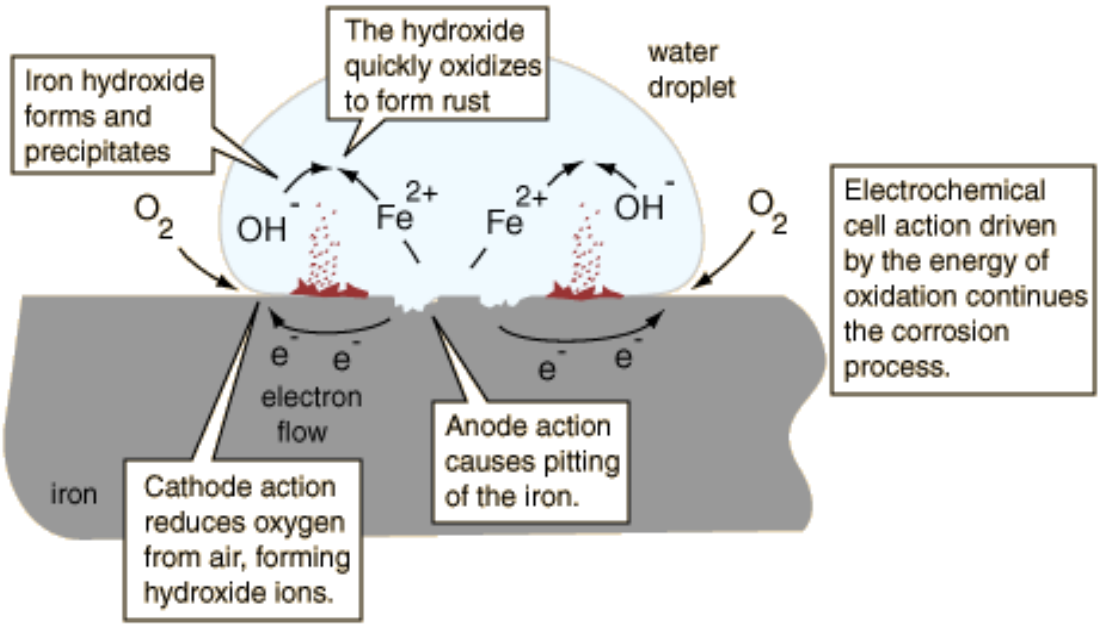

Figure 11. Corrosion process [16]

2.2.1.1 Anodic Reaction

An anodic reaction occurs when metal atoms are ionized and move to a solution, while the electrons remain on the surface of the original metal [14] as shown on the Equation (4).

$$Fe \rightarrow Fe_{aq}^{2+} + 2e^{-} \quad (4)$$

where *Fe* is the metallic iron, Fe^{2+} is the double negative charges of ferrous iron, and e^{-} is the electron that remains in the original metal.

2.2.1.2 Cathodic Reaction

A cathodic reaction occurs when the electrons that remain in the metal are taken by chemical species (i.e., O_2 and CO_2). This reactions consumes electrons and is called a reduction reaction. The cathodic reaction is represented on the Equation (5).

$$R + e^{-} \rightarrow R^{-} \quad (5)$$

2.2.2 Corrosion Types

2.2.2.1 Galvanic Corrosion

Galvanic corrosion occurs when two different types of metals are placed in a corrosive or conductive solution. The corrosion reaction proceeds as a result of the potential difference that exists between the two different metals. When the metals are laid in contact or electrically connected, the potential difference between the metals generates electron flow between them. The less corrosion-resistant metal is more corroded, and the corrosion process in the more resistant metal is reduced, as compared to when these different metal types are not in contact. In a galvanic reaction, the less corrosion-resistant metal acts as anodic and more resistant metal acts as cathodic, and the corrosion rate is influenced by the corrosion potential difference between the two metals [15].

One simple method to detect galvanic corrosion is using Zero Resistance Ammetry (ZRA). Real-time measurement of the galvanic corrosion rate can be obtained by employing a sensor [15, 17]. The methods to prevent galvanic corrosion are summarized as follow [14]:

1. Select appropriate material
2. Avoid mixing different types of tube
3. Implement cathodic protection
4. Add inhibitors

2.2.2.2 Crevice Corrosion

Crevices and other shielded areas on the surface of metals can be exposed to corrosive substances. As a result, local corrosion can be generated on the crevices and other shielded areas because of the low quantity of stagnant corrosive substances created by holes, deposits on the surface, lap joints, surfaces of the gasket, and crevices under bolt and rivet heads [18].

When stagnant corrosive substances lie on the crevice geometry, a highly corrosive micro-environment will be generated. This condition is similar to the pitting corrosion case. Localized corrosion starts when chemical components, such as oxygen form an electrical concentration cell. Some methods to limit crevice corrosion include [15]:

1. Use higher alloys
2. Use welds for joints (avoid using bolted or riveted joints)
3. Uses non-absorbent gaskets
4. Use continuous welding in lap joints

2.2.2.3 Pitting Corrosion

Pitting corrosion is a very extreme type of localized corrosion attack. The corrosion reaction starts when a passive layer formation is attacked, and the potential hydrogen (pH) is reduced in the interface between passive layers and electrolytes. Slow passive film dissolution begins and finally the material breaks [15, 17]. The removal of a corrosive-protecting layer from the external part of the casing due to scratching when the casing is running into hole (RIH) could lead to the occurrence of pitting corrosion. In a geothermal well, pitting corrosion on the external part of the casing can lead to premature casing collapse [9]. Pitting corrosion types are shown in Figure 12.

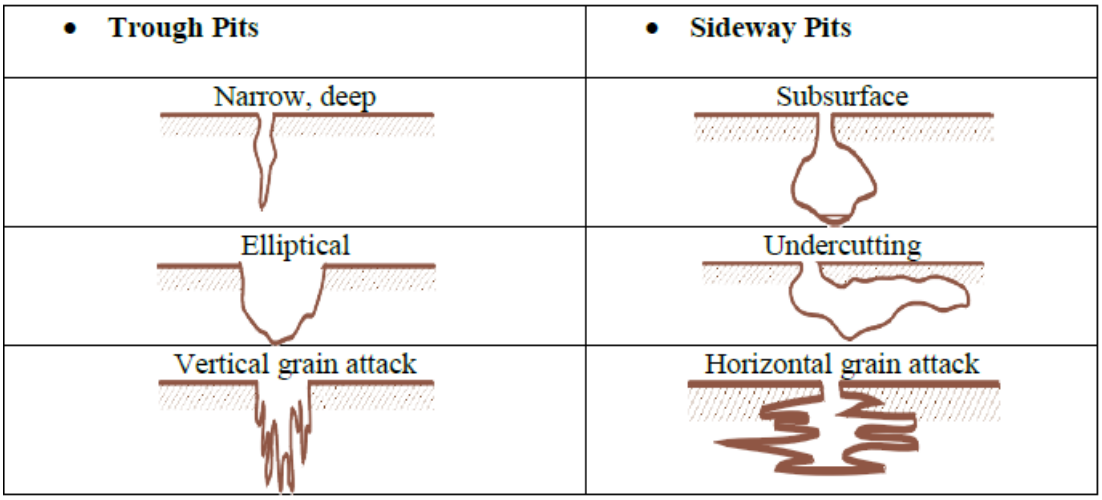

Figure 12. Pitting corrosion types [8]

This corrosion produces small or large holes in the metal that may lie close to other pits or be isolated, creating a rough surface. In general, a pit is defined as a cavity or hole with surface diameter approximately the same as or less than its depth. Pitting corrosion is the most destructive and dangerous corrosion type. The small percentage of weight loss of the structure caused by pitting can lead to equipment failure. It is also very complicated to detect pitting because of various depths and numbers of pits can occur under identical conditions. Some methods can be implemented to control pitting, such as [14]:

1. Select corrosive-resistant material
2. Fluid chemistry control
3. Use inhibitors
4. Use material coating

2.2.2.4 Intergranular Corrosion

Intergranular corrosion may arise under tensile stress along the boundaries of the grain [15, 17]. During a uniform attack, the grain interfaces are very reactive and display intergranular corrosion. A localized attack in the adjacent and at the grain boundaries with relatively small corrosion of the grains is also defined as intergranular corrosion. This corrosion induces the fallout of grains or alloy disintegration and makes the alloy lose strength [19].

This corrosion type can also be caused by contamination at the boundaries of the grain or by enrichment or depletion of the alloying elements in the grain boundary area. For example, chromium depletion in the grain boundary condition induces intergranular corrosion of stainless steel. Prevention of this corrosion form can be achieved by [19]:

1. Using low carbon (e.g., 304L, 316L) grade stainless steels
2. Using strong carbide-formers (titanium and niobium) to stabilize elements in the stainless steel
3. Applying post-weld heat practice

2.2.2.5 Erosion Corrosion

Erosion corrosion occurs when there is an acceleration of material degradation or attack on metal due to flow between a corrosive fluid relative to the surface area of metal. The flow is relatively fast, and therefore creates a mechanical wear effect or abrasion. The corrosion process removes metal from the surface area and precipitates to form solid products which are mechanically discarded from the surface area of the metal [14].

Erosion corrosion is indicated by the appearance of grooves, gullies, waves, rounded holes, and valleys in the surface area of the metal. In many circumstances, material failure due to erosion corrosion can occur in a short time. These are some prevention methods for erosion corrosion type, including [14]:

1. Smooth out irregularities
2. Change the pipe diameter gradually
3. Change the pipe material to different metal type

2.2.2.6 Cavitation

Cavitation is similar in form to erosion corrosion. It occurs when the protective film in the tube or pipe is removed from the surface during fluid flow. The gas or vapor bubbles which occur on the fluid stream due to low pressure conditions collide with the metal surface. Therefore, the bubbles collapse or implode and generate shockwaves that are strong enough to remove the protective film which is laid above the metal surface [14].

2.2.2.7 Stress Corrosion Cracking

A combination of tensile stress and corrosive conditions in the surrounding area can lead to stress corrosion cracking. Stress corrosion cracking is very dangerous and difficult to measure because the metal material does not indicate any corrosion form in its surface area. Instead, the corrosion forms fine cracks and goes deep inside the material while the surface part of metal remains unattacked [14].

The fine cracks which occur in the material have a transgranular or intergranular shape microstructure. In macroscopic terms, this corrosion form has brittle fracture characteristics. Stress corrosion cracking is categorized as a catastrophic corrosion type because the fine cracks it causes are very difficult to detect. The following methods can be implemented to prevent stress corrosion cracking [14]:

1. Decrease the overall stress limit and take stress concentration into account in design
2. Select appropriate material for the environmental conditions
3. Reduce thermal and residual stresses
4. Build compressive stresses in the surface area of the material

2.2.3 Corrosive Gases

2.2.3.1 Carbon Dioxide Corrosion

Carbon dioxide (CO_2) corrosion is commonly found in oil and gas fields. It occurs because many fields produces not only oil and gas, but also some byproducts such as CO_2. The CO_2 corrosion mechanism involves an electrochemical reaction in which CO_2 transforms from the gas phase into the aqueous phase and reacts with water to form carbonic acid. The carbonic acid is dissociated and reacts with iron to produce Fe_2O_3 precipitation [20]. An increase in temperature accelerates the CO_2 corrosion reaction and the increase of pH decelerates the CO_2 corrosion process. The common types of corrosion induced by CO_2 presence are pitting corrosion, raindrop corrosion, erosion corrosion, and corrosion fatigue [8, 14]. The presence of CO_2 on the formation water could induce the corrosion on the external part of the casing [21].

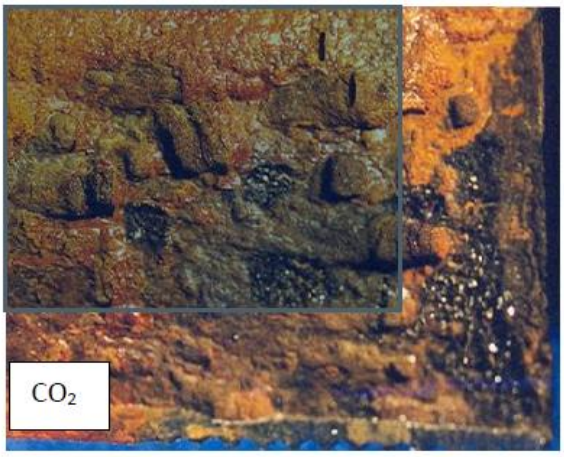

Figure 13. CO_2 pitting corrosion [14]

2.2.3.2 Oxygen Corrosion

The presence of oxygen (O_2) can induce corrosion in oil field equipment including casing and tubing. In an oil or gas well or water injection well, there is a high possibility of this corrosion form due to the presence of oxygen in water. The process of oxygen corrosion is quite fast and causes severe damage to casing or tubing as shown in Figure 14. To avoid this type of corrosion, oxygen must be removed. There are some oxygen removal methods, such as chemical scavenging using bisulfates [8, 14].

Figure 14. Corrosion on water injection tubing [8]

2.2.3.3 Hydrogen Sulfide Corrosion

As a byproduct of oil and gas well, hydrogen sulfide (H_2S) presents a risk of corrosion in tubing or casing. H_2S is difficult to detect since it is colorless and odorless and is very dangerous because it is poisonous and inflammable. H_2S corrosion occurs when there is a reaction between steel and produced fluids which contain H_2S. The steel is exposed to H_2S and becomes anodic [20]. Therefore the steel becomes corroded and pitting corrosion is formed [14]. H_2S content of the formation water induces corrosion on the external part of the casing due to the presence of anaerobic bacteria in the well. The anaerobic bacteria produces H_2S from metabolizing sulfate ions (SO_4) contained in the water and soil in the wellbore environment. This metabolism process of bacteria induces the corrosion process on the casing [21]. Figure 15 shows H_2S corrosion on the external part of casing.

Figure 15. H_2S pitting corrosion due to bacteria metabolism on external part of casing [21]

3. Theory

This chapter presents the theory of tubing stress, failure criterion and burst-casing analytical and empirical models. For the analysis, the model will be compared with FEM simulation result.

3.1 Stress and Failure Analysis

This section discusses the theory of stress and failure analysis on a circular cylinder. The theory is used for computing limit curves, collapse and burst equations, and maximum allowable tensile load on the tubing/casing/drill pipe [22]. Three models are used to evaluate stress in tubing/casing: triaxial, biaxial, and API Burst/Barlow.

Assume a circular pipe with wall thickness t, and inner radius, r. The pipe is subjected to internal pressure P_i and external pressure P_o. Axial load F_a and torque are also applied on the pipe [22]. Figure 16 illustrates the material elements exposed to stress σ_h, σ_θ, and σ_z in three perpendicular directions.

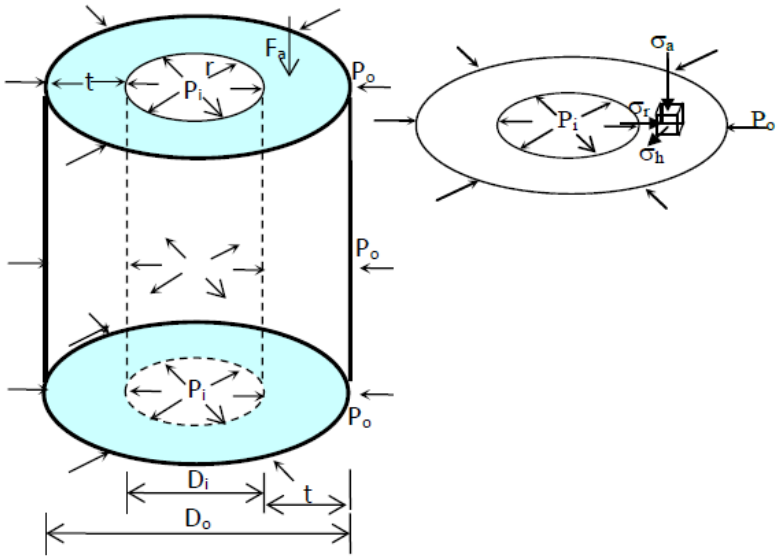

Figure 16. Triaxial stress on circular pipe [22]

3.2 Cylinder Types

There are two categories of circular cylinder which are used in stress and failure analysis theory.

1. Thick-walled cylinder is defined when

$$t > \frac{1}{10} r_i \tag{6}$$

2. Thin-walled cylinder is defined when

$$t < \frac{1}{10} r_i \tag{7}$$

where *t* is defined as the thickness of the cylinder and *r* is defined as the inner cylinder radius

3.2.1 Thick-Walled Cylinder

The thick-walled cylinder is defined in Equation (6). For the analysis of this particular cylinder, assume uniform pressure is imposed on the cylinder. Stresses are produced across the thickness of the cylinder in the radial, axial and circumferential directions as described in Figure 17. These stresses are called the radial, axial, and tangential stresses respectively. The stress field of the thick-walled cylinder must be derived in order to design safe operation limits [22].

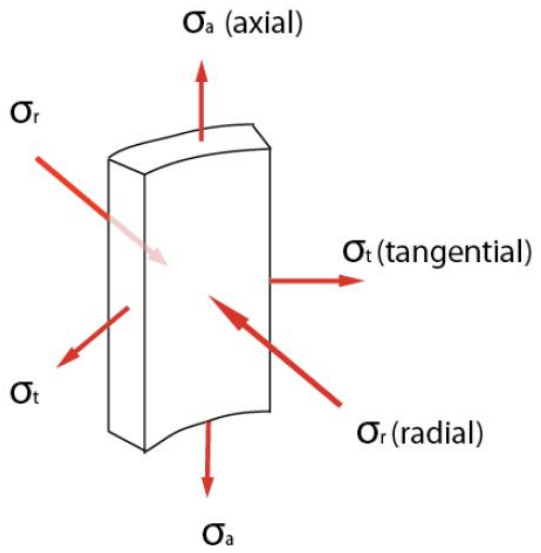

Figure 17. Stress fields in thick-walled cylinder [22]

3.2.1.1 Stress Fields in Thick-Walled Cylinder

Using a combination of the equilibrium equation, compatibility and constitutive relations, and suitable boundary conditions, the stress field across the cylinder wall thickness can be derived [22]. Following are the derivation result of the stress field across the wall thickness of a cylinder.

3.2.1.1.1 Radial Stress

$$\sigma_r = \frac{p_a a^2 - p_b b^2}{b^2 - a^2} - \frac{a^2 b^2}{(b^2 - a^2) r^2}(p_a - p_b) + \sigma_r(\Delta T) \quad (8)$$

3.2.1.1.2 Hoop Stress

$$\sigma_\theta = \frac{p_a a^2 - p_b b^2}{b^2 - a^2} - \frac{a^2 b^2}{(b^2 - a^2) r^2}(p_a - p_b) + \sigma_\theta(\Delta T) \quad (9)$$

3.2.1.1.3 Axial Stress

Prior to solving the axial stress, the "real force", F_a and "effective force", F_e must be defined. The actual axial force in the pipe wall is called real force, and the effective force is the axial force when the effects of pressure are neglected [22].

$$\sigma_a = \frac{F_a}{A} + \frac{P_a a^2 - P_b b^2}{(b^2 - a^2)} + \sigma_a(\Delta T) \quad (10)$$

Equations (8) to (10) are the solutions for thick-walled cylinders.

Moreover, the relationship between real and effective force can be written as

$$F_a = F_a + P_a A_a - P_b A_b \quad (11)$$

Equation (11) is applied for a thin-walled cylinder case. Hence Equation (11) is used for the drilling pipe case since most of drilling pipes are thin-walled cylinders [22].

Figure 18 illustrates the stress distribution across the wall of the cylinder for a thick-walled cylinder case [22].

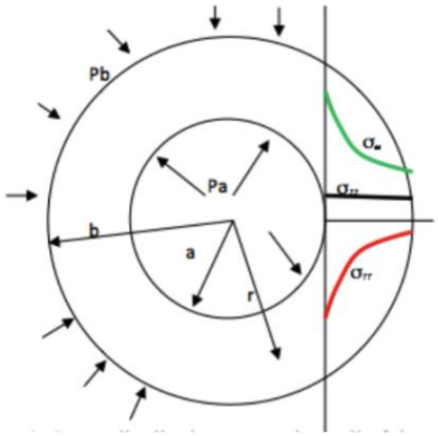

Figure 18. Stress distribution across cylinder wall [23]

3.2.2 Thin-Walled Cylinder

A thin-walled cylinder is using Equation (7). For the analysis of a thin-walled cylinder, assume a thin-walled cylinder subject to internal pressure, P_i [22] as illustrated in Figure 19.

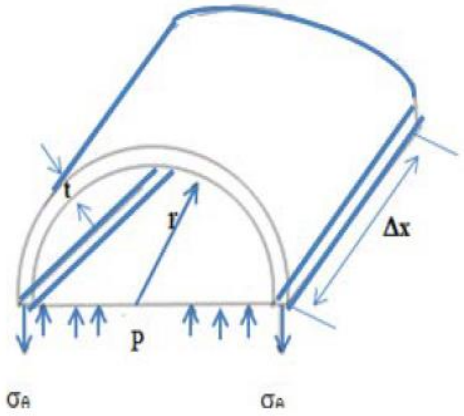

Figure 19. Free body diagram of an open-ended thin-walled cylinder [22]

where Δx is defined as the length of the cylinder, t is defined as the thickness of the cylinder and P is defined as the pressure at the cylinder wall.

The analysis of a thin-walled cylinder is categorized into two cases: open-ended thin-walled cylinder and closed-ended thin-walled cylinder [22].

3.2.2.1 Case 1: Open-Ended Thin-Walled Cylinder

3.2.2.1.1 Hoop Stress

For case 1, only hoop stress exists [22].

$$2\sigma_\theta . t\Delta X = 2.r.\Delta X.P \tag{12}$$

Hence, the solution for hoop stress is

$$\sigma_\theta = \frac{P.r}{t} \tag{13}$$

3.2.2.1.2 Axial Stress

Axial stress does not exist in the case of an open-ended thin-walled cylinder [22].

3.2.2.2 Case 2: Closed-Ended Thin-Walled Cylinder

In case 2, the hoop and axial stress exist in the case of the closed-ended thin-walled cylinder [22].

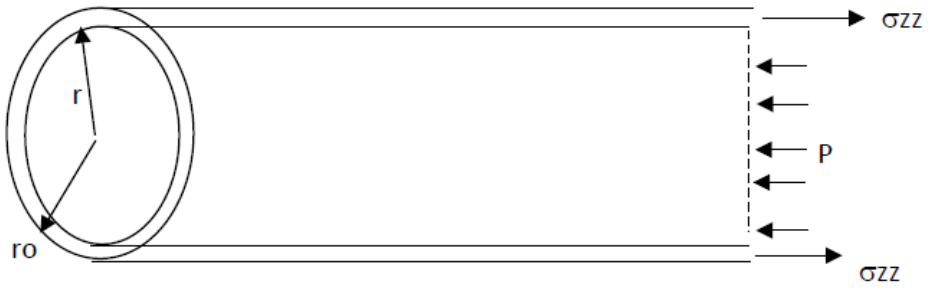

Figure 20. Free body diagram of the closed-ended thin-walled cylinder [22]

3.2.2.2.1 Hoop Stress

The solution for hoop stress on the closed-ended thin-walled cylinder case is the same as for the open-ended thin-walled cylinder case [22].

$$\sigma_\theta = \frac{P.r}{t} \tag{14}$$

3.2.2.2.2 Axial Stress

From the balance of force concept [22], the axial force is given as

$$\sigma_z.\pi(r_o^2 - r^2) = \pi.r^2.P \tag{15}$$

Alternatively, Equation (15) can be written as

$$\sigma_z.\pi(2.r.t + r^2) = \pi.r^2.P \tag{16}$$

By assuming t^2 is very small, $2.r.t + r^2$ is approximated into 2.r.t form. Equation (16) can be written as

$$\sigma_z.2.\pi.r.t = \pi.r^2.P \tag{17}$$

The axial stress on the closed-ended thin wall cylinder is obtained by

$$\sigma_z = \frac{P.r}{2.t} \tag{18}$$

3.3 Shear Stress

Shear occurs due to applied moment on the cylinder. Shear stress is approximated for a thin-walled cylinder as follows [24]:

$$\tau = \frac{T}{2\pi . r^2 . t} \tag{19}$$

3.4 Bending Stress

When a beam is subjected to uniform load on the top fibers of the beam, the top part of the fibers experiences normal compressive stress. The neutral horizontal plane has zero stress and the bottom part of the fibers experiences normal tensile stress [25].

In a high dogleg well, bending stress could occur. The highest bending stress arises at the outer part of the pipe [8]. The value of bending stress caused by dogleg can be determined by the following equation:

$$\sigma_{DL} = \pm \frac{ED}{2R} = \pm (\pi . E . DL . D_O)/432000 \tag{20}$$

where *DL* is defined as the dogleg severity in degree/100 ft depth and *R* is defined as the radius of curvature. If the result is positive, it means that the pipe is subject to tensile stress and the highest stress is located on the outside part of the bent pipe while the negative result indicates that the pipe is subject to compressive stress and the highest stress appears on the inside part of the bent pipe [22].

3.5 Failure Criterion

3.5.1 Tresca Failure Criterion

The maximum and minimum principal stress concept has been developed into Tresca failure criterion. The Tresca failure criterion neglects the intermediate principal stress and is derived from maximum shear stress theory equating with yield stress (σ_y) [22]. The criterion for Tresca failure is

$$\sigma_y = \sigma_{max} - \sigma_{min} \tag{21}$$

3.5.2 Von Mises Failure Criterion

One function of the Von Mises failure criterion is to define the yielding of steel under combined states of stress. This criterion takes intermediate principal stress into account. The Von Mises failure criterion is often used to compute the yielding point of a cylindrical structure. As an example, the initial yield of the casing is based on the combination of three principal stresses: axial stress (σ_a), radial stress (σ_r), and hoop stress (σ_θ), and the shear stress due to torque (τ) [22]. The following equation is used to determine material yielding:

$$\sigma_{VME} = \sqrt{\frac{1}{2}\{(\sigma_\theta - \sigma_r)^2 + (\sigma_r - \sigma_a)^2 + (\sigma_a - \sigma_\theta)^2\} + 3\tau^2} \qquad (22)$$

When no torque is assumed, the shear stress term is removed from Equation (22). The yield limit of the pipe is obtained by setting the Von Mises stress, σ_{vme} equal to the yield stress, σ_y.

3.5.3 Maximum Principal Stress Theory

By plotting two principal stresses, a bi-axial failure envelope is formed. The stress state inside the envelope is defined as safe, while the outside of the envelope is defined as failure [22]. Figure 21 illustrates the comparison of three failure criterion in one biaxial failure envelope. Maximum principal stress is pink (square), Tresca failure criterion is blue (hexagonal), and Von Mises failure criterion is green (ellipse).

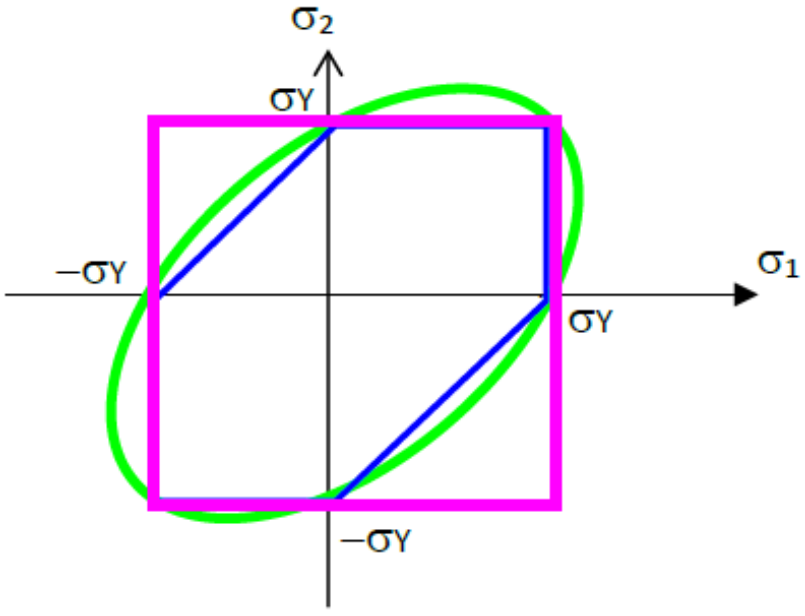

Figure 21. Comparison of three failure criterion [22]

3.6 Safety Factor Design

Internal pressure P_i, external pressure P_o, real axial force F_a, and torque T are needed to determine combined stress limits in the tubing. For practicality, only the pressure difference between internal pressure P_i, and external pressure P_o, is computed. If the pressure difference result is positive, it indicates a "burst" condition. When the pressure difference result is negative, a "collapse" condition is indicated [22].

The design factor due to triaxial stress intensity is obtained by the following equation,

$$SF = \frac{\sigma_y}{\sigma_{VME}} \tag{23}$$

The Von Mises failure criterion is used to plot the limits curve to illustrate which part of the pipe would show yielding first. The maximum equivalent stress is frequently observed on the inside surface of the pipe. Hence, the radial stress is solved by reducing Equation (8) and hoop stress is obtained by reducing Equation (9) by assuming $r = r_i$.

3.6.1 Radial Stress

By assuming $r = r_i$, Equation (8) is reduced to

$$\sigma_r = -P_i \tag{24}$$

3.6.2 Hoop Stress

By assuming $r = r_i$, Equation (9) is reduced to

$$\sigma_\theta = \frac{d_o^2 + d_i^2}{d_o^2 - d_i^2} P_i - \frac{2d_o^2}{d_o^2 - d_i^2} P_o \tag{25}$$

Equation (25) can be written as

$$\sigma_\theta = (\beta - 1)P_i - \beta P_o \tag{26}$$

Note: $P_i = P_a$, and $P_o = P_b$ when using Figure 18 as reference.

Solving for β,

$$\beta = \frac{2d_o^2}{d_o^2 - d_i^2} \tag{27}$$

Jan and Aadnøy [26] developed three-dimensional stress analysis to calculate burst and collapse of tubing and casing. The analysis assumes that temperature effect, torque, and bending stress are neglected. Equation (23) it is known that the safety factor is the ratio of the real yield stress to the theoretical yield stress. Hence, the safety factor is computed as

$$SF = \frac{\sqrt{2}\sigma_y}{\sqrt{[(\sigma_a - \sigma_h)^2 + (\sigma_h - \sigma_r)^2 + (\sigma_r - \sigma_a)^2]}} \tag{28}$$

By inserting Equation (24) and Equation (25), the dimensionless parameters are obtained.

For *x* parameter,

$$x = \frac{(P_i + \sigma_a)}{\sigma_y} \tag{29}$$

For *y* parameter,

$$y = \frac{\beta(P_i - P_o)}{\sigma_y} \tag{30}$$

In terms of dimensionless parameters, the safety factor could be computed as

$$z = SF = \frac{1}{\sqrt{x^2 - xy + y^2}} = \frac{\sigma_y}{\sigma_{VME}} \tag{31}$$

Solving Equation (31) for y gives

$$y = \frac{x}{2} \pm \sqrt{\frac{1}{SF^2} - \frac{3}{4}x^2} \tag{32}$$

A positive sign indicates tensile force for a burst condition, whereas a negative sign indicates compressive force for a collapse condition [22]. Equation (32) is an ellipse Equation [22]. Figure 22 illustrates the ellipse of curve limits for the various safety factors.

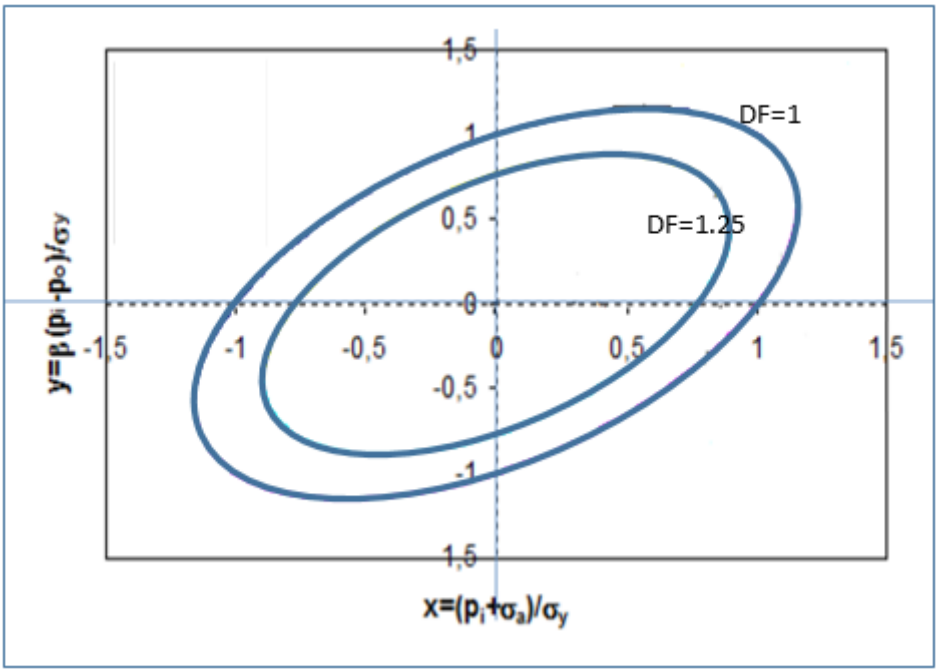

Figure 22. Three-dimensional design factor on two-dimensional plane [22]

3.7 Triaxial Design Factor

Triaxial load includes burst, collapse, and axial failure modes. Therefore, triaxial design factor should be categorized as the highest failure mode compared to other failure modes (burst, collapse and axial failure modes). However, the limit which is produced by triaxial design factor cannot be applied in all conditions. On a Von Mises stress plot, the triaxial limit only applies to the top or bottom right of the plot as illustrated in Figure 23. Observation shows that the material limit using the triaxial design factor is higher than when using collapse design factor. Hence, the triaxial load becomes more relevant for calculating collapse and tension limits [8].

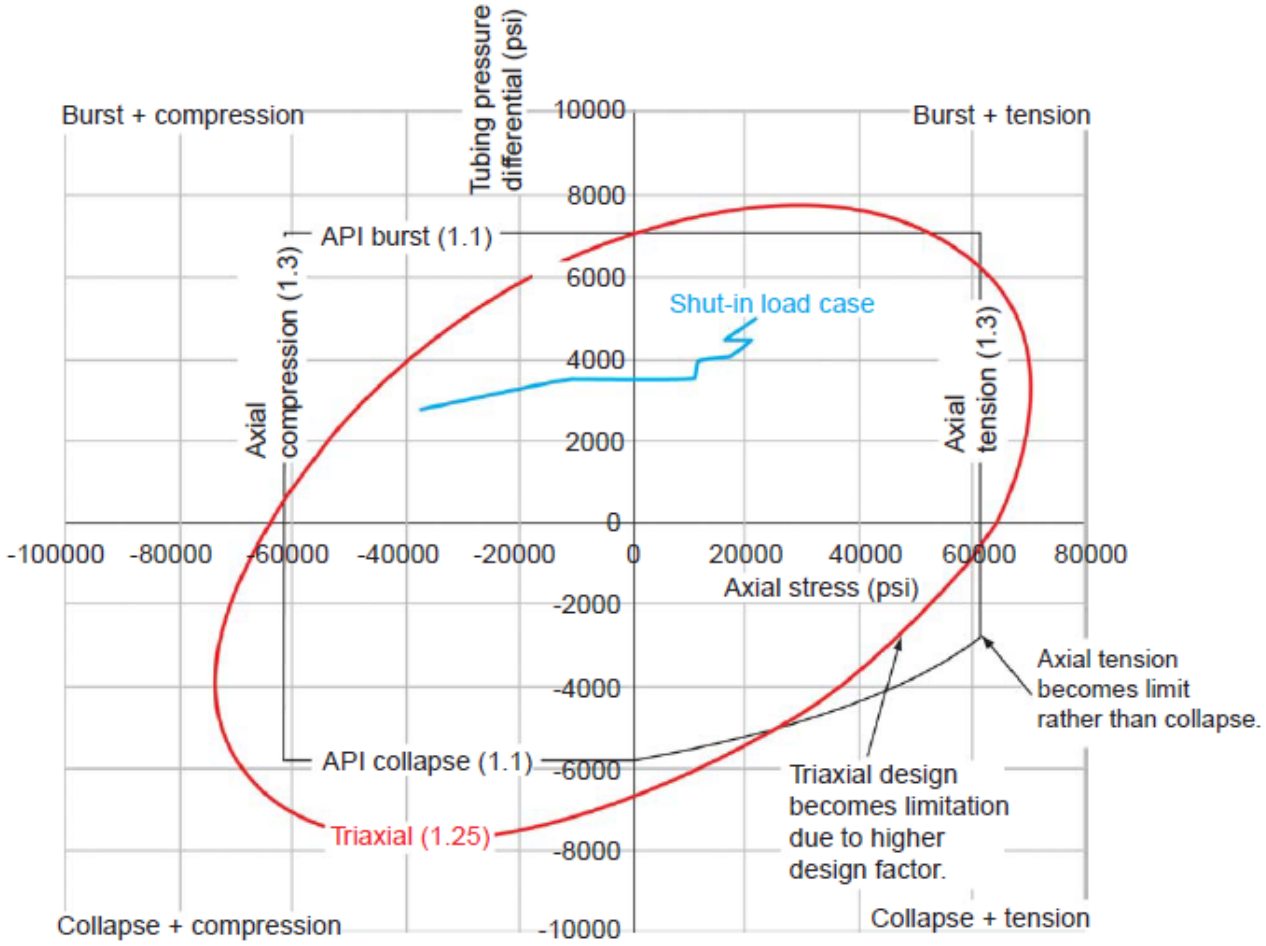

Figure 23. Design limit plot with triaxial design included L-80 material [8]

3.7.1 Collapse Pressure

The collapse pressure equation is obtained by inserting Equation (24) and (25) into Equation (22) [22]. Solving for the external pressure gives

$$P_o = \frac{-\sigma_a + 2\beta P_i - P_i \pm \sqrt{-3\sigma_a^2 - 6\sigma_z P_i - 3P_i^2 + 4\sigma_y^2}}{2\beta} \tag{33}$$

The solution of P_o is the maximum collapse pressure using the triaxial design equation. There could be one or two solutions for collapse pressure design [22].

3.7.2 Burst Pressure

By solving for P_i in Equation (34), burst pressure using the triaxial design equation is computed [22].

$$P_i = \frac{\beta\sigma_a - 2\sigma_a + 2\beta^2 P_o - \beta P_o \pm \sqrt{-3\beta^2\sigma_a^2 - 6\beta^2\sigma_a P_o - 3\beta^2 P_o^2 + 4(\beta^2 - \beta + 1)\sigma_y^2}}{2(\beta^2 - \beta + 1)} \quad (34)$$

There are two P_i solutions: positive square roots and negative square roots. The burst pressure is only represented by positive real numbers [22].

3.8 Burst and Collapse Model

3.8.1 API Burst/Barlow Model

Burst is a type of tensile failure which causes a rupture along the pipe axis. This failure develops when the difference between the internal pressure and external pressure reaches the limit of the pipe's mechanical strength [27]. Burst condition in the casing takes place during well control operations, pressure integrity tests, pumping operations, and production operations [28].

Consider a thin-walled cylinder with both ends closed. Furthermore, this closed-ended cylinder is loaded by internal pressure. As a result of the pressure loading, axial stresses and hoop stresses arise on the cylinder as illustrated in Figure 24 [27].

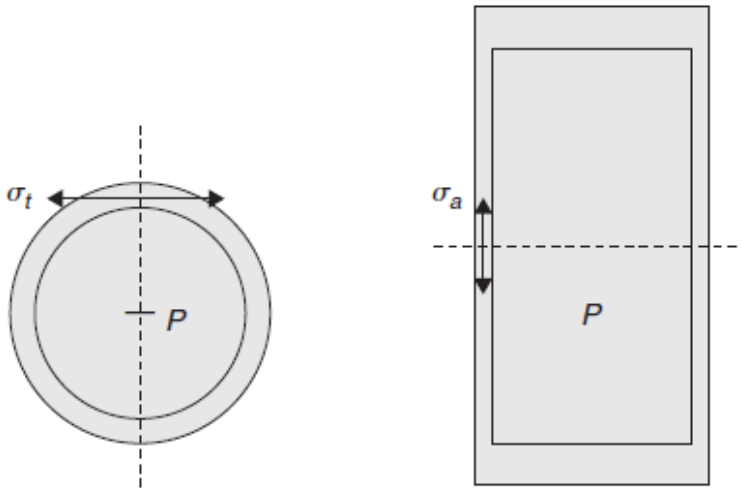

Figure 24. Stresses in internally loaded thin-walled cylinder [27]

When a thin-walled cylinder is loaded by internal pressure, the stress on the circumference of the cylinder is twice the axial stress [27]. Therefore, when the cylinder fails, it breaks on the axis as shown in Figure 25.

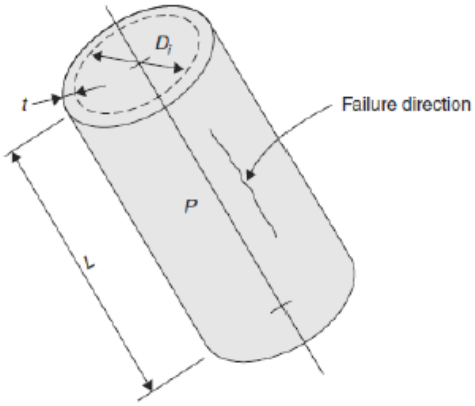

Figure 25. Stress on thin-walled cylinder [27]

By assuming that the tangential stress is equal to the tensile strength of the material [27]. The burst equation is computed by the following formula:

$$P_{burst} = 2\sigma_{tensile}[\frac{t}{D_i}] \tag{35}$$

Alternatively, when using the outer diameter,

$$P_{burst} = 2\sigma_{tensile}[\frac{t}{D_o}] \tag{36}$$

From the API Bulletin 5C3 [29], the burst pressure in the casing is computed by using internal yield pressure formula as shown in the following equation:

$$P_B = 0.875[\frac{2Y_p t}{D}] \tag{37}$$

where P_B is the minimum burst pressure (psi), Y_P is the minimum yield strength (psi), t is nominal wall thickness (inch), D is nominal outside pipe diameter (inch), and 0.875 is the tolerance correction.

Equation (37) is also known as the Barlow Equation [28].

3.8.2 API Collapse Model

The casing tends to collapse when the external pressure is higher than the internal pressure. Collapse on the casing could occur during cementing operations, trapped fluid expansion, and well evacuation [28]. Collapse is considered to be geometric failure instead of a material failure, and it is categorized as casing deformation [27].

Collapse strength of the casing is the function of slenderness ratio (*D/t*) of the casing. According to API Bulletin 5C3, there are four collapse regimes which are functions of the yield strength and slenderness ratio. These are: yield strength collapse, plastic collapse, transition collapse, and elastic collapse [28].

3.8.1.1 Yield strength collapse

In thick-walled pipes (*D/t* < 15±), the tangential stress surpasses the material yield strength before collapse instability failure occurs [28]. The yield strength collapse is computed by the following equation,

$$P_{Y_P} = 2Y_P[\frac{(D/t)-1}{(D/t)^2}] \quad (38)$$

Pipe nominal dimensions are used for the collapse equations. The *D/t* ratio values for the yield strength collapse equation are provided in Table 3.

Table 3. P-110 Yield Strength Collapse Model [29]

Grade	Maximum D/t
P-110	12.44

3.8.1.2 Plastic collapse

Plastic collapse types have been established from experimental data from 2,488 tests of certain types of seamless casing (K-55, N-80, and P-110). No analytical models have been developed to predict collapse behavior accurately in the plastic collapse range. The analysis of data regression gives a 95% confidence level that 99.5% of the pipes manufactured to American Petroleum Institute (API) specifications will collapse when the collapse pressure is higher than plastic collapse pressure [28]. The minimum collapse pressure for the plastic region of collapse is

$$P_P = Y_P\left[\frac{A}{D/t} - B\right] - C \quad (39)$$

The values of *A*, *B*, and *C* factors and the *D/t* value range for plastic collapse are shown in Table 4,

Table 4. P-110 Plastic Collapse Model [29]

Grade	A	B	C	D/t Range
P-110	3.181	0.0819	2852	12.44-20.41

3.8.1.3 Transition collapse

The transition collapse value is determined by numerical curve fitting between the plastic collapse and elastic collapse ranges [28]. The minimum collapse pressure for the region between plastic collapse and elastic collapse is

$$P_T = Y_P \left[\frac{F}{D/t} - G\right] \quad (40)$$

The values of *F*, and *G* factors and *D/t* value range for transition collapse formula are shown in Table 5

Table 5. P-110 Transition Collapse Model [29]

Grade	F	G	D/t Range
P-110	2.066	0.0532	12.44-20.41

3.8.1.4 Elastic collapse

The elastic collapse mode is developed from elastic instability failure theory. This collapse criterion is not a function of casing or tubing yield strength and is suitable for the case of thin-walled pipe (*D/t* > 25±) [28]. The minimum collapse pressure equation for the elastic range is

$$P_E = \frac{46.95\ x\ 10^6}{(D/t)[(D/t) - 1]^2} \quad (41)$$

The value of D/t for the elastic collapse equation is shown in Table 6

Table 6. P-110 Elastic Collapse Model [29]

Grade	Minimum D/t range
P-110	26.22

3.9 Fracture Mechanics

Designing the structure against fracture is a vital area of research. However, the elastic stress analysis performed by structural designers is not sufficient when the fracture of material occurs. This can happen due to the change of local stress in the material to such an extent that the structure is not able to withstand the load that occurs from the fracture. Propagation in the structure will occur when the fracture reaches a certain critical length. Moreover, this can happen when the stress values are still under the yield stress of the material [30].

3.9.1 Energy Balance Approach

A. A. Griffith (1893-1963) is well known developing the study of fracture mechanics. By applying an energy-balance approach, Griffith estimates the strain energy per unit in a stressed material during fracture [30]:

$$U^* = \frac{1}{V}\int f\, dx = \int \frac{f}{A}\frac{dx}{L} = \int \sigma d\epsilon \tag{42}$$

For linear material ($\sigma_y = E\epsilon$), the strain energy per unit volume is

$$U^* = \frac{E\epsilon^2}{2} = \frac{\sigma^2}{2E} \tag{43}$$

When a crack is growing through a solid part of the material to the depth *a*, the material region adjoining the free surface area is unloaded and releases its strain energy. The amount of energy which is released can be computed by Griffith's formula [30].

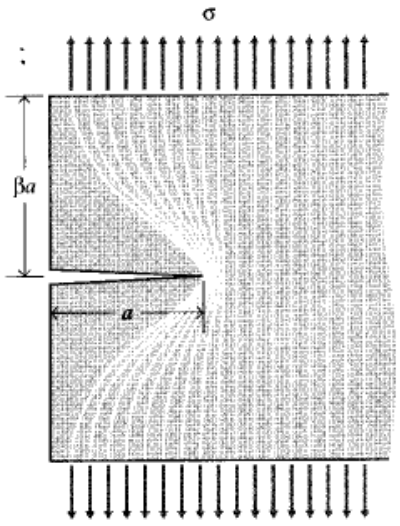

Figure 26. Idealization of unloaded region near crack flanks [30]

3.9.2 Modes of Fractures

An alternative method called the stress intensity approach has been developed to analyse the fracture process that considers the stress state on the area adjacent to the tip of a crack. In engineering practice, this alternative method has proven to be more beneficial than the method developed by Griffith. The stress intensity approach categorizes three types of cracks, termed modes I, II, and III. Mode I is a normal opening mode, while modes II and III are shear sliding modes [30]. The illustration of fracture modes is shown in Figure 27.

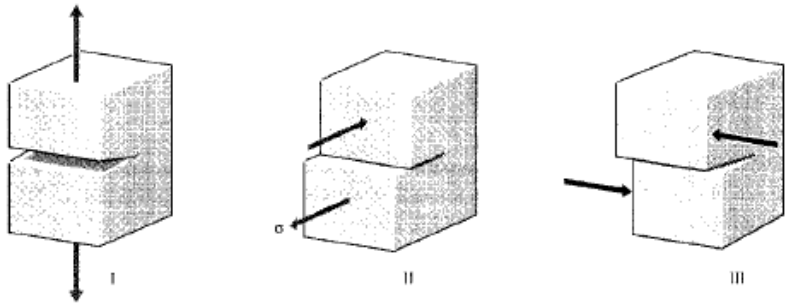

Figure 27. Three types of fracture modes [30]

4. Finite Element Method (FEM) Modelling

The term “finite element” was introduced in 1960. This method was used by engineers to obtain solution approximation in stress analysis, fluid flow, heat transfer, and other areas. FEM has been employed in engineering since the early 1960s. From the late 1960s until the early 1970s, numerous engineering problems were solved by the application of this method [31]. FEM is the common method used for structural mechanic discretization. The FEM physical concept is the partition of the mathematical model into smaller part of elements called finite elements [32]. The building and solving process of FEM involves three stages: idealization, discretization, and solution. Abaqus software is used for FEM modelling and analysis in this thesis study.

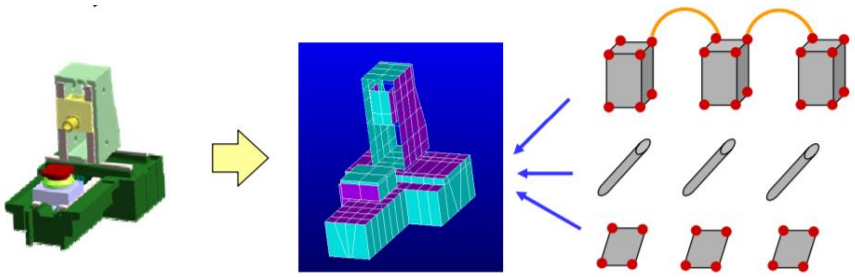

Figure 28. Finite element method concept [31]

4.1 Idealization

Idealization transforms the physical form of the FEM system into a mathematical model and can only be processed by a human. Therefore, idealization is an essential step in engineering design process. Idealization generates a model that acts as an instrument to simulate and predict the behavior of the system [32]. Figure 29 illustrates the simplification of the FEM simulation process

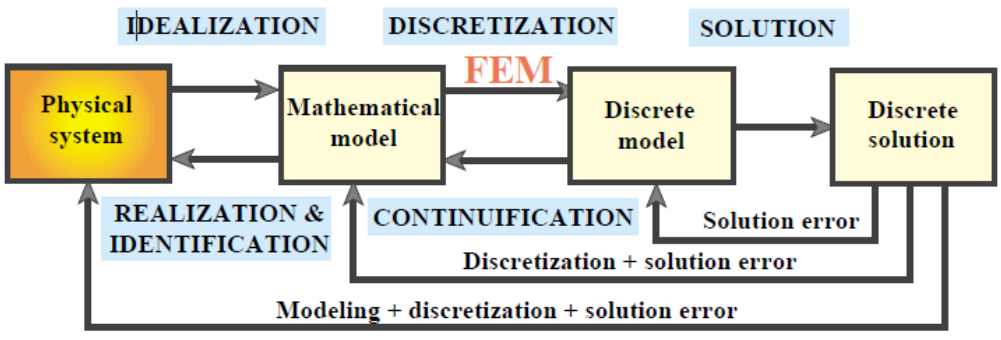

Figure 29. Physical simulation process simplification [32]

This process is an abstraction of a physical form in reality. The numerical results from the idealization are interpreted back into a physical form to explain the behavior aspect of the system [32].

There are four mathematical models that can be used in idealization [32]:

1. A very thin plate model (based on Von Karman's membrane-bending theory)
2. A thin plate model (i.e. Kirchoff's plate theory)
3. A moderately thick plate model (i.e. Mindlin-Reissner plate theory)
4. A very thick plate model (three-dimensional elasticity base)

4.2 Discretization

Discretization comprises multiple decomposition processes. In FEM simulation, discretization is important in order to make a numerical simulation practical. The process involves the reduction of the number of degrees of freedom. As a result of this reduction, a discrete model is produced for the simulation. The discretization model works in the dimensions of both space and time [32]. The example of discretization process on the object is illustrated in Figure 30.

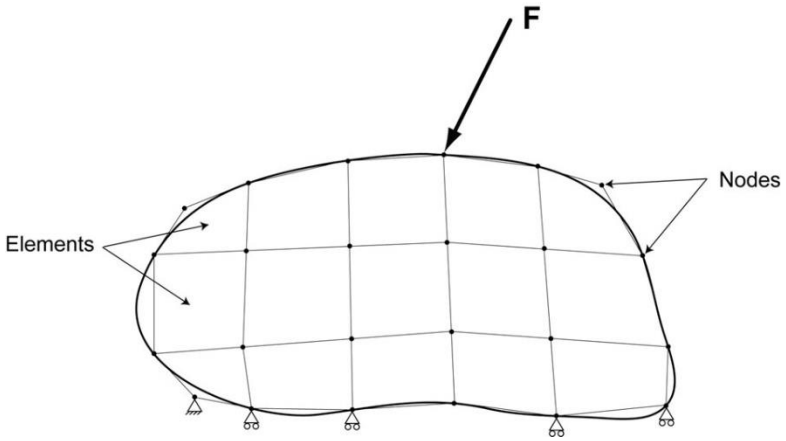

Figure 30. Discretization process example [33]

4.3 Element Geometry

The element geometry is described by assigning the locations of geometric nodal points. For practicality, the components use simple geometries. For a one-dimensional plane, the components are regular and in the form of straight lines or arched sections. In a two-dimensional plane, the components are trilateral or rectangle-shaped. In a three-dimensional plane, tetrahedral, wedges/prisms, and cuboid shapes prevail.

4.4 Error Sources

Modelling errors are very important in engineering. However, it is difficult and expensive to assess an error itself. A process is therefore required by which the models are validated through comparison of experimental results.

Discretization errors also very important. The solution calculated by a discrete model is only an estimation of the solution based on a mathematical model. The difference in results between both solutions is measured quantitatively and called discretization error [32].

A discrete model solution is more accurate when the number of degrees of freedom is also increased. Errors from discretization will reach zero when the number of degrees of freedom is very large or close to infinity [32].

4.5 Degrees of Freedom (DOF)

The components of DOF indicate the state of the component. DOF also functions as a referrer to which the nearest component are connected. Degrees of freedom are characterized as values or derivatives of a variable in primary field in connector points at node [32].

4.6 FEM Modelling and Simulation

FEM simulations are based on models which are built from scratch. Several steps are required to obtain the models and the results of the FEM simulations as shown in Figure 31. The first step is geometry building to create a model based on cylindrical pipe geometry. The models are categorized into undamaged model type and damaged model with various wear percentages. The next step is to add the material properties to the model. Then loads are applied to the model, input problem type is determined, the boundary conditions of the model are set, and meshing on the model is assigned before starting the simulation on the model.

Due to the irregularity of wear shape in the casing, various models of wear are introduced to represent the shapes of local wear as regular geometric shapes. Specifically, a crescent-shaped model, wedged shaped model, and rectangle-shaped model are used. The models are categorized into single scar model and double scars model. The double scars model is a combination of two of the three models, with two model types. Model 1 has both scars are located on the internal part of the production casing, and Model 2 has one scar is located on the internal of the production casing and another scar located on the external part of the production casing.

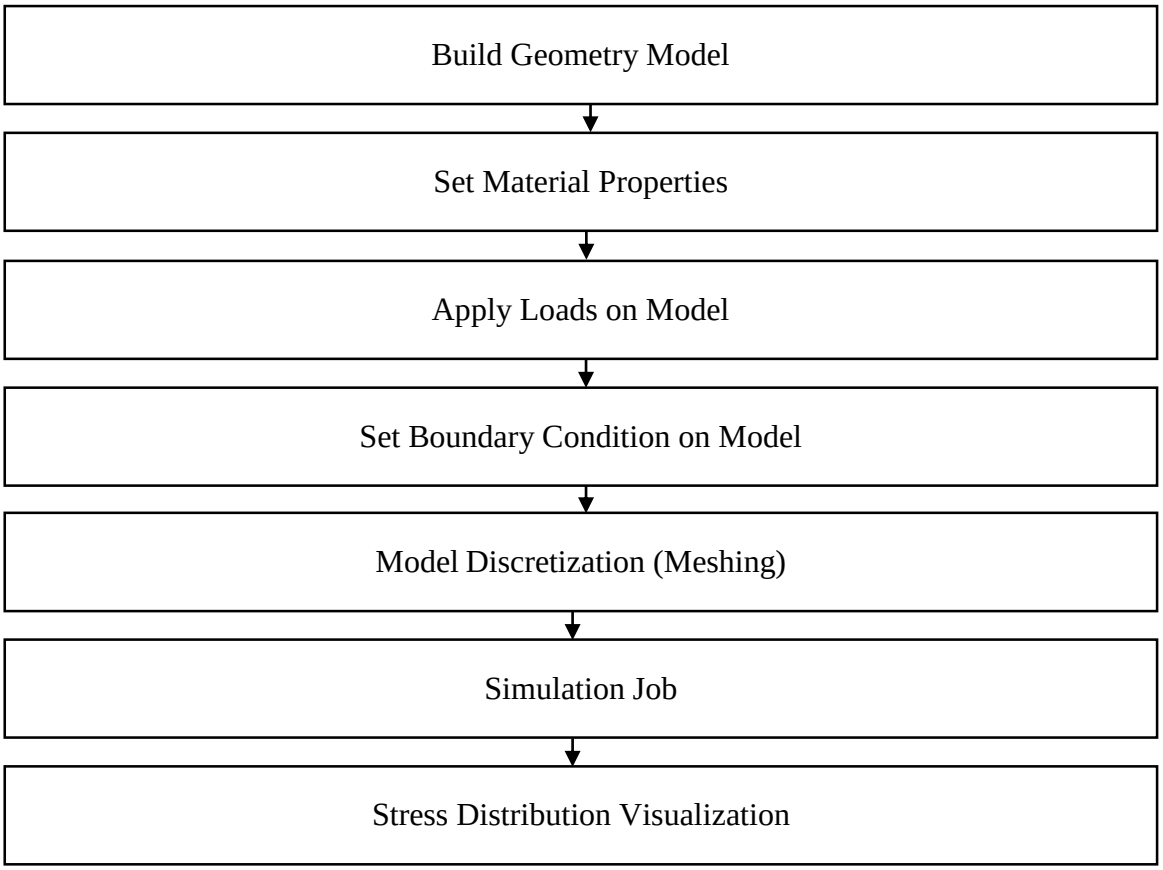

Figure 31. FEM simulation steps in Abaqus software

4.7 Modelling Assumption

The tubular experiences several loadings including temperature, bending, and pressure among others. However, the assumptions for this simulation are

- Isothermal condition ($\Delta T = 0$)
- Straight tubular, where bending stress = 0

4.8 FEM Simulation Data

All data for the FEM simulations in this thesis work are hypothetical. Table 7 presents the hypothetical casing data used for the simulation. Wear percentage data are assumed from tubing and casing wear measurement data from Ekofisk and Gullfaks Fields [1, 2, 5]. For the pressure loading data, the external pressure is set at 500 psi and internal pressure is set varying from 1000 psi to 10000 psi for the burst scenario, while the internal pressure is set at 500 psi and external pressure is set varying from 1000 psi to 10000 psi for the collapse scenario. A reference model is built for both burst and collapse scenarios in this simulation.

Table 7. Casing Specification Data for Simulation

Specification	
Casing Type	Production Casing
Casing Grade	P-110
Yield Strength	11000 psi
Yield Strength Included SF 8/7	96250 psi
Weight	47 lbs/ft
Outer Diameter	9.625 in
Inner Diameter	8.681 in
Wall Thickness	0.472 in

4.8.1 Wear Percentage

As previously mentioned, the wear percentage data are hypothetical and based on measurement from the Ekofisk Field, where tubing wear shows maximum wear up to 47% [1], and the Gullfaks Field, where maximum wear of 35% is observed [2]. Based on these field measurement data, the production casing wear was assumed up to 45% for the FEM simulation. The wear percentage data are based on removed wall thickness percentage for the production casing and computed into the depth of indentation in the production casing. From the depth of indentation data, a locally worn production casing model is built. The wear percentages vary from 5% to 45% with an increment of 5% for each model and 0% as a reference model. Figure 32 shows an example of locally worn production casing, while Figure 33 shows an example of uniformly worn production casing. The FEM simulation is executed for each wear model to obtain the maximum Von Mises stress value results for the production casing wall. Furthermore, the Von Mises stress results are compared to the material yield strength after including the safety factor. From the data comparison results, the trend line of the de-rated burst and collapse strengths of the production casing are generated by implementing linear interpolation. Table 8 presents the wear percentage parameters for the production casing.

Table 8. Wear Percentage Parameters of Production Casing

Wear Percentage (%)	Wear Nominal Thickness	Depth of Indentation
0	0	0.000
5	0.05	0.024
10	0.1	0.047
15	0.15	0.071
20	0.2	0.094
25	0.25	0.118
30	0.3	0.142
35	0.35	0.165
40	0.4	0.189
45	0.45	0.212

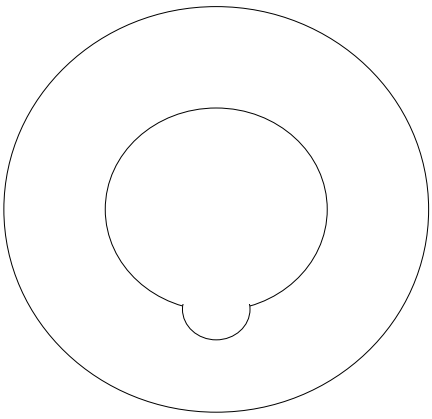

Figure 32. Local wear

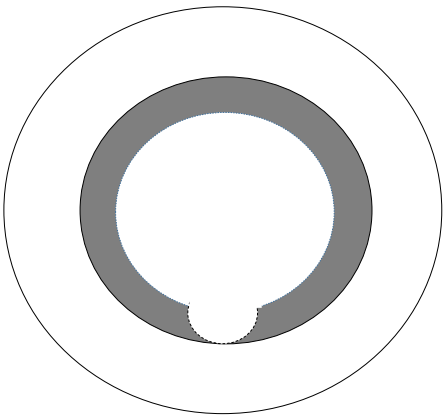

Figure 33. Local wear removed

4.8.2 Building Simulation Model

The model for the FEM simulation is built based on a cylindrical pipe model. This model is built based on the real production casing specification as shown in Table 7. To simulate the wear effects on the burst and collapse strengths of the casing, nine wear shape models are built with specific geometry and wear location. These are the single crescent and single wedge-shaped wear models. The double scars model is divided into two models. Model 1 has both scars located on the inside part of the casing, while model 2 has one scar located on the internal part of the casing and the other located on the external part of the casing.

4.8.2.1 Single Scar

4.8.2.1.1 Crescent-shaped Wear

The crescent-shaped wear model is built using the assumption of production casing wear due to contact between the casing and a tool joint or coiled tubing operation.

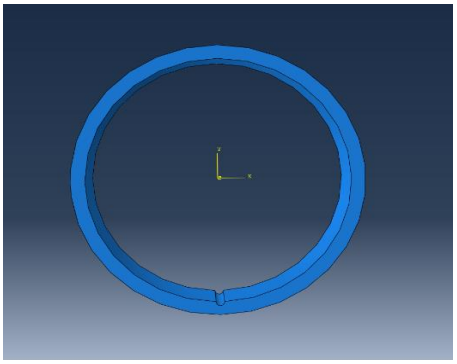

Figure 34. Crescent-shaped wear

4.8.2.1.2 Wedge-shaped Wear

The wedge-shaped wear model is categorized into three different wear width types: 0.2 wear width, 0.25 wear width, and 0.3 wear width. Wedge-shaped wear is assumed to be the type of wear that occurs due to pitting corrosion. See Figures 35, 36, and 37.

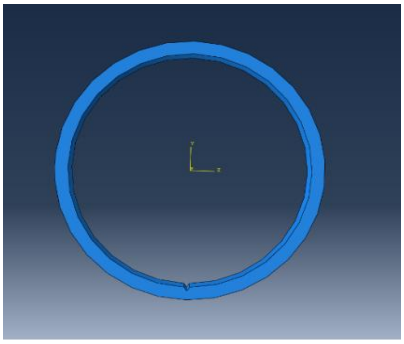

Figure 35. 0.2 width wedge-shaped wear

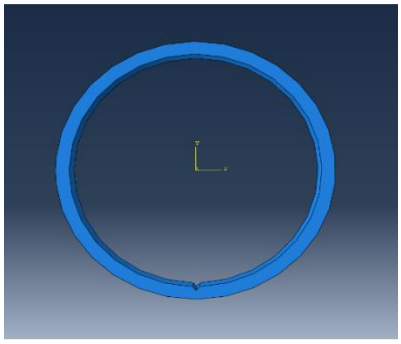

Figure 36. 0.25 width wedge-shaped wear

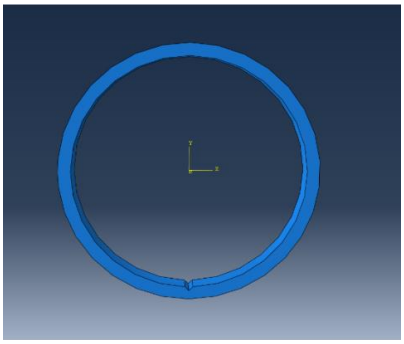

Figure 37. 0.3 width wedge-shaped wear

4.8.2.2 Double Scars (Model 1)

The double scars model is built assuming continuous contact between the casing wall and the tool joint or drill string. This model also takes into consideration that the pitting corrosion process occurs in more than one location. Therefore, the wear on the casing wall not only occurs at one point but also is located on two points as modeled in this simulation. The wear geometry

for the double scars model is approximated by dual crescent-shaped wear (Figure 38) and dual wedge-shaped wear models (Figure 39).

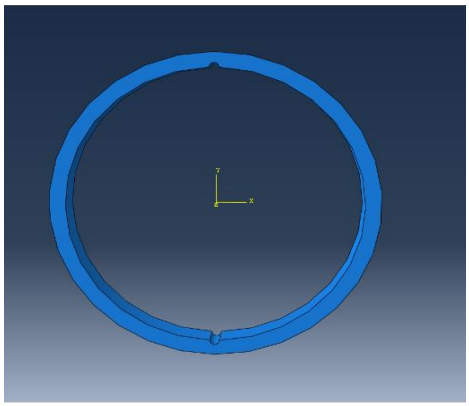

Figure 38. Dual crescent-shaped wear

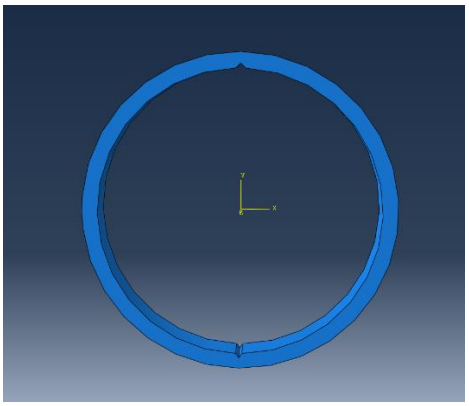

Figure 39. Dual wedge-shaped wear

4.8.2.3 Double Scars (Model 2)

Another type of wear is casing wear on the external part of the production casing. This wear occurs when the casing is running into hole (RIH) and being scratched by the borehole wall or other drilling equipment. Due to this scratching, the corrosion-protective layer is removed and pitting corrosion on the outer part appears. The outer part wear is approximated by three types of geometry: crescent-shaped wear (Figure 40), wedge-shaped wear (Figure 41), and rectangle-shaped wear (Figure 42).

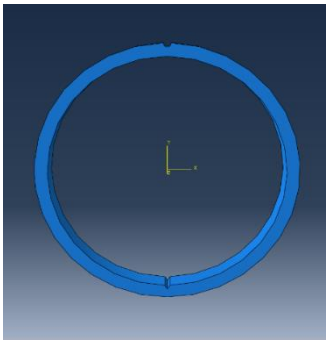

Figure 40. External crescent-shaped wear

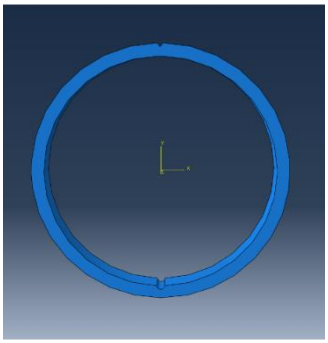

Figure 41. External wedge-shaped wear

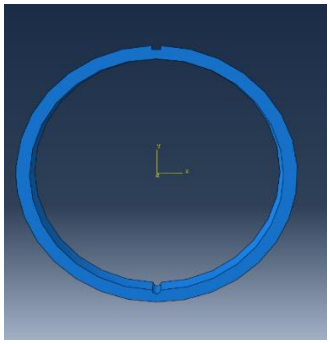

Figure 42. External rectangle-shaped wear

4.8.3 Material

This FEM simulation model uses elastic material type and has linear and isotropic properties. Mechanical properties of the model, such as Young's modulus (E) and Poisson's ratio (v) are set on typical values for steel mechanical properties.

Table 9. Material Properties

Material Type	Elastic
Material Properties	Linear, Isotropic
Young's Modulus	30 x 10^6 psi
Poisson's Ratio	0.25

4.8.4 Meshing/Model Discretization

The division of a geometry model into small fine elements is called model discretization or meshing. The meshing process generates the coarsest element which is used to cover the dominating behavior of the system. This process is implemented to distribute the load on the geometry model uniformly through the elements. However, the stress concentrations in the geometry areas where cracks and corners appear are very high. The meshing process gives an acceptable level of accuracy when compared to the results from theoretical data [15]. The FEM simulation for this thesis work uses a bilinear Q8 element with a degree of freedom of 8.

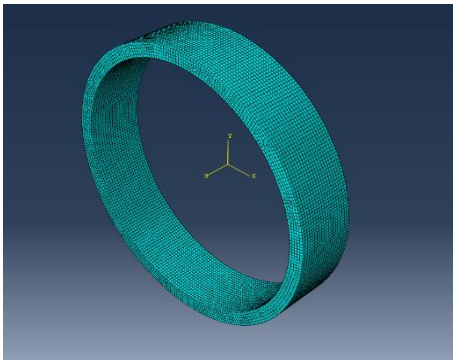

Figure 43. Meshing process

4.8.5 Boundary Condition

This thesis work only simulates and analyses a production casing cross-section. Therefore, the boundary condition on the FEM simulation to investigate the effect of local wear on the production casing is set to open-ended.

4.8.6 Loading

Since the temperature effect is neglected, only pressure acts as loading on the model. The internal loadings are set varying from 1000 psi to 10000 psi, while the external loading is set static at 500 psi for the burst case. For the collapse case, the external loadings are set varying

from 1000 psi to 10000 psi, while the external loading is set at 500 psi. Variations in loading are implemented in order to obtain the trend line of the de-rated burst and collapse strength of the production casing. Internal loading is due to the fluid inside the A-Annulus while external loading is due to fluid leaks in the B-Annulus.

Table 10. Burst Case Pressure Loading Data

Burst Case	
Internal Pressure (psi)	External Pressure (psi)
1000	500
2000	
3000	
4000	
5000	
6000	
7000	
8000	
9000	
10000	

Table 11. Collapse Case Pressure Loading Data

Collapse Case	
Internal Pressure (psi)	External Pressure (psi)
500	1000
	2000
	3000
	4000
	5000
	6000
	7000
	8000
	9000
	10000

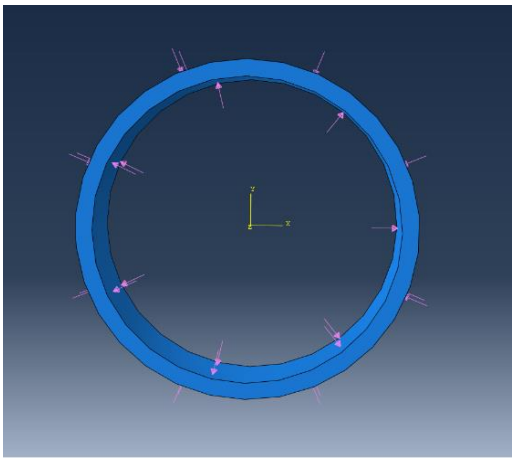

Figure 44. Loading on model

4.8.7 Von Mises Stress Field Result

The results of the FEM simulation using Abaqus software are presented in a stress distribution visualization which illustrates the distribution of Von Mises stress as the result of FEM numerical computation along the wall thickness of the cylinder model from the lowest to the highest. Figure 45 shows the stress distribution visualization of the undamaged 9 5/8 in production casing when it is loaded by internal pressure 1000 psi and external pressure 500 psi.

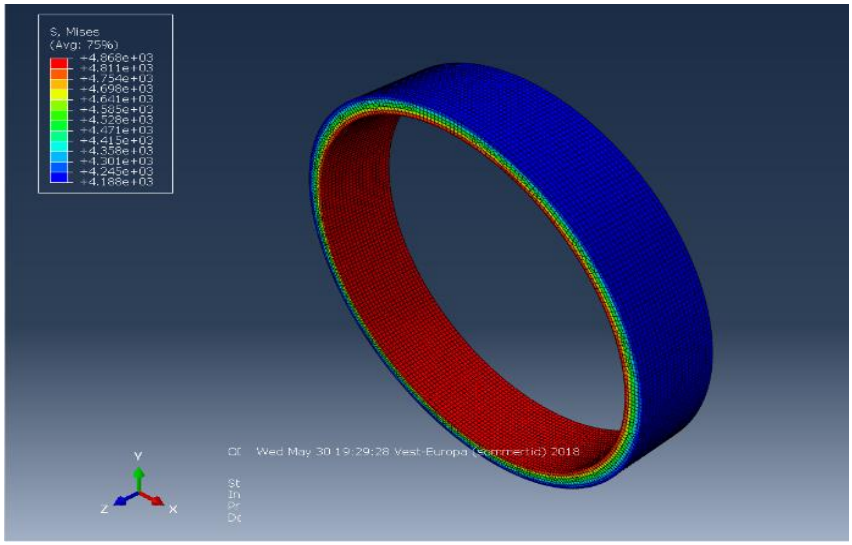

Figure 45. Stress distribution visualization

5. Simulation Results

This chapter presents the simulation results of the production casing de-rated burst and collapse pressures. The wear types introduced in the production casing are presented in Chapter 4.

5.1 Burst Case Results

In this thesis work, the API Burst/Barlow model is used to predict the maximum burst pressure limit on the production casing. The API Burst/Barlow model is chosen since the computation of undamaged casing or reference scenarios using API Burst/Barlow model are similar to the results of the maximum burst pressure limit of the undamaged casing or reference scenario in the FEM simulation.

5.1.1 Reference Model (0% Wear)

The reference model is built based on the undamaged production casing scenario. All of the simulated production casing models use the same reference model. The simulation shows that the Von Mises stress on the production casing reaches 96650 psi when it is loaded by internal pressure 10000 psi. The production casing reaches its yield limit when it is loaded by internal pressure between 9000-10000 psi (safety factor is included). The Von Mises stresses computed from the FEM simulation in production casing are shown in Table 12.

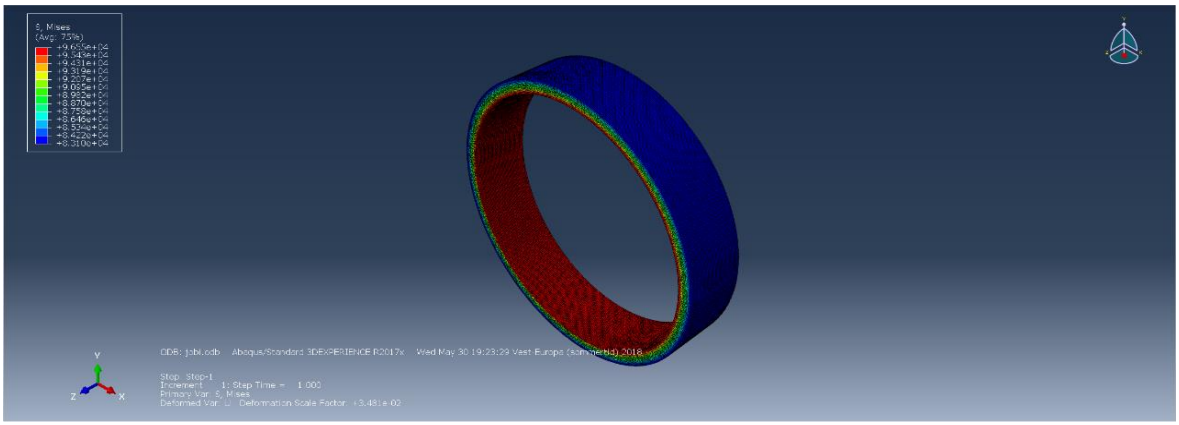

Figure 46. Simulated burst model with 0% wear and internal pressure 10000 psi

Table 12. Internal Pressure with Von Mises Stress for 0% Wear Model

Wear	Internal Pressure (psi)	Von Mises Stress (psi)
0%	1000	4900
	2000	15070
	3000	25250
	4000	35440
	5000	45630
	6000	55810
	7000	66000
	8000	76180
	9000	86370
	10000	96550

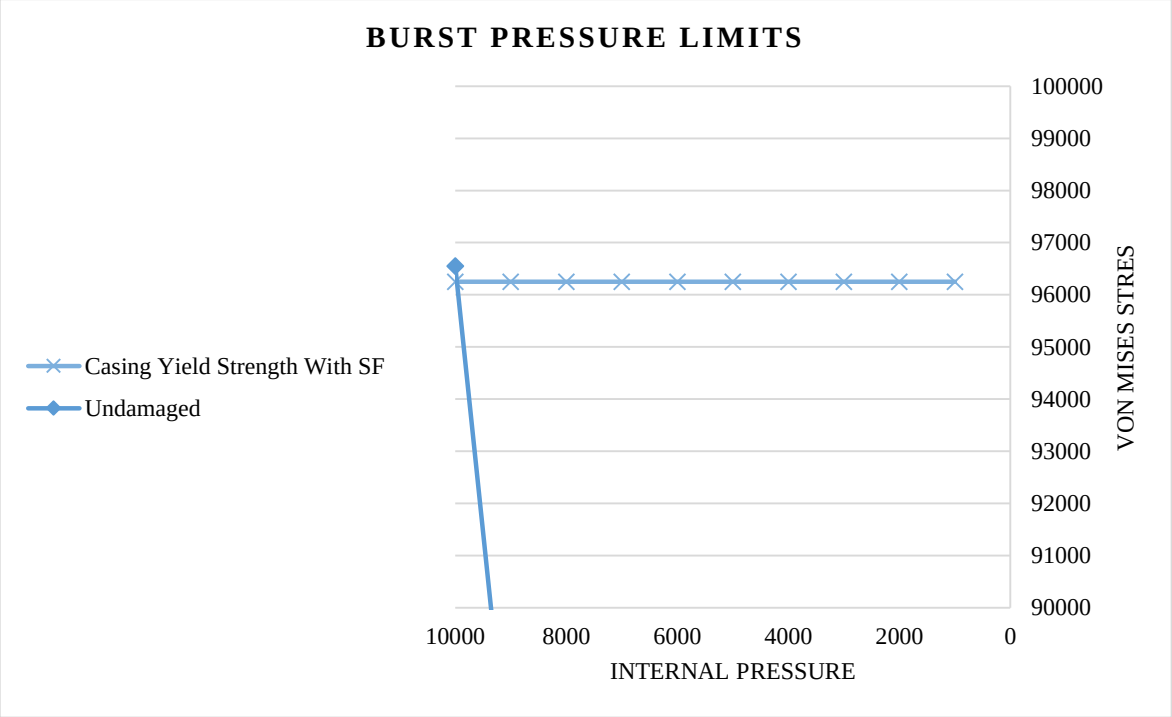

Figure 47. Internal pressure with Von Mises stress graph for 0% wear model

By the interpolation, the maximum internal pressure of the production casing before the material yields is 9470 psi (safety factor included).

5.1.1.1 Uniform Wear Model Comparison

Two models are made to examine the validity of the Finite Element Method (FEM) for the burst analysis on locally worn production casing. The first model is the undamaged reference production casing model and the second model is the 10% uniform wear production casing model. The FEM simulation results for both models are compared with the results from the API Burst/Barlow model for undamaged and 10% uniform wear model as shown in Table 13.

Table 13. Comparison between API Burst/Barlow and FEM Results

Wear Percentage	API Burst/Barlow	Simulated Results
0%	9440	9470
10%	8496	8540

The data presented in Table 13 show that there are similarities between the results of API Burst/Barlow model and the FEM model. It can be concluded that FEM is valid for the analysis of the burst scenario in the case of production casing.

5.1.2 Single Scar Scenario

5.1.2.1 Single Crescent-shaped Wear

The results of the simulations for single crescent-shaped wear in a production casing are presented in this section.

5.1.2.1.1 Single Crescent Wear (10% Wear Model)

For the 10% single crescent-shaped wear model, the maximum internal pressure before the production casing started to yield is 7344 psi. Compared to the reference model (0% wear), there is a reduction by 22% of the maximum internal pressure in the production casing.

5.1.2.1.2 Single Crescent Wear (30% Wear Model)

In the 30% single crescent-shaped wear model, the maximum internal pressure before the production casing material yielded is 3749 psi. The simulated result has a reduction of 60% compared to the undamaged reference model (0% wear).

5.1.2.1.3 Single Crescent Wear (45% Wear Model)

The result from the 45% single crescent wear model shows that the maximum internal yield pressure for the production casing is 2463 psi. This simulated result has a 74% reduction compared to the reference model (0% wear).

5.1.2.1.4 Burst Pressure Limits Results

Figure 48 presents the linear slopes for the wear percentages of the different internal pressures for all the simulated scenarios. The maximum internal yield pressure for the production casing decreases as the wear percentage increases. Table 14 shows the maximum internal yield pressure of the production casing for all simulated wear percentage scenarios, from 0% to 45%. The maximum internal yield pressure is obtained by solving the linear interpolation.

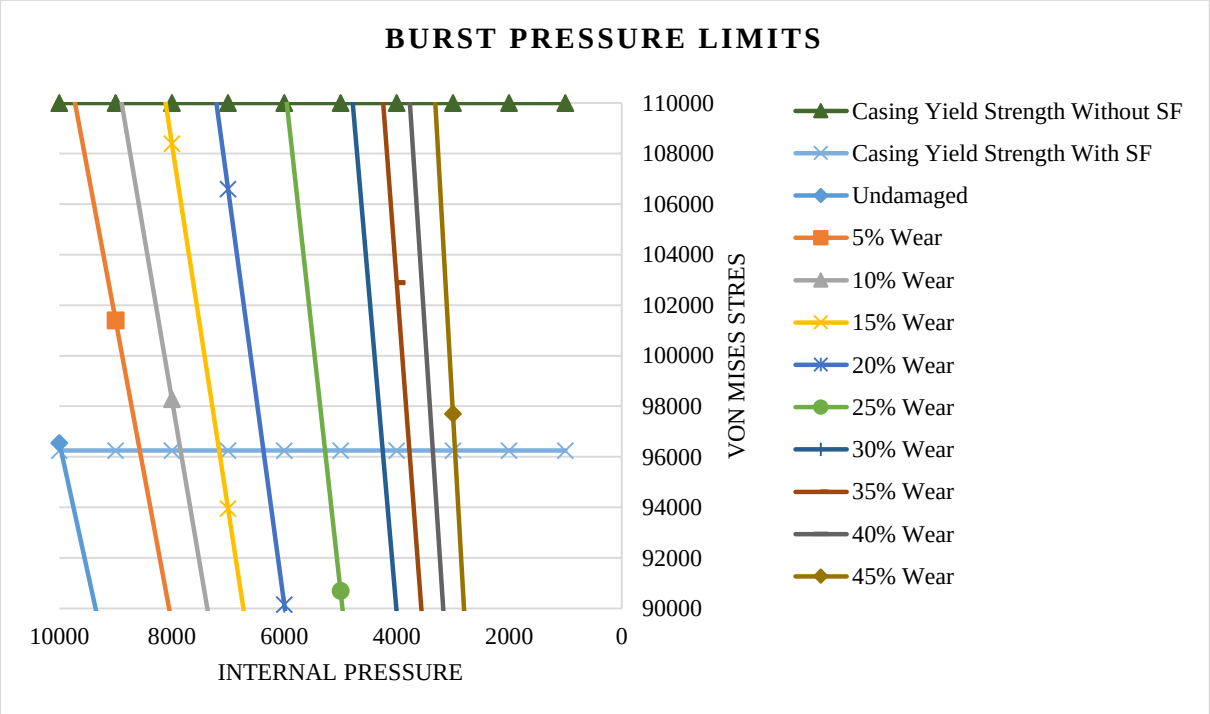

Figure 48. Internal pressure with respective Von Mises stress for different wear depths (single crescent-shaped wear model)

Table 14. Linear Interpolation for Maximum Internal Pressure

Wear (%)	Burst Pressure (psi)
0%	9470
5%	8067
10%	7344
15%	6662
20%	5869
25%	4775
30%	3749
35%	3275
40%	2858
45%	2463

Figure 49 presents the safe and failure zones for the maximum operating internal yield pressure. The area below the curve represents the safe zone, while the area above the curve is the failure zone. The burst pressure model developed from the simulation is also shown.

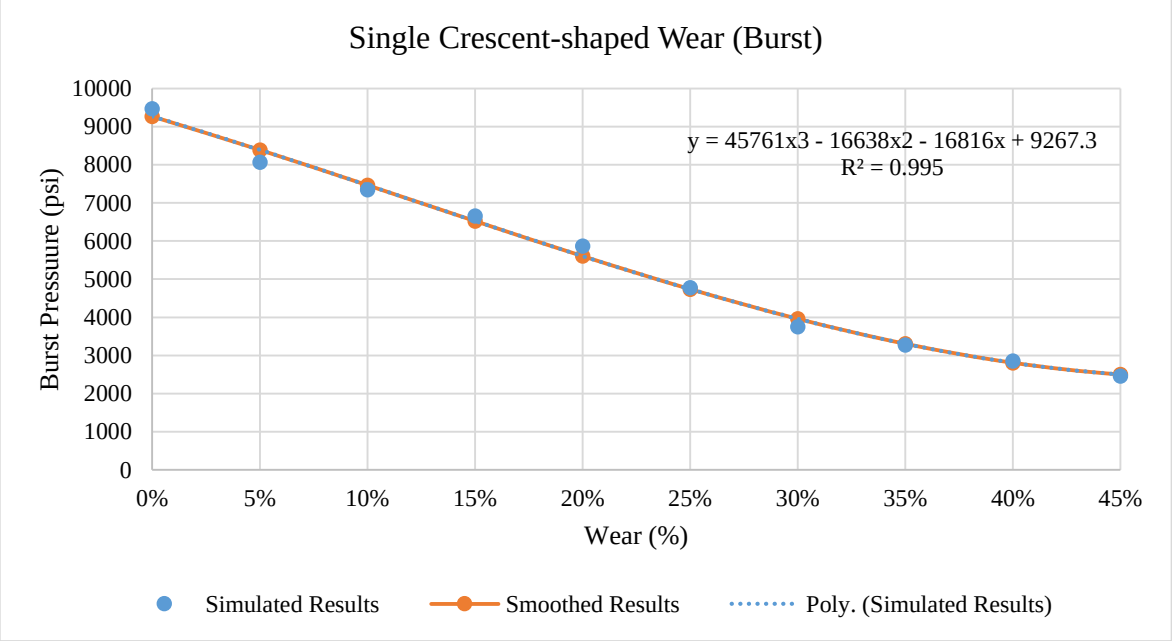

Figure 49. Safe and failure zones for maximum internal pressure on single crescent-shaped wear

The burst pressure model from the simulation is:

$$P_{burst} = 45761\ x\ Wear^3 - 16638\ x\ Wear^2 - 16816\ x\ Wear + 9267.3 \qquad (44)$$

The coefficient of determination of this model (R^2) is 0.995. This value suggests that the data from the simulation fit the statistical model. This simulated model already includes the safety factor. The comparison between the simulated model and the API Burst/Barlow model (Equation (37)) is presented in Figure 50.

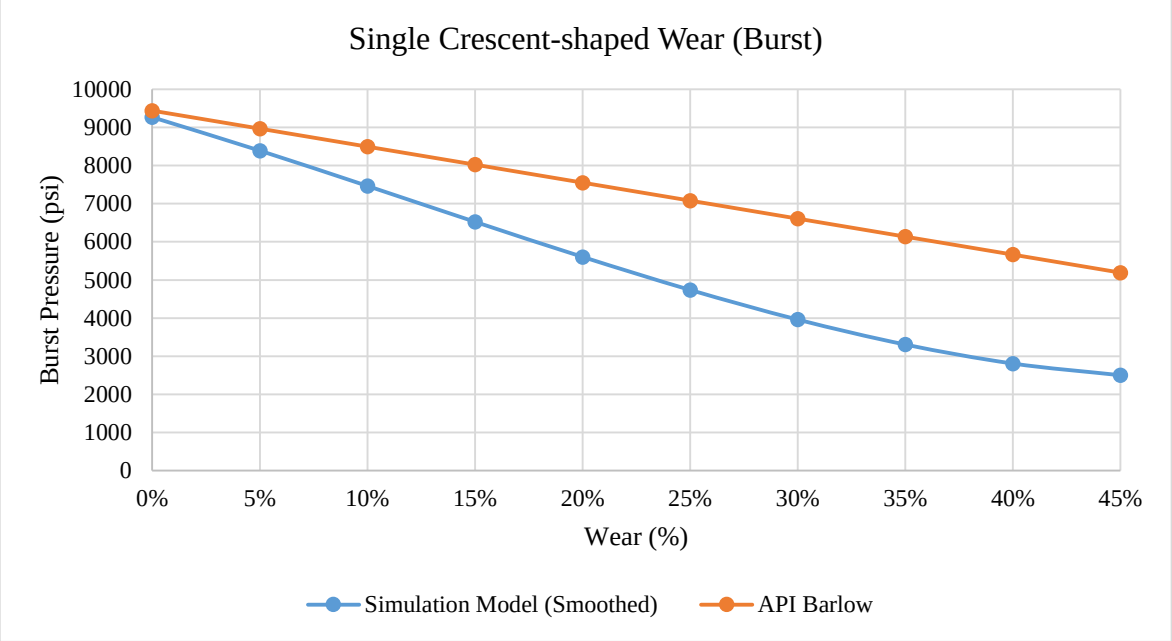

Figure 50. Comparison between API Burst/Barlow model and the simulation results

5.1.2.2 Single Wedge-shaped Wear

Wedge-shaped wear in production casing is divided based on three different wear widths: 0.2, 0.25, and 0.3 unit width.

5.1.2.2.1 Wedge-shaped 0.2 Width Wear

5.1.2.2.1.1 Wedge-shaped 0.2 Width Wear (10% Wear Model)

The result for the 10% wedge-shaped model shows that the maximum internal yield pressure for the production casing is 6823 psi. This simulated result is a 28% reduction from the reference model (0% wear).

5.1.2.2.1.2 Wedge-shaped 0.2 Width Wear (30% Wear Model)

For the 30% single wedge-shaped wear model, the maximum internal pressure before the production casing started to yield is 4859 psi. Compared to the reference model (0% wear), there is a reduction by 49% of the maximum internal pressure in the production casing.

5.1.2.2.1.3 Wedge-shaped 0.2 Width Wear (45% Wear Model)

In the 45% wedge-shaped wear model, the maximum internal pressure before the production casing material yielded is 3075 psi. The simulated result has a reduction of 68% compared to the undamaged reference model (0% wear).

5.1.2.2.1.4 Burst Pressure Limits Results

Figure 51 represents the linear slopes for the wear percentages of different internal pressures for all wedge-shaped 0.2 width scenarios. The maximum internal yield pressure for the production casing decreases as the wear percentage increases. Table 15 shows the maximum internal yield pressure of the production casing for all simulated wear percentage scenarios, from 0% to 45%. The maximum internal yield pressure is obtained by solving the linear interpolation.

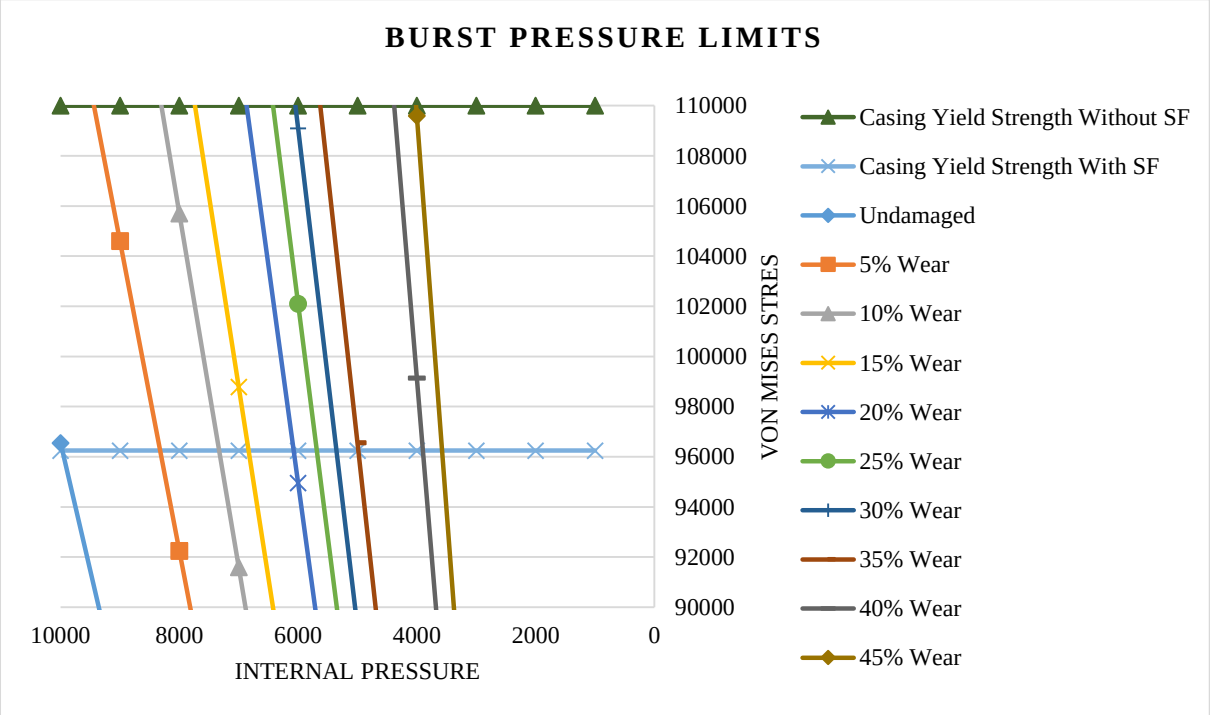

Figure 51. Internal pressure with respective Von Mises stress for different wear depths (0.2 width single wedge-shaped wear model)

Table 15. Linear Interpolation for Maximum Internal Pressure

Wear (%)	Burst Pressure (psi)
0%	9470
5%	7821
10%	6823
15%	6332
20%	5572
25%	5180
30%	4859
35%	4488
40%	3396
45%	3075

Figure 52 presents the safe and failure zones for the maximum operating internal yield pressure in the 0.2 width wedge-shaped scenario. The area below the curve represents the safe zone, while the area above the curve is the failure zone. The burst pressure model developed from the simulation is also shown.

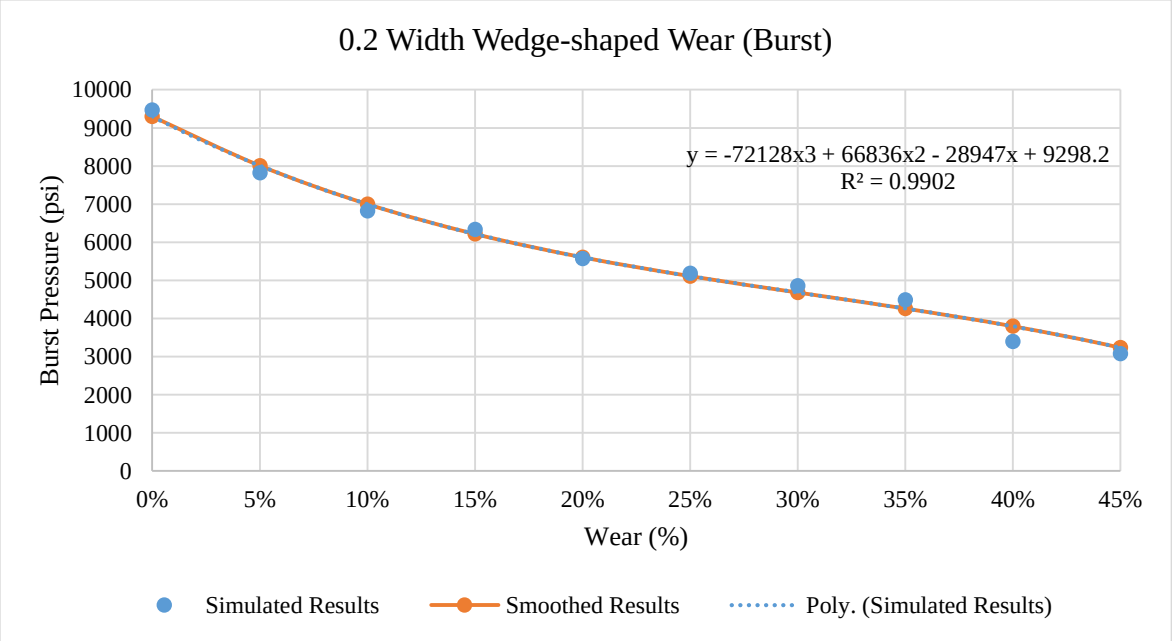

Figure 52. Safe and failure zones for maximum internal pressure on 0.2 width single wedge-shaped wear

The burst pressure model from the simulation is:

$$P_{burst} = -72128\ x\ Wear^3 + 66836\ x\ Wear^2 - 28947\ x\ Wear + 9298.2 \qquad (45)$$

The coefficient of determination of this model (R^2) is 0.9902. This value suggests that the data from the simulation fit the statistical model. This simulated model already includes the safety factor. Figure 53 shows a comparison of the simulated model with the API Burst/Barlow model.

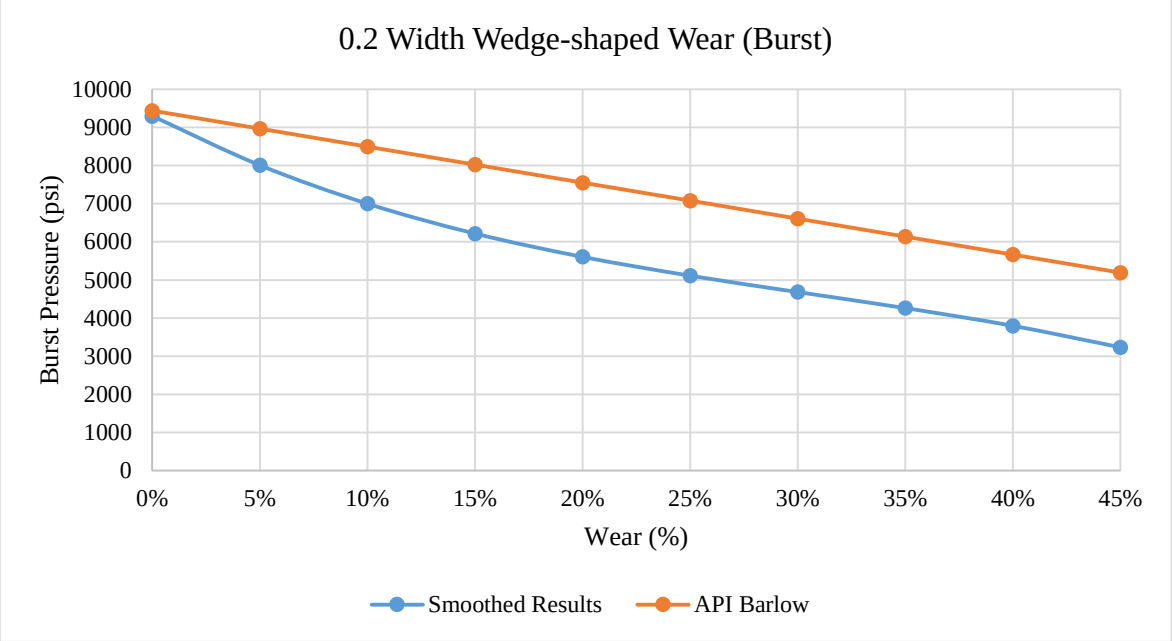

Figure 53. Comparison between API Burst/Barlow model and the simulation results

5.1.2.2.2 Wedge-shaped 0.25 Width Wear

5.1.2.2.2.1 Wedge-shaped 0.25 Width Wear (10% Wear Model)

The result from the 10% single wedge-shaped model shows that the maximum internal yield pressure for the production casing is 6446 psi. This simulated result is a 32% reduction from the reference model (0% wear).

5.1.2.2.2.2 Wedge-shaped 0.25 Width Wear (30% Wear Model)

For the 30% single wedge-shaped wear model, the maximum internal pressure before the production casing started to yield is 4429 psi. Compared to the reference model (0% wear), there is a reduction by 53% of the maximum internal pressure in the production casing.

5.1.2.2.2.3 Wedge-shaped 0.25 Width Wear (45% Wear Model)

In the 45% single wedge-shaped wear model, the maximum internal pressure before the production casing material yielded is 2888 psi. The simulated result has a reduction of 70% compared to the undamaged reference model (0% wear).

5.1.2.2.2.4 Burst Pressure Limits Results

Figure 54 presents the linear slopes for the wear percentages of the different internal pressure for all wedge-shaped 0.25 width scenarios. The maximum internal yield pressure for the production casing decreases as the wear percentage increases. Table 16 shows the maximum internal yield pressure of the production casing for all simulated wear percentage scenarios, from 0% to 45%. The maximum internal yield pressure is obtained by solving the linear interpolation.

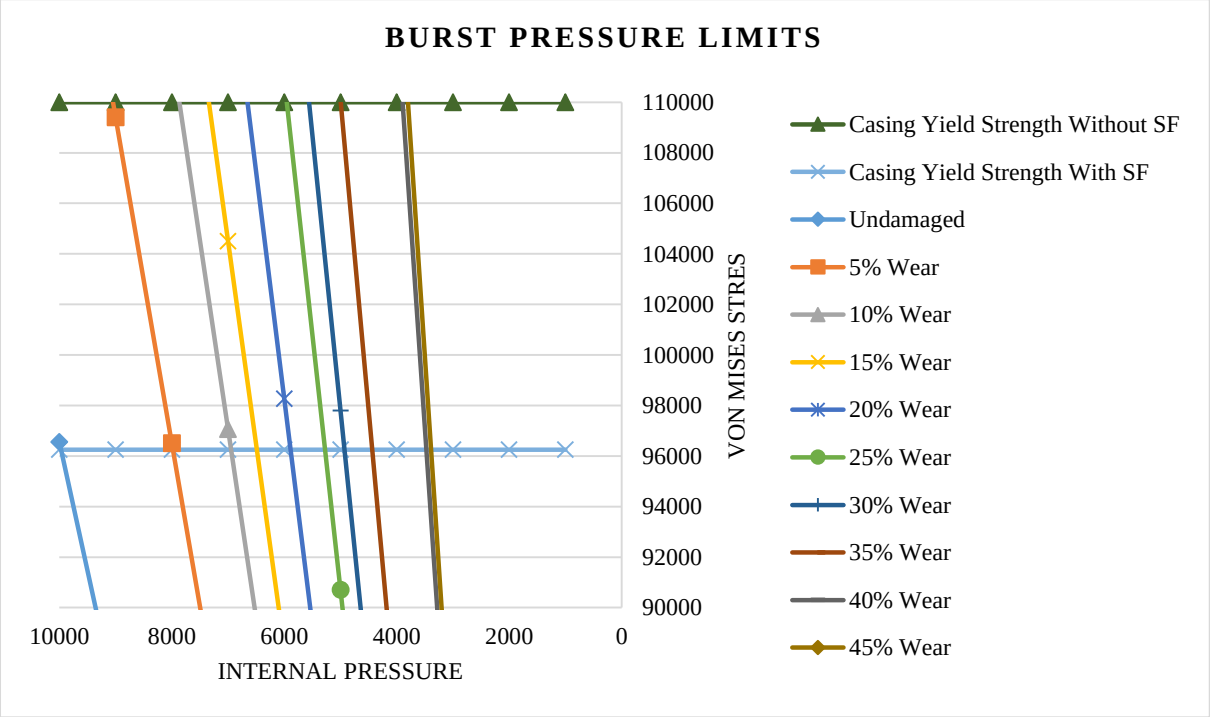

Figure 54. Internal pressure with respective Von Mises stress for different wear depths (0.25 width single wedge-shaped wear model)

Table 16. Linear Interpolation for Maximum Internal Pressure

Wear (%)	Burst Pressure (psi)
0%	9470
5%	7481
10%	6446
15%	5988
20%	5388
25%	4770
30%	4429
35%	3941
40%	2972
45%	2888

Figure 55 presents the safe and failure zones for the maximum operating internal yield pressure in the 0.25 width wedge-shaped scenario. The area below the curve represents the safe zone, while the area above the curve is the failure zone. The burst pressure model developed from the simulation is also shown.

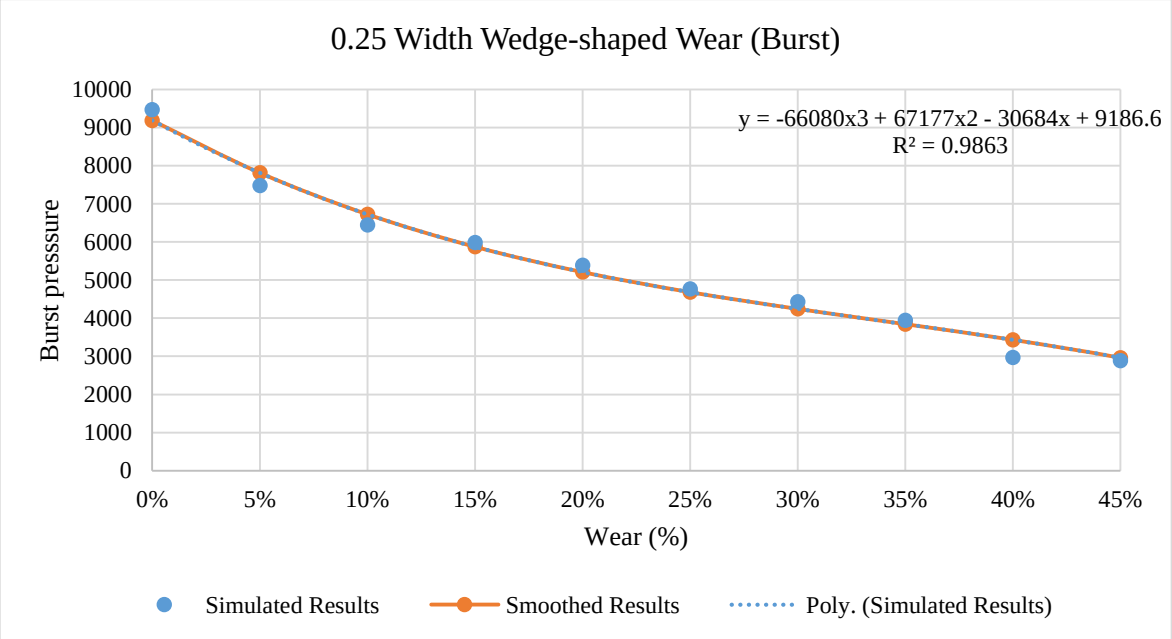

Figure 55. Safe and failure zones for maximum internal pressure on 0.25 width single wedge-shaped wear

The burst pressure model from the simulation is:

$$P_{burst} = -66080\ x\ Wear^3 + 67177\ x\ Wear^{\ 2} - 30684\ x\ Wear + 9186.6 \qquad (46)$$

The coefficient of determination of this model (R^2) is 0.9863. This value suggests that the data from the simulation fit the statistical model. This simulated model already includes the safety factor. Figure 56 shows the comparison between the simulated model and the API Burst/Barlow model.

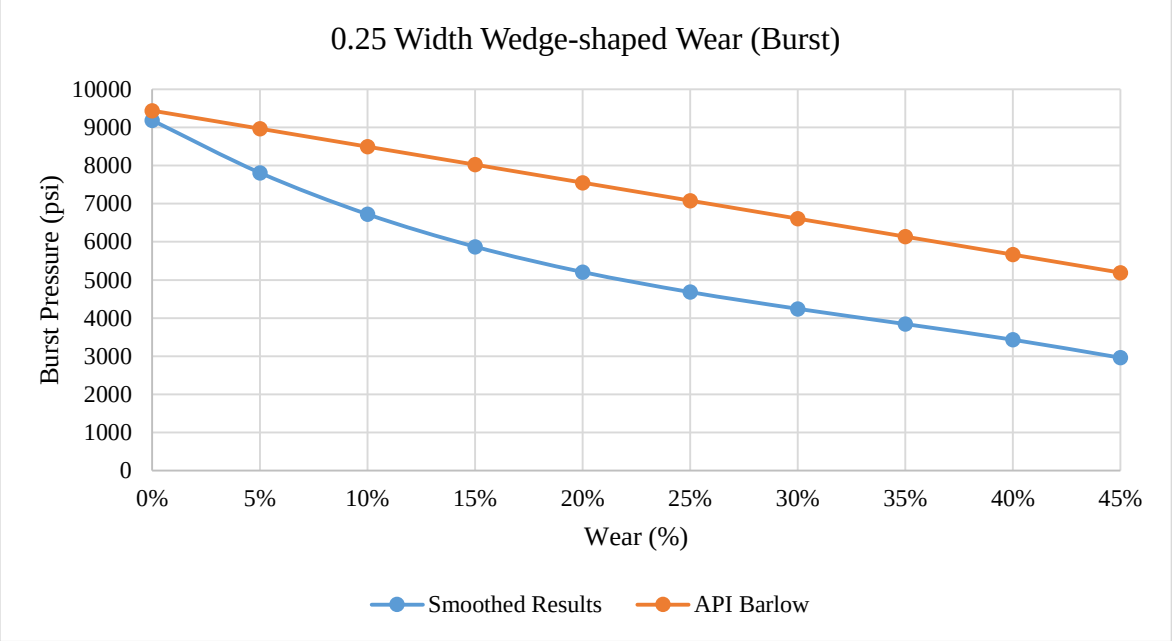

Figure 56. Comparison between API Burst/Barlow model and the simulation results

5.1.2.2.3 Wedge-shaped 0.3 Width Wear

5.1.2.2.3.1 Wedge-shaped 0.3 Width Wear (10% Wear Model)

The result from the 10% wedge-shaped 0.3 width model shows that the maximum internal yield pressure for the production casing is 6383 psi. This simulated result is a 33% reduction from the reference model (0% wear).

5.1.2.2.3.2 Wedge-shaped 0.3 Width Wear (30% Wear Model)

For the 30% single wedge-shaped wear model, the maximum internal pressure before the production casing started to yield is 3945 psi. Compared to the reference model (0% wear), there is a reduction by 58% of the maximum internal pressure in the production casing.

5.1.2.2.3.3 Wedge-shaped 0.3 Width Wear (45% Wear Model)

In the 45% single crescent wear model, the maximum internal pressure before the production casing material yielded is 2596 psi. The simulated result has a reduction of 73% compared to the reference model (0% wear).

5.1.2.2.3.4 Burst Pressure Limits Results

Figure 57 represents the linear slopes for the wear percentages of the different internal pressures for all wedge-shaped 0.3 width scenarios. The maximum internal yield pressure for the production casing decreases as the wear percentage increases. Table 17 shows the maximum internal yield pressure of the production casing for all simulated wear percentage scenarios, from 0% to 45%. The maximum internal yield pressure is obtained by solving the linear interpolation.

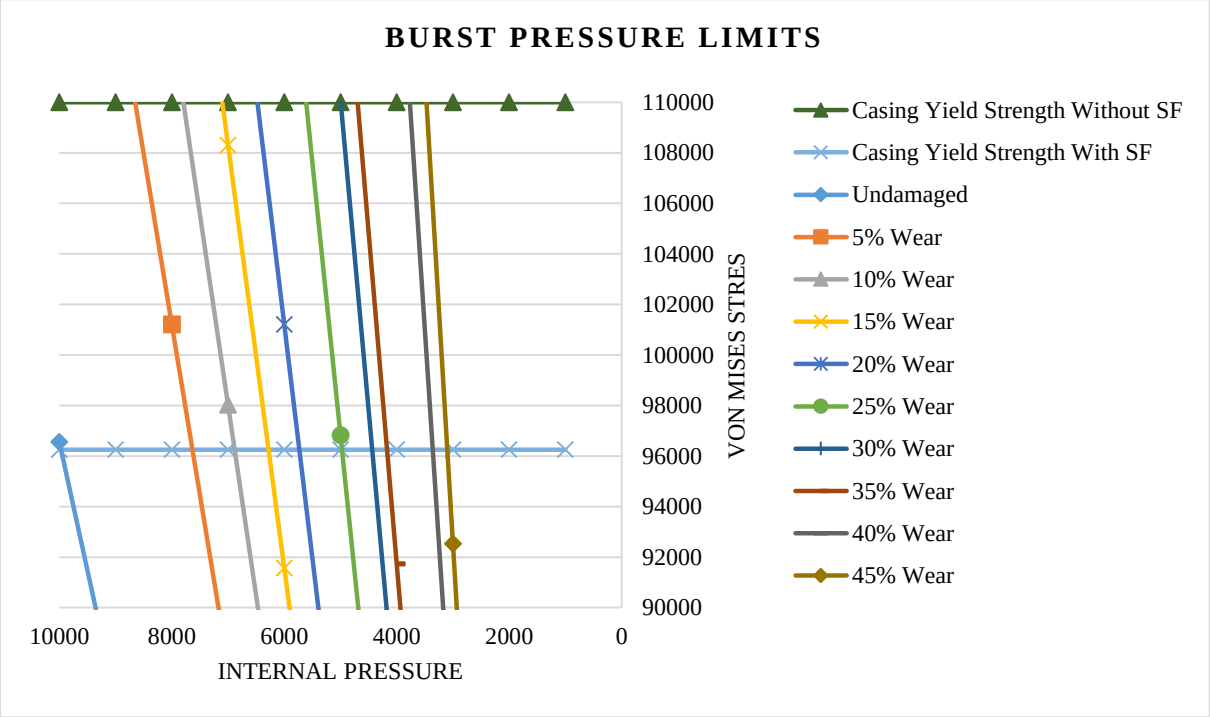

Figure 57. Internal pressure with respective Von Mises stress for different wear depths (0.3 width single wedge-shaped wear model)

Table 17. Linear Interpolation for Maximum Internal Pressure

Wear (%)	Burst Pressure (psi)
0%	9470
5%	7133
10%	6383
15%	5778
20%	5231
25%	4460
30%	3945
35%	3673
40%	2859
45%	2596

Figure 58 presents the safe and failure zones for the maximum operating internal yield pressure in the 0.3 width wedge-shaped scenario. The area below the curve represents the safe zone, while the area above the curve is the failure zone. The burst pressure model developed from the simulation is also shown.

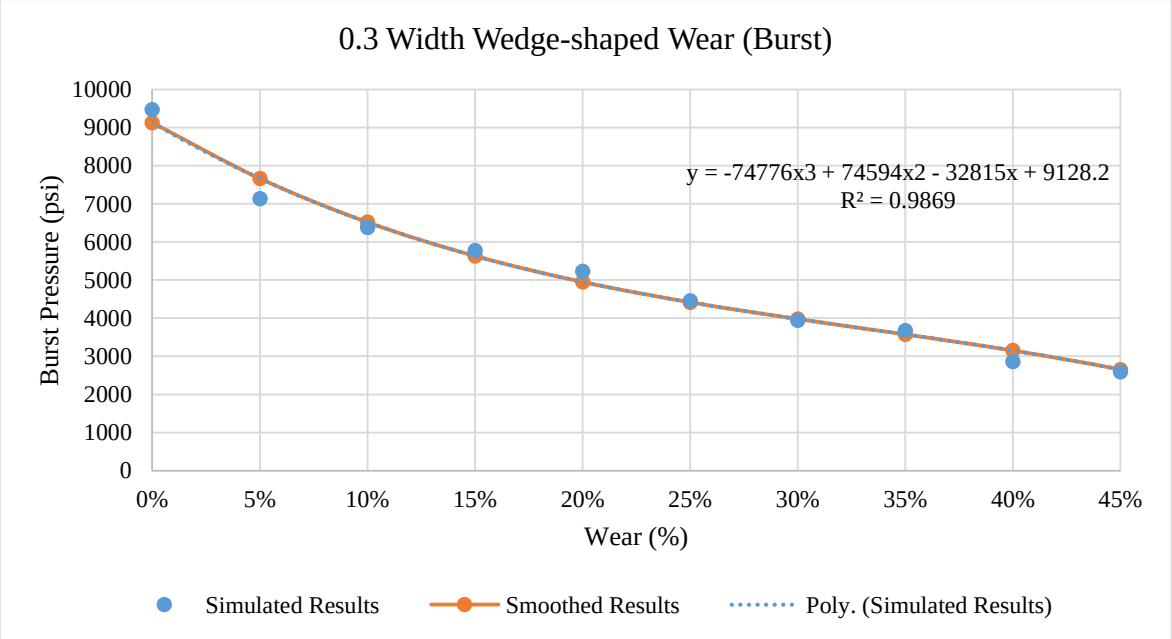

Figure 58. Safe and failure zones for maximum internal pressure on 0.3 width single wedge-shaped wear

The burst pressure model from the simulation is:

$$P_{burst} = -74766\ x\ Wear^3 + 74594\ x\ Wear^{\ 2} - 32815\ x\ Wear + 9128.2 \qquad (47)$$

The coefficient of determination of this model (R^2) is 0.9869. This value suggests that the data from the simulation fits the statistical model. This simulated model already includes the safety factor. Figure 59 shows the comparison between the simulated model and the API Burst/Barlow model.

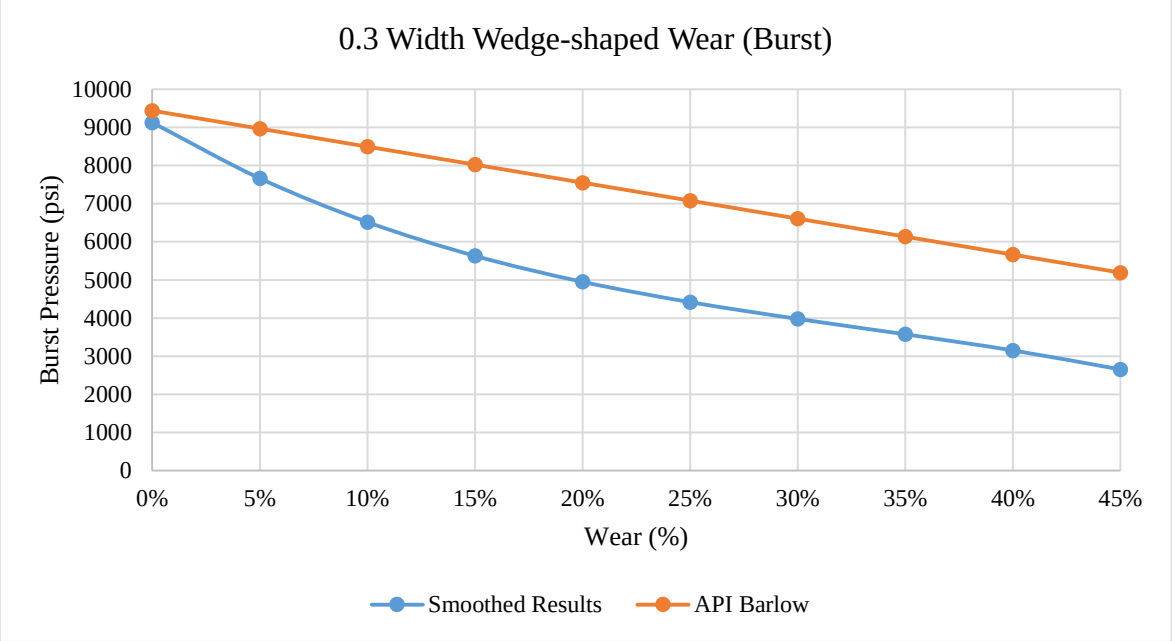

Figure 59. Comparison between API Burst/Barlow model and the simulation results

5.1.3 Double Scars Scenario (Model 1)

The modelling of scars in the production casing is divided into two types: model 1 with both scars on the internal part of the production casing, and model 2 with one scar located on the internal part of the production casing and one scar located on the external part of the production casing.

5.1.3.1 Double Crescent-shaped Wear (Model 1)

5.1.3.1.1 Double Crescent-shaped Wear (10% Wear Model)

For the 10% double crescent-shaped wear model, the maximum internal pressure before the production casing started to yield is 7092 psi. Compared to the reference model (0% wear), there is a reduction by 25% of the maximum internal pressure in the production casing.

5.1.3.1.2 Double Crescent-shaped Wear (30% Wear Model)

In the 30% double crescent-shaped wear model, the maximum internal pressure before the production casing material yielded is 3434 psi. The simulated result has reduction of 64% compared to the undamaged reference model (0% wear).

5.1.3.1.3 Double Crescent-shaped Wear (45% Wear Model)

The result from the 45% double crescent-shaped wear model shows that the maximum internal yield pressure for the production casing is 2339 psi. This simulated result is a 75% reduction from the reference model (0% wear).

5.1.3.1.4 Burst Pressure Limits Results

Figure 60 represents the linear slopes for the wear percentages of the different internal pressures for all simulated scenarios. The maximum internal yield pressure for the production casing decreases as the wear percentage increases. Table 18 shows the maximum internal yield pressure of the production casing for all simulated wear percentage scenarios, from 0% to 45%. The maximum internal yield pressure is obtained by solving the linear interpolation.

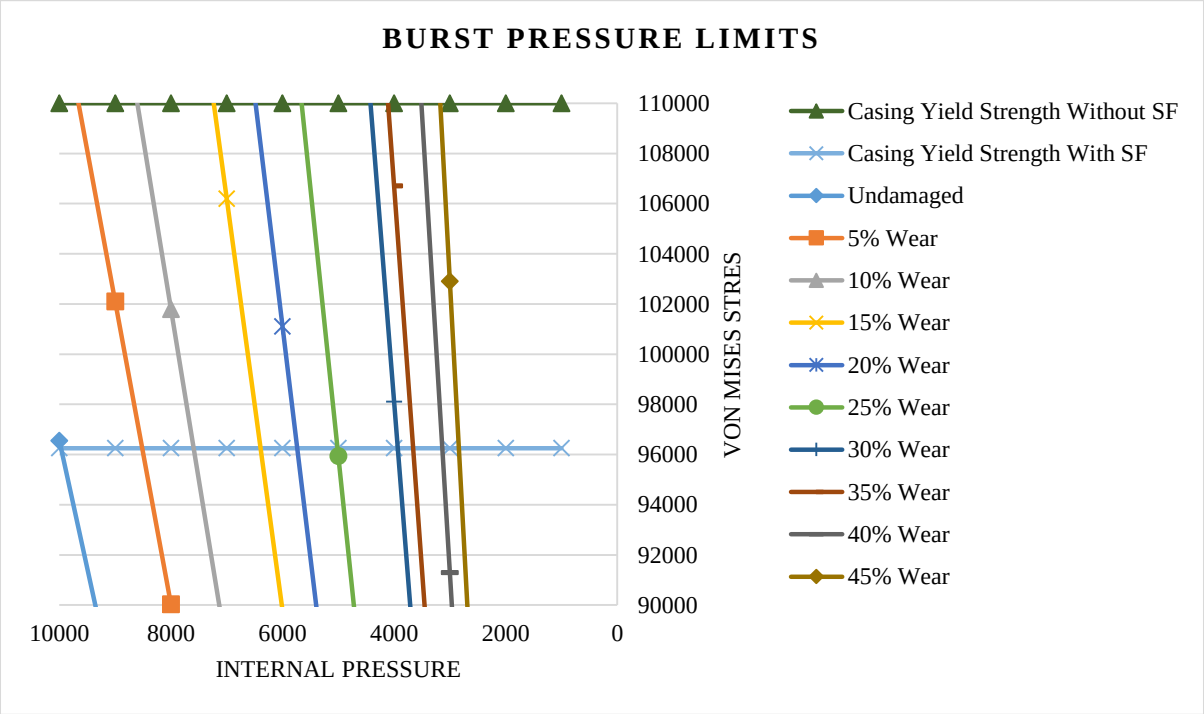

Figure 60. Internal pressure with respective Von Mises stress for different wear depths (double crescent-shaped wear model)

Table 18. Linear Interpolation for Maximum Internal Pressure

Wear (%)	Burst Pressure (psi)
0%	9470
5%	8013
10%	7092
15%	5890
20%	5236
25%	4515
30%	3434
35%	3157
40%	2635
45%	2339

Figure 61 shows the safe and failure zones for the maximum operating internal yield pressure. The area below the curve represents the safe zones, while the area above the curve is the failure zone. The burst pressure model developed from the simulation is also shown.

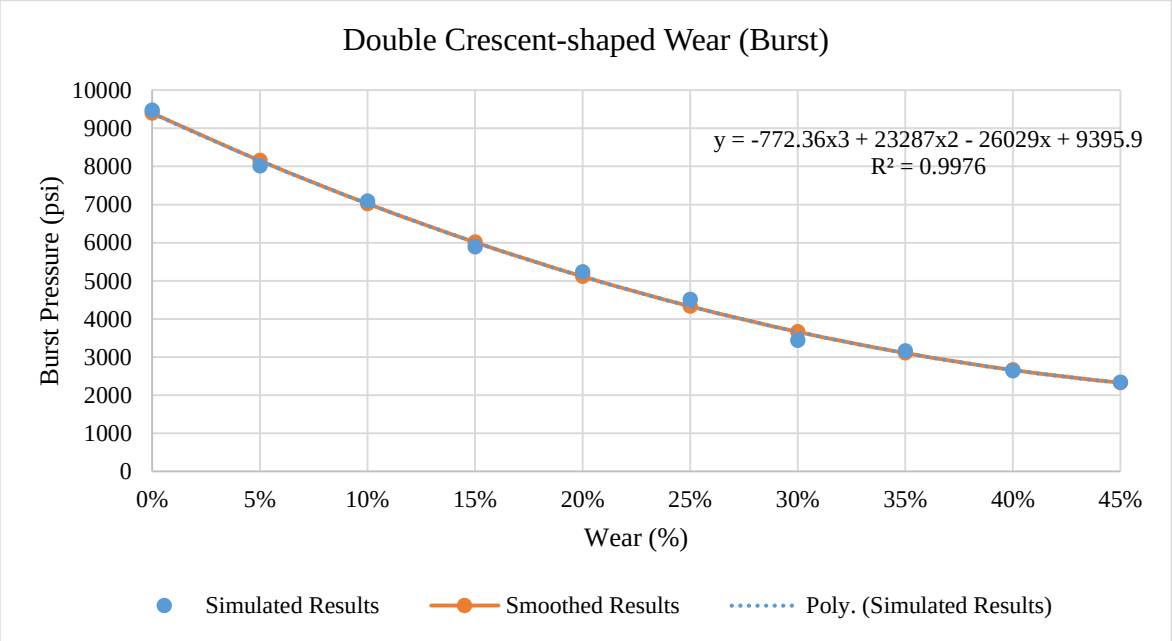

Figure 61. Safe and failure zones for maximum internal pressure on double crescent-shaped wear

The burst pressure model from the simulation is:

$$P_{burst} = -772.36\ x\ Wear^3 + 23287\ x\ Wear^2 - 26029\ x\ Wear + 9395.9 \qquad (48)$$

The coefficient of determination of this model (R^2) is 0.9976. This value suggests that the data from the simulation fit the statistical model. This simulated model already includes the safety factor. Figure 62 presents the comparison between the simulated model and the API Burst/Barlow model.

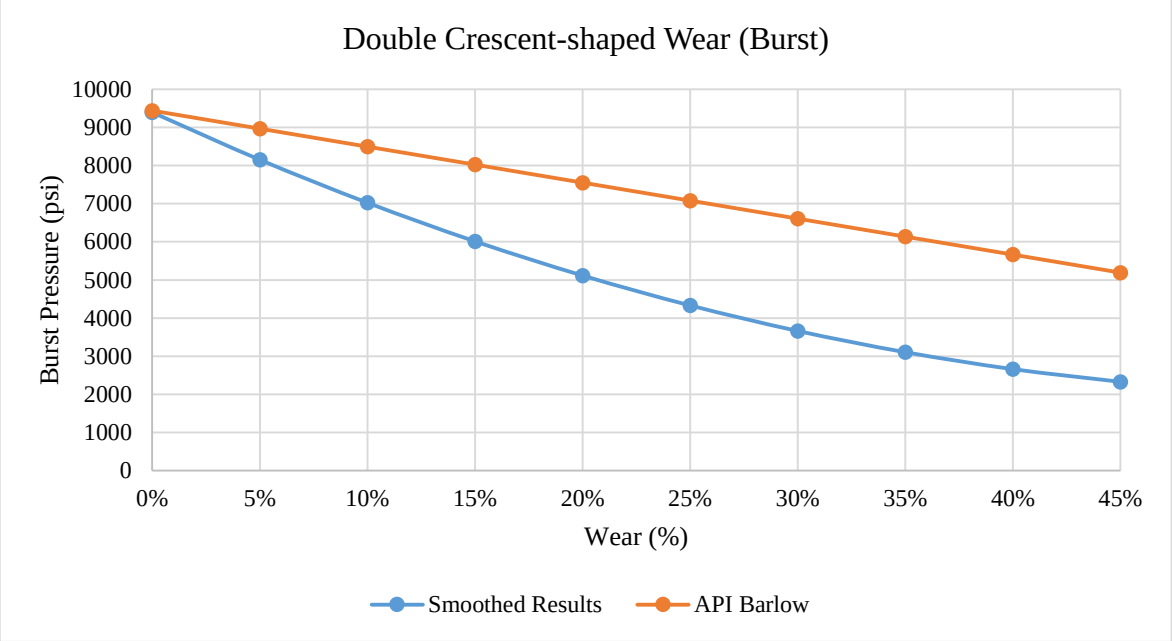

Figure 62. Comparison between API Burst/Barlow model and the simulation results

5.1.3.2 Double Wedge-shaped Wear

5.1.3.2.1 Double Wedge-shaped Wear (10% Wear Model)

For the 10% double wedge-shaped wear model, the maximum internal pressure before the production casing started to yield is 5590 psi. Compared to the reference model (0% wear), there is a reduction by 41% of the maximum internal pressure in the production casing.

5.1.3.2.2 Double Wedge-shaped Wear (30% Wear Model)

The simulation result for the 30% double wedges wear model has a reduction of 63% from the undamaged reference model (0% wear). The maximum internal pressure before the production casing material yielded from the simulation is measured at 3476 psi

5.1.3.2.3 Double Wedge-shaped Wear (45% Wear Model)

The result for the 45% double wedges wear model shows that the maximum internal yield pressure for the production casing is 2286 psi. This simulated result is a 76% reduction from the reference model (0% wear).

5.1.3.2.4 Burst Pressure Limits Results

Figure 63 represents the linear slopes for the wear percentages of the different internal pressures for all simulated scenarios. The maximum internal yield pressure for the production casing decreases as the wear percentage increases. Table 19 presents the maximum internal yield pressure of the production casing for all simulated wear percentage scenarios, from 0% to 45%. The maximum internal yield pressure is obtained by solving the linear interpolation.

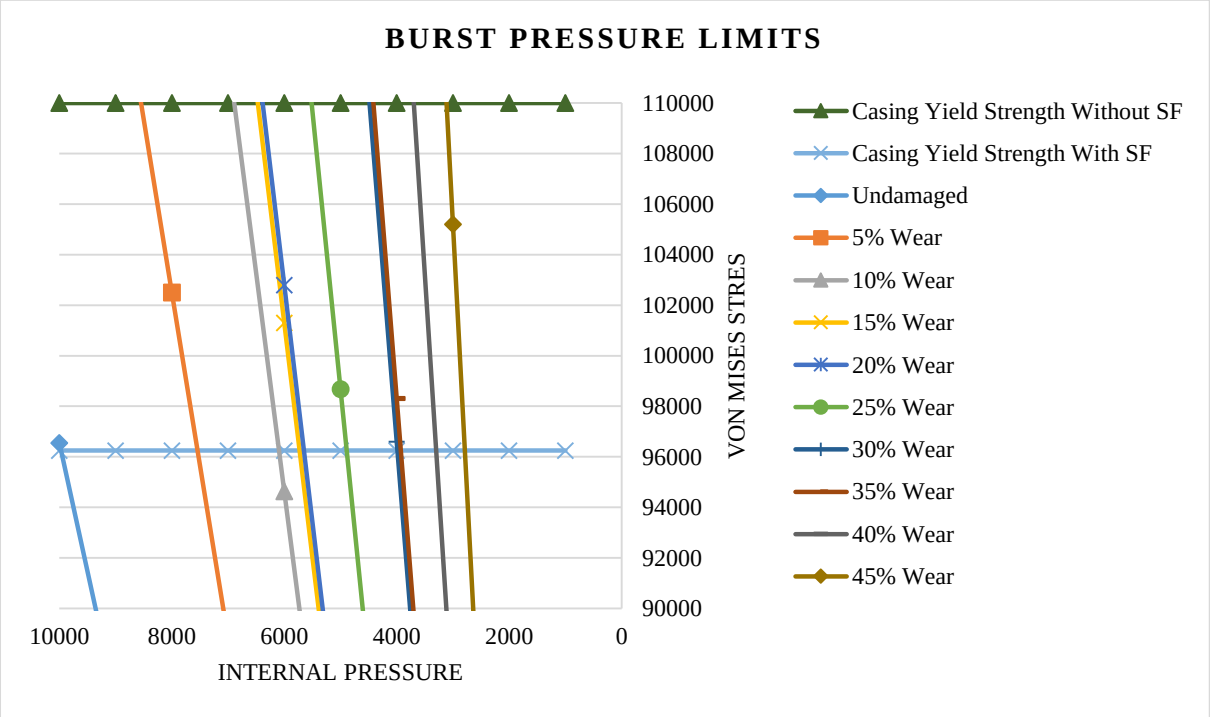

Figure 63. Internal pressure with respective Von Mises stress for different wear depths (double wedge-shaped wear model)

Table 19. Linear Interpolation for Maximum Internal Pressure

Wear (%)	Burst Pressure (psi)
0%	9470
5%	7044
10%	5590
15%	5227
20%	5150
25%	4389
30%	3476
35%	3431
40%	2797
45%	2286

Figure 64 presents the safe and failure zones for the maximum operating internal yield pressure. The area below the curve represents the safe zone, while the area above the curve is the failure zone. The burst pressure model developed from the simulation is also shown.

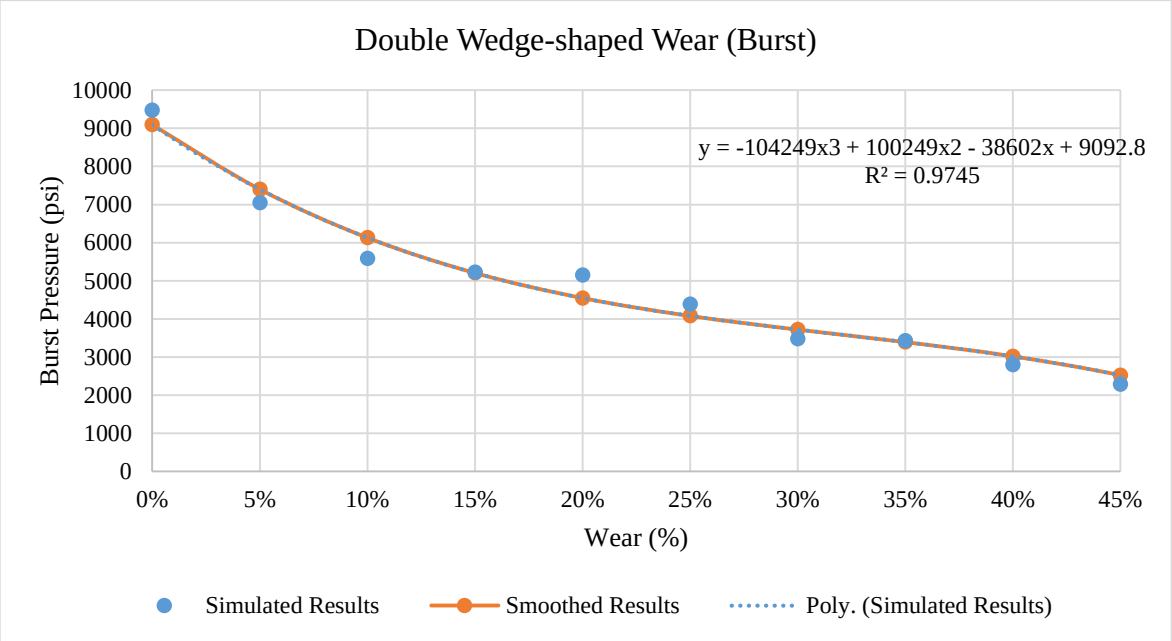

Figure 64. Safe and failure zones for maximum internal pressure on double wedge-shaped wear

The burst pressure model from the simulation is:

$$P_{burst} = -104249\ x\ Wear^3 + 100249\ x\ Wear^{\ 2} - 38602\ x\ Wear + 9092.8 \qquad (49)$$

The coefficient of determination of this model (R^2) is 0.9745. This value suggests that the data from the simulation fit the statistical model. This simulated model already includes the safety factor. Figure 65 shows the comparison between the simulated model and the API Burst/Barlow model.

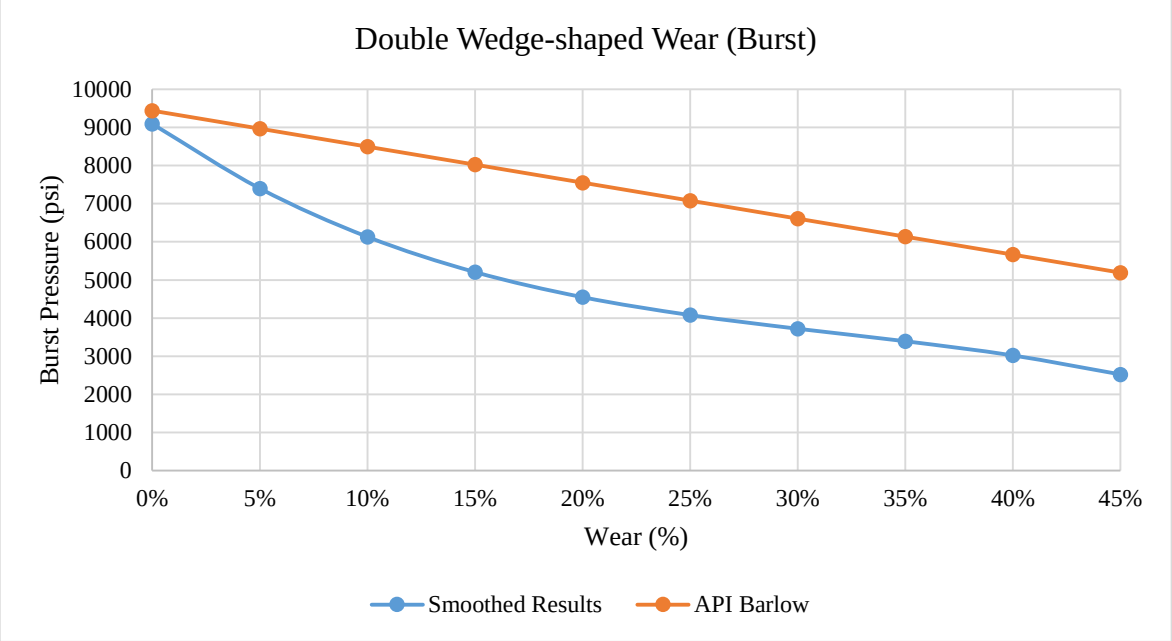

Figure 65. Comparison between API Burst/Barlow model and the simulation results

5.1.4 Double Scars Scenario (Model 2)

5.1.4.1 Wedge-shaped Wear (inside) and Crescent-shaped Wear (outside)

5.1.4.1.1 Wedge-shaped Wear (inside) and Crescent-shaped Wear (outside) (10% Wear Model)

The result from the 10% wear model shows that the maximum internal yield pressure for the production casing is 6283 psi. This simulated result is a 34% reduction from the reference model (0% wear).

5.1.4.1.2 Wedge-shaped Wear (inside) and Crescent-shaped Wear (outside) (30% Wear Model)

For the 30% wear model, the maximum internal pressure before the production casing started to yield is 4198 psi. Compared to the reference model (0% wear), there is a reduction by 56% of the maximum internal pressure in the production casing.

5.1.4.1.3 Wedge-shaped Wear (inside) and Crescent-shaped Wear (outside) (45% Wear Model)

In the 45% wear model, the maximum internal pressure before the production casing material yielded is 2436 psi. The simulated result is a reduction of 74% from the undamaged reference model (0% wear).

5.1.4.1.4 Burst Pressure Limits Results

Figure 66 represents the linear slopes for the wear percentages of the different internal pressures for all simulated scenarios. The maximum internal yield pressure for the production casing decreases as the wear percentage increases. The maximum internal yield pressure of the production casing for all simulated wear percentage scenarios from 0% to 45% are shown in Table 20. The maximum internal yield pressure is obtained by solving the linear interpolation.

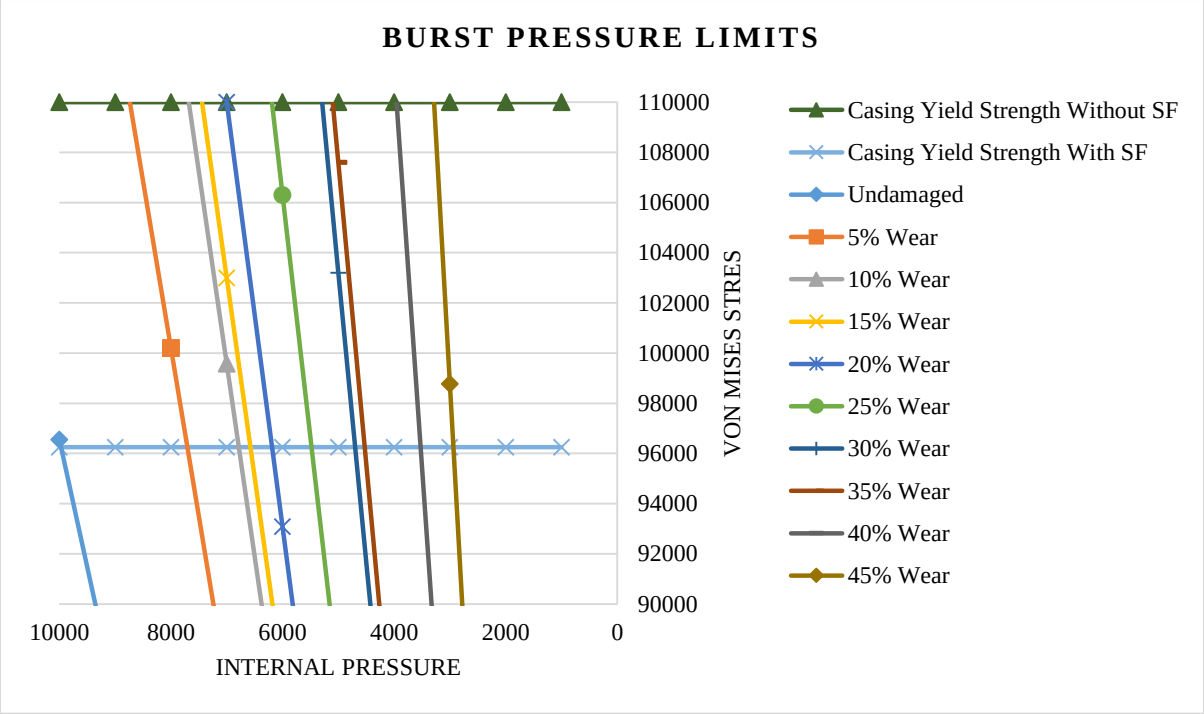

Figure 66. Internal pressure with respective Von Mises stress for different wear depths (mixed-shape wear model)

Table 20. Linear Interpolation for Maximum Internal Pressure

Wear (%)	Burst Pressure (psi)
0%	9470
5%	7203
10%	6283
15%	6073
20%	5687
25%	4969
30%	4198
35%	4021
40%	3022
45%	2436

Figure 67 shows the safe and failure zones for the maximum operating internal yield pressure. The area below the curve represents the safe zone, while the area above the curve is the failure zone. The burst pressure model developed from the simulation is also shown.

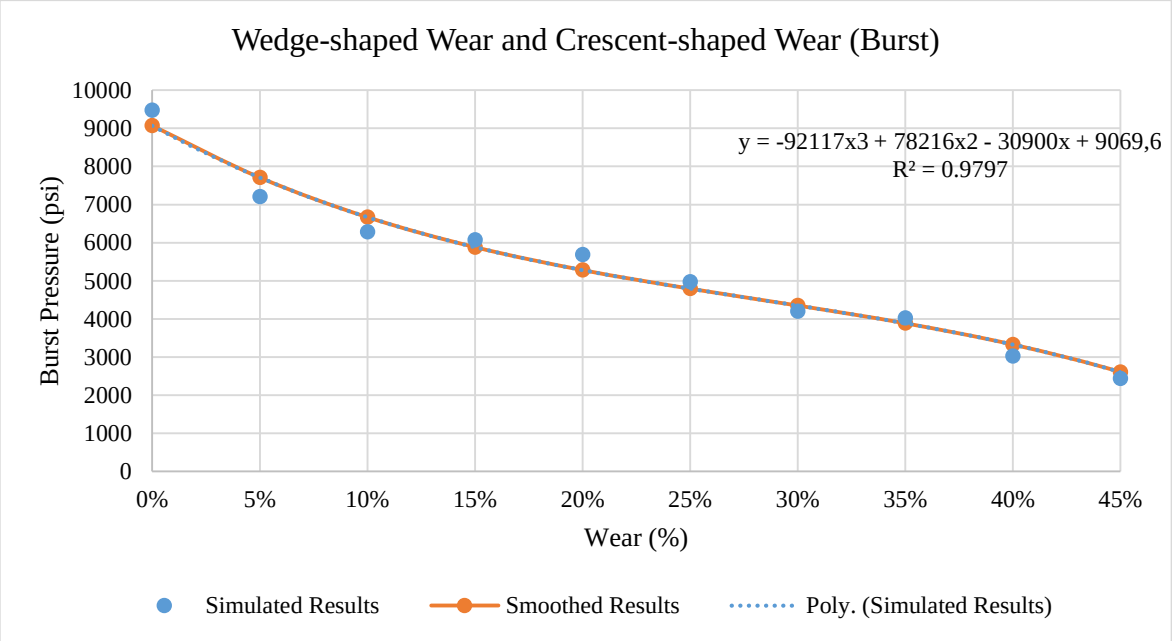

Figure 67. Safe and failure zones for maximum internal pressure on mixed-shape wear

The burst pressure model from the simulation is:

$$P_{burst} = -92117\ x\ Wear^3 + 78216\ x\ Wear^{\,2} - 30900\ x\ Wear + 9069.6 \qquad (50)$$

The coefficient of determination of this model (R^2) is 0.9797. This value suggests that the data from the simulation fit the statistical model. This simulated model already includes the safety factor. Figure 68 presents the comparison between simulated model and the API Burst/Barlow model.

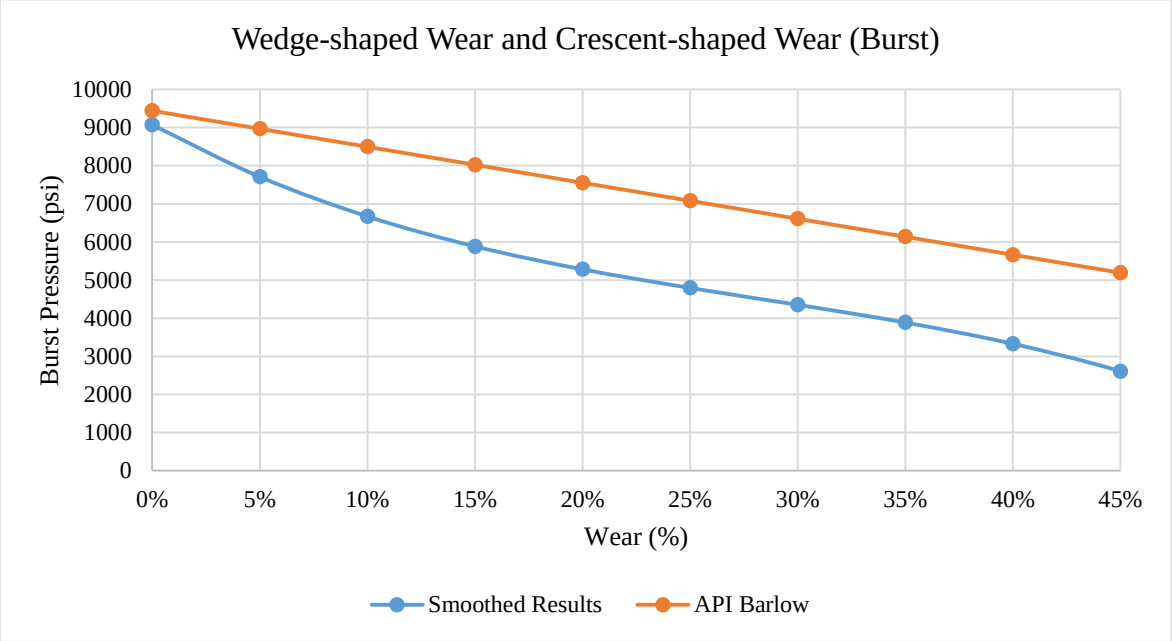

Figure 68. Comparison between API Burst/Barlow model and the simulation results

5.1.4.2 Crescent-shaped Wear (inside) and Wedge-shaped Wear (outside)

5.1.4.2.1 Crescent-shaped Wear (inside) and Wedge-shaped Wear (outside) (10% Wear Model)

The result from the 10% wear model shows that the maximum internal yield pressure for the production casing is 5920 psi. This simulated result is a 37% reduction from the reference model (0% wear).

5.1.4.2.2 Crescent-shaped Wear (inside) and Wedge-shaped Wear (outside) (30% Wear Model)

For the 30% wear model, the maximum internal pressure before the production casing started to yield is 3778 psi. Compared to the reference model (0% wear), there is a reduction by 60% of the maximum internal pressure in the production casing.

5.1.4.2.3 Crescent-shaped Wear (inside) and Wedge-shaped Wear (outside) (45% Wear Model)

In the 45% wear model, the maximum internal pressure before the production casing material yielded is 2421 psi. The simulated result has a reduction of 74% compared to the undamaged reference model (0% wear).

5.1.4.2.4 Burst Pressure Limits Results

Figure 69 shows the linear slopes for the wear percentages of the different internal pressures for all simulated scenarios. The maximum internal yield pressure for the production casing decreases as the wear percentage increases. Table 21 presents the maximum internal yield pressure of the production casing for all simulated wear percentage scenarios, from 0% to 45%. The maximum internal yield pressure is obtained by solving the linear interpolation.

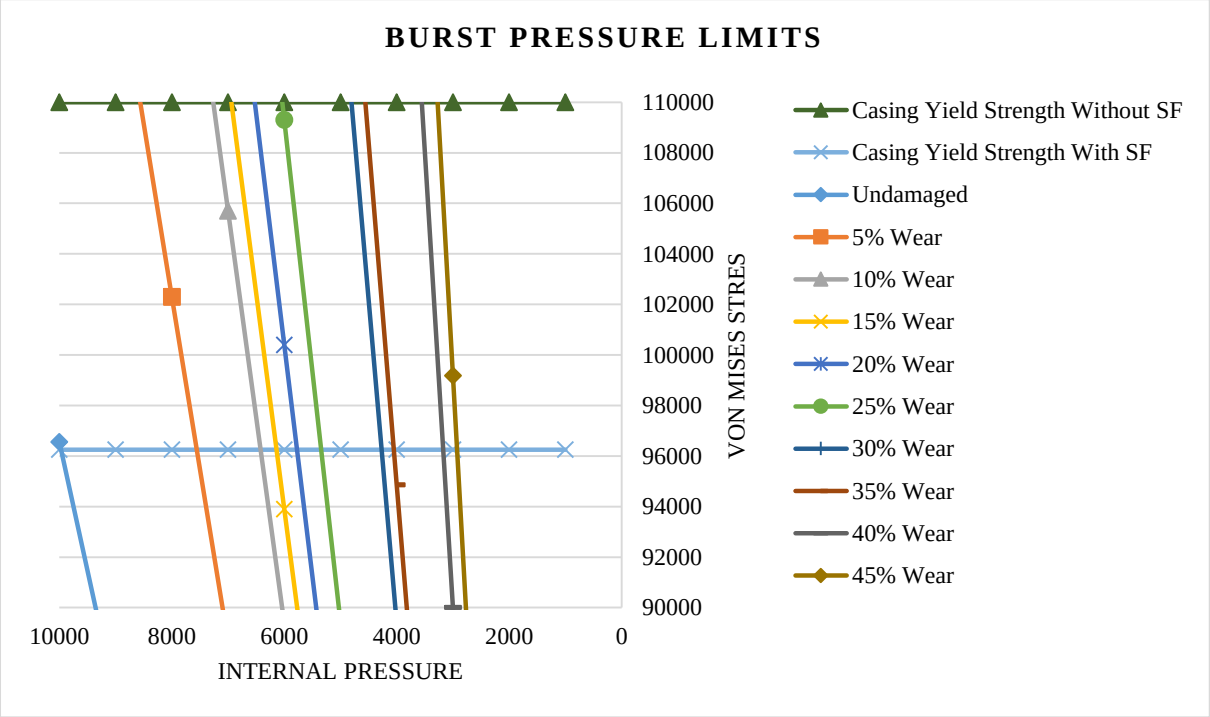

Figure 69. Internal pressure with respective Von Mises stress for different wear depths (mixed-shape wear model)

Table 21. Linear Interpolation for Maximum Internal Pressure

Wear (%)	Burst Pressure (psi)
0%	9470
5%	7058
10%	5920
15%	5637
20%	5273
25%	4839
30%	3778
35%	3542
40%	2673
45%	2421

Figure 70 presents the safe and failure zones for the maximum operating internal yield pressure. The area below the curve represents the safe zone, while the area above the curve is the failure zone. The burst pressure model developed from the simulation is also shown.

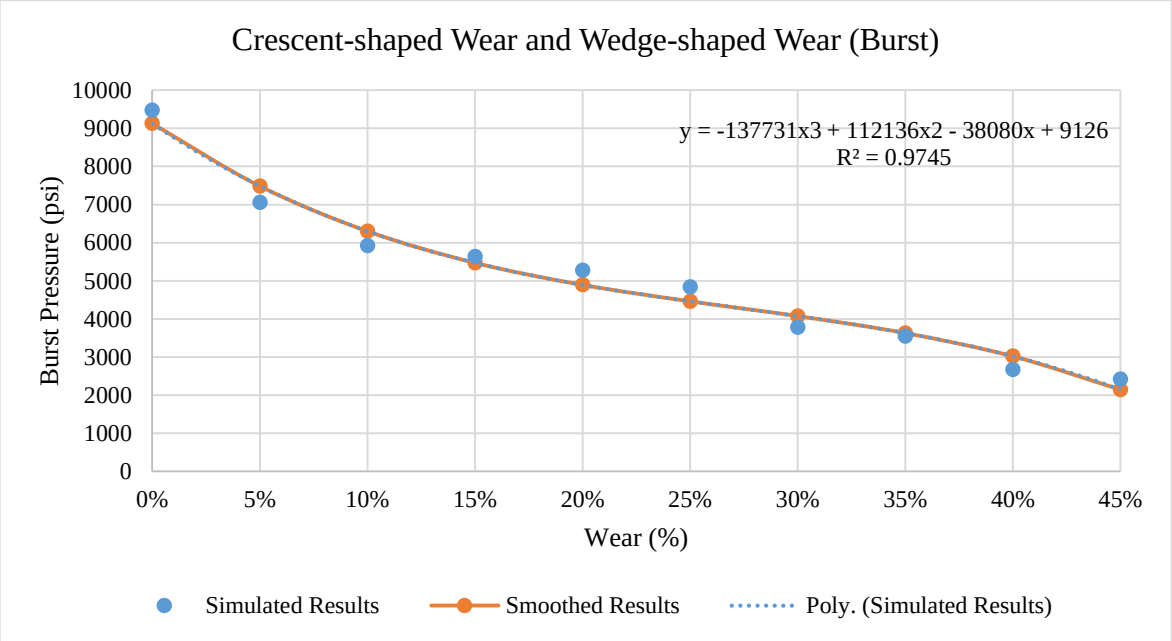

Figure 70. Safe and failure zones for maximum internal pressure on mixed-shape wear

The burst pressure model from the simulation is:

$$P_{burst} = -137731\ x\ Wear^3 + 112136\ x\ Wear^{\,2} - 38080\ x\ Wear + 9126 \qquad (51)$$

The coefficient of determination of this model (R^2) is 0.9745. This value suggests that the data from the simulation fit the statistical model. This simulated model already includes the safety factor. Figure 71 shows a comparison between the simulated model and the API Burst/Barlow model.

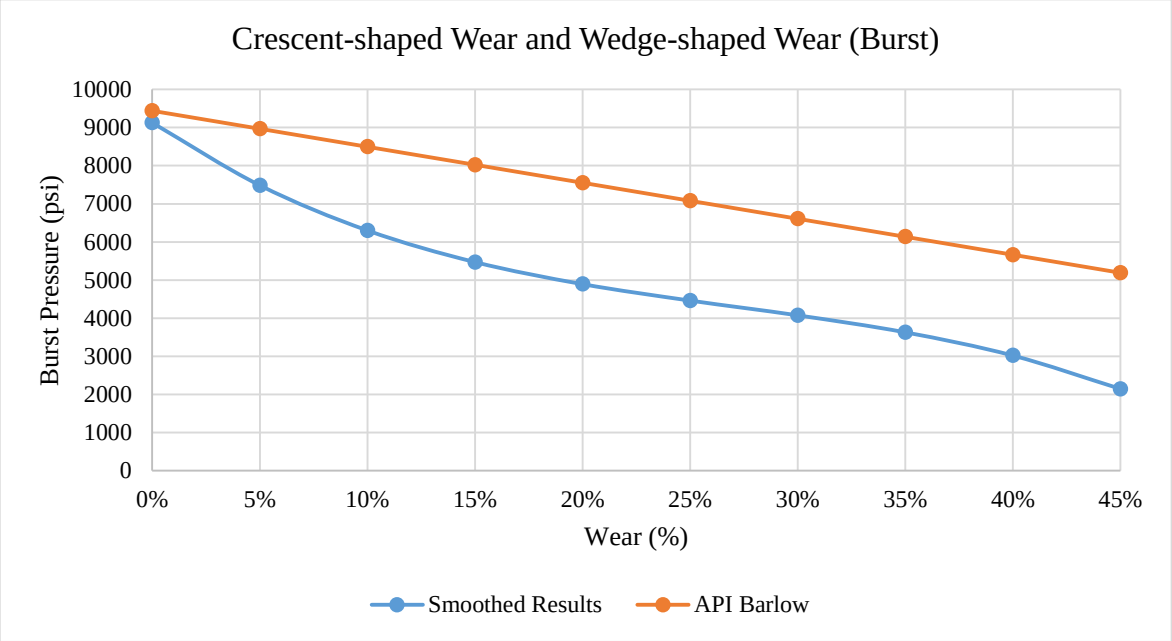

Figure 71. Comparison between API Burst/Barlow model and the simulation results

5.1.4.3 Crescent-shaped Wear (inside) and Rectangle-shaped Wear (outside)

5.1.4.3.1 Crescent-shaped Wear (inside) and Rectangle-shaped Wear (outside) (10% Wear Model)

For the 10% wear model, the maximum internal pressure before the production casing started to yield is 5881 psi. Compared to the reference model (0% wear), there is a reduction by 38% of the maximum internal pressure in the production casing.

5.1.4.3.2 Crescent-shaped Wear (inside) and Rectangle-shaped Wear (outside) (30% Wear Model)

In the 30% wear model, the maximum internal pressure before the production casing material yielded is 3580 psi. The simulated result is a reduction of 62% from the undamaged reference model (0% wear).

5.1.4.3.3 Crescent-shaped Wear (inside) and Rectangle-shaped Wear (outside) (50% Wear Model)

The result from the 45% wear model shows that the maximum internal yield pressure for the production casing is 2223 psi. This simulated result is a 72% reduction from the reference model (0% wear).

5.1.4.3.4 Burst Pressure Limits Results

Figure 72 represents the linear slopes for the wear percentages of the different internal pressures for all simulated scenarios. The maximum internal yield pressure for the production casing decreases as the wear percentage increases. Table 22 shows the maximum internal yield pressure of the production casing for all simulated wear percentage scenarios, from 0% to 45%. The maximum internal yield pressure is obtained by solving the linear interpolation.

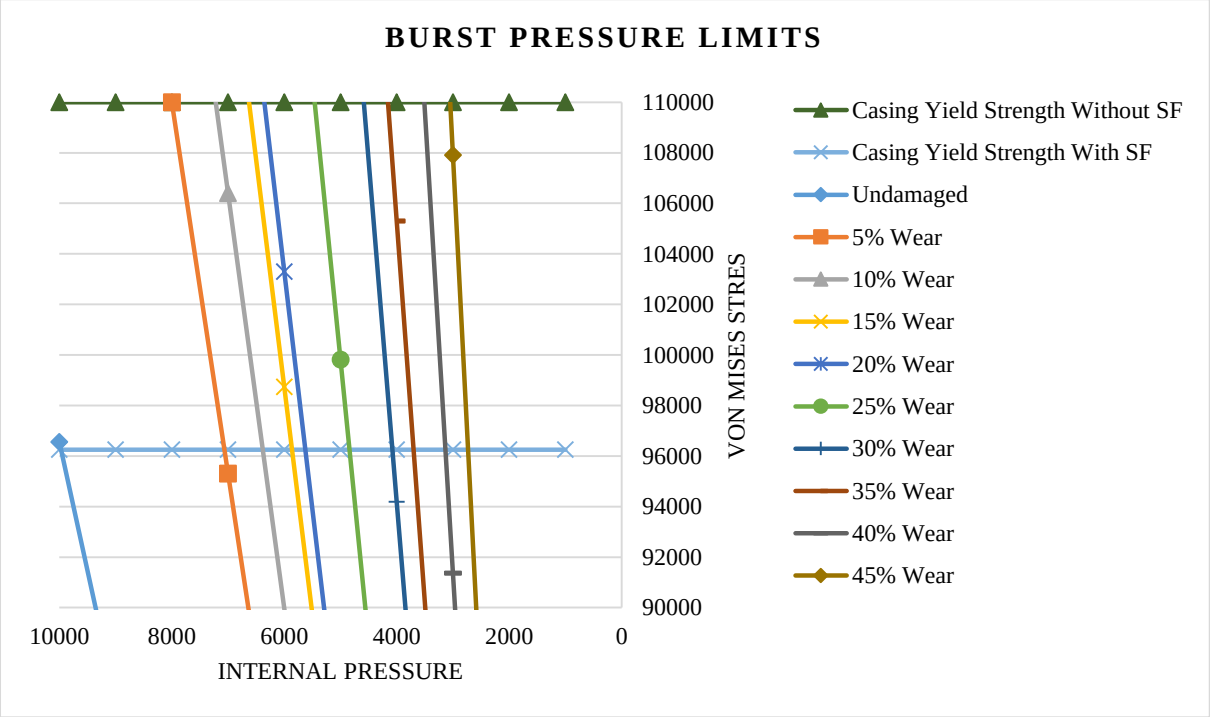

Figure 72. Internal pressure with respective Von Mises stress for different wear depths (mixed-shape wear model)

Table 22. Linear Interpolation for Maximum Internal Pressure

Wear (%)	Burst Pressure (psi)
0%	9470
5%	6565
10%	5881
15%	5364
20%	5127
25%	4336
30%	3580
35%	3204
40%	2630
45%	2223

Figure 73 shows the safe and failure zones for the maximum operating internal yield pressure. The area below the curve represents the safe zone while, the area above the curve is the failure zone. The burst pressure model developed from the simulation is also shown.

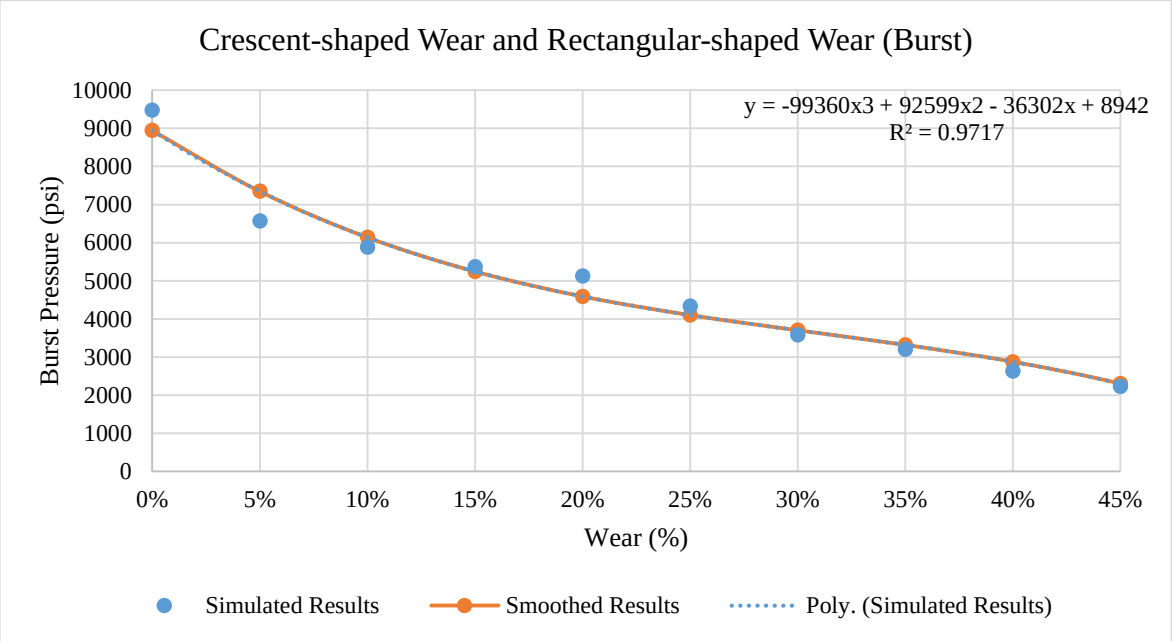

Figure 73. Safe and failure zones for maximum internal pressure on mixed-shape wear

The burst pressure model from the simulation is:

$$P_{burst} = -99360\ x\ Wear^3 + 92599\ x\ Wear^{\,2} - 36302\ x\ Wear + 8942 \qquad (52)$$

The coefficient of determination of this model (R^2) is 0.9717. This value suggests that the data from the simulation fit the statistical model. This simulated model already includes the safety factor. Figure 74 presents a comparison between the simulated model and the API Burst/Barlow model.

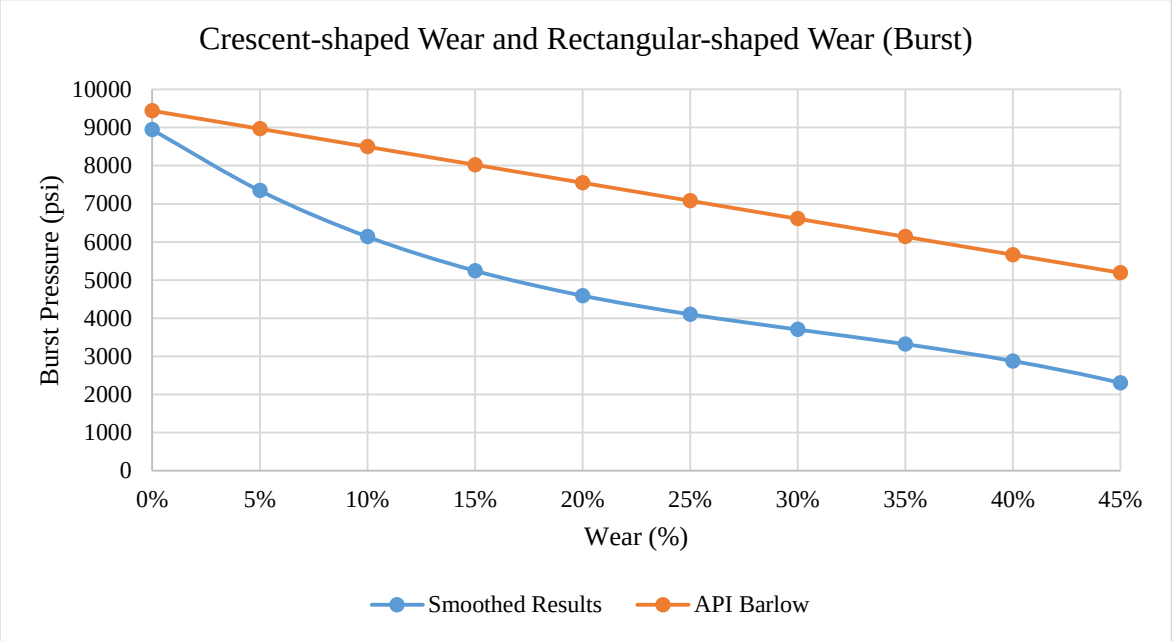

Figure 74. Comparison between API Burst/Barlow model and the simulation results

5.2 Collapse Case Results

In this thesis, the triaxial collapse model is used to predict the maximum collapse pressure limit on the production casing instead of the API Collapse model. The triaxial collapse model is used because the computation results for the undamaged casing or reference scenario using the triaxial collapse model are similar to the results of maximum collapse pressure limit of the undamaged casing or reference scenario in the FEM simulation. By contrast, the API Collapse model gives a significantly lower estimation of the maximum collapse pressure of the undamaged casing or reference scenario compared to the FEM simulation result.

5.2.1 Reference Model – 0% Wear

The reference model is built based on the undamaged production casing scenario. All of the simulated production casing models use the same reference model (Figure 75). The simulation shows that the Von Mises stress on the production casing reaches 101500 psi when it is loaded by an internal pressure of 10000 psi. The production casing reaches the yield limit when loaded by external pressure between 9000-10000 psi (safety factor is included). The Von Mises stresses calculated from the FEM simulation for the production casing are shown in Table 23.

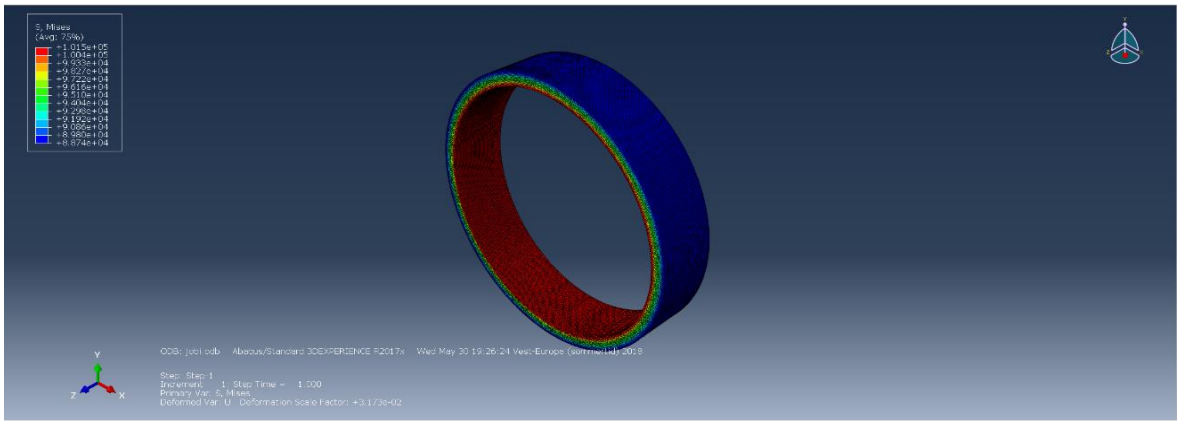

Figure 75. Simulated collapse model with 0% wear and external pressure 10000 psi

Table 23. External Pressure with Von Mises Stress for 0% Wear Model

Wear (%)	External Pressure (psi)	Von Mises Stress (psi)
0%	1000	5595
	2000	16240
	3000	26890
	4000	37540
	5000	48190
	6000	58840
	7000	69490
	8000	80150
	9000	90800
	10000	101500

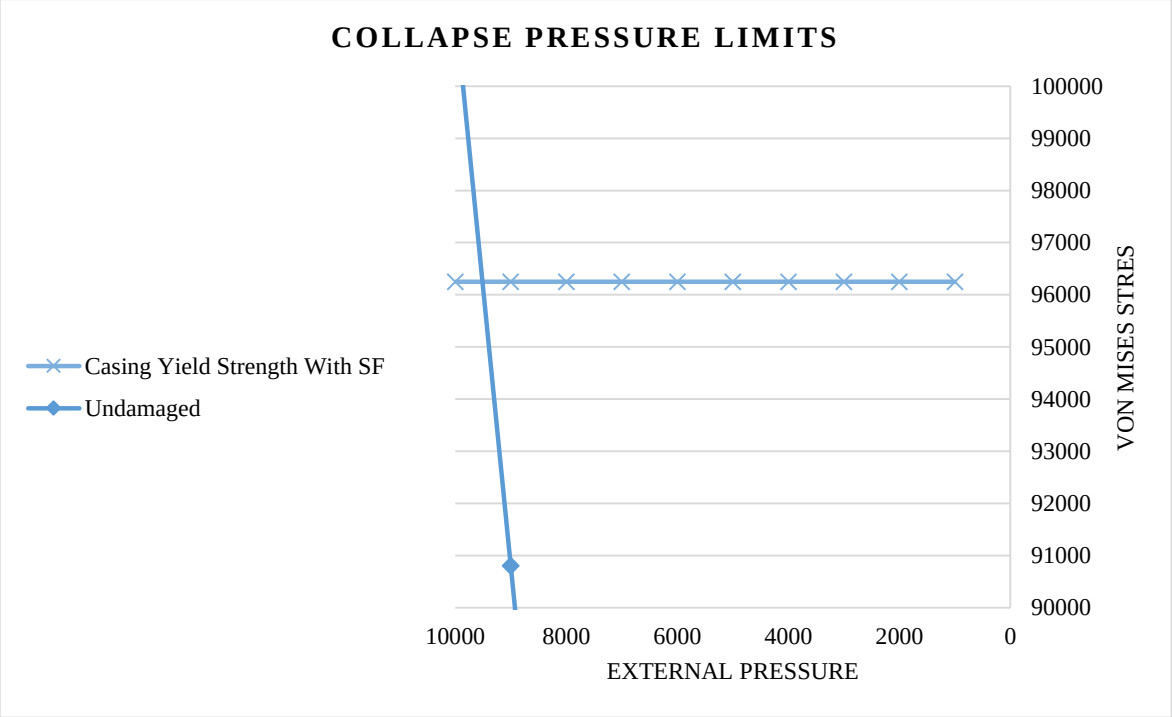

Figure 76. External pressure with Von Mises stress graph for 0% wear model

By the interpolation, the maximum external pressure of the production casing before the material yields is 9005 psi (safety factor included).

5.2.1.1 Uniform Wear Model Comparison

In a process similar to that described in part 5.1.1.1 of the thesis, two models are made to examine the validity of the Finite Element Method (FEM) for the collapse analysis of locally worn production casing. The first model is an undamaged reference production casing model and the second model is the 10% uniform wear production casing model. The FEM simulation results from both models are compared with the results from the triaxial collapse model for undamaged and 10% uniform wear model as shown in Table 24.

Table 24. Comparison between Triaxial Collapse and FEM Results

Wear Percentage	Triaxial Collapse	Simulated Results
0%	8977	9005
10%	8121	8160

The data presented in Table 24 show that there are similarities between the results of the triaxial collapse model and the FEM model. It can be concluded that the FEM method is valid for the analysis of the collapse scenario of production casing.

5.2.2 Single Scar Scenario

5.2.2.1 Crescent-shaped

The simulation result for single crescent-shaped wear in a production casing is presented in this section.

5.2.2.1.1 Single Crescent-shaped Wear (10% Wear Model)

For the 10% single crescent-shaped wear model, the maximum external pressure before the production casing started to yield is 7040 psi. Compared to the reference model (0% wear), there is a reduction of 22% of the maximum external pressure in the production casing.

5.2.2.1.2 Single Crescent-shaped Wear (30% Wear Model)

In the 30% single crescent-shaped wear model, the maximum external pressure before the production casing material yielded is 3660 psi. The simulated result is a reduction of 59% from the undamaged reference model (0% wear).

5.2.2.1.3 Single Crescent-shaped Wear (45% Wear Model)

The result from the 45% single crescent-shaped wear model shows that the maximum external yield pressure for the production casing is 2422 psi. This simulated result is a 73% reduction from the reference model (0% wear).

5.2.2.1.4 Collapse Pressure Limits Results

Figure 77 presents the linear slopes for wear percentages of the different external pressures for all simulated scenarios. The maximum external yield pressure for the production casing decreases as the wear percentage increases. Table 25 presents the maximum external yield pressure of the production casing for all simulated wear percentage scenarios, from 0% to 45%. The maximum external yield pressure is obtained by solving the linear interpolation.

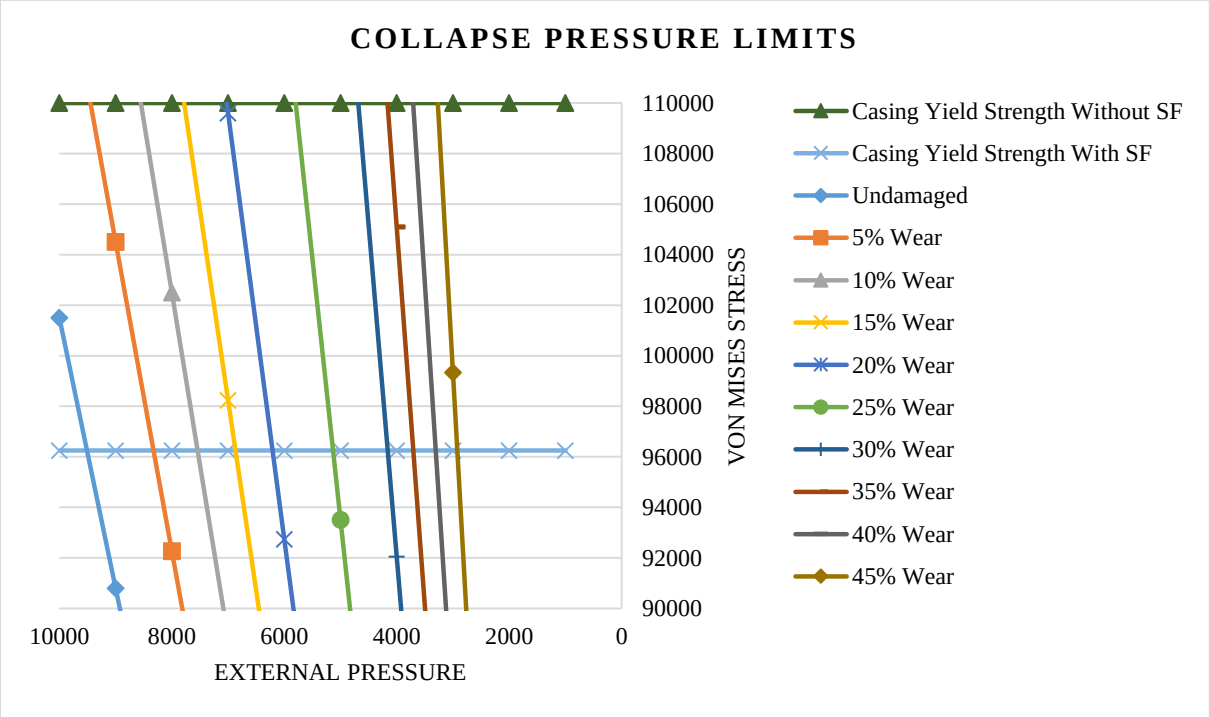

Figure 77. External pressure with respective Von Mises stress for different wear depths (single crescent-shaped wear model)

Table 25. Linear Interpolation for Maximum External Pressure

Wear (%)	Collapse Pressure (psi)
0%	9005
5%	7829
10%	7040
15%	6368
20%	5705
25%	4632
30%	3660
35%	3204
40%	2806
45%	2422

Figure 78 shows the safe and failure zones for the maximum operating external yield pressure. The area below the curve represents the safe zone, while the area above the curve is the failure zone. The collapse pressure model developed from the simulation is also shown.

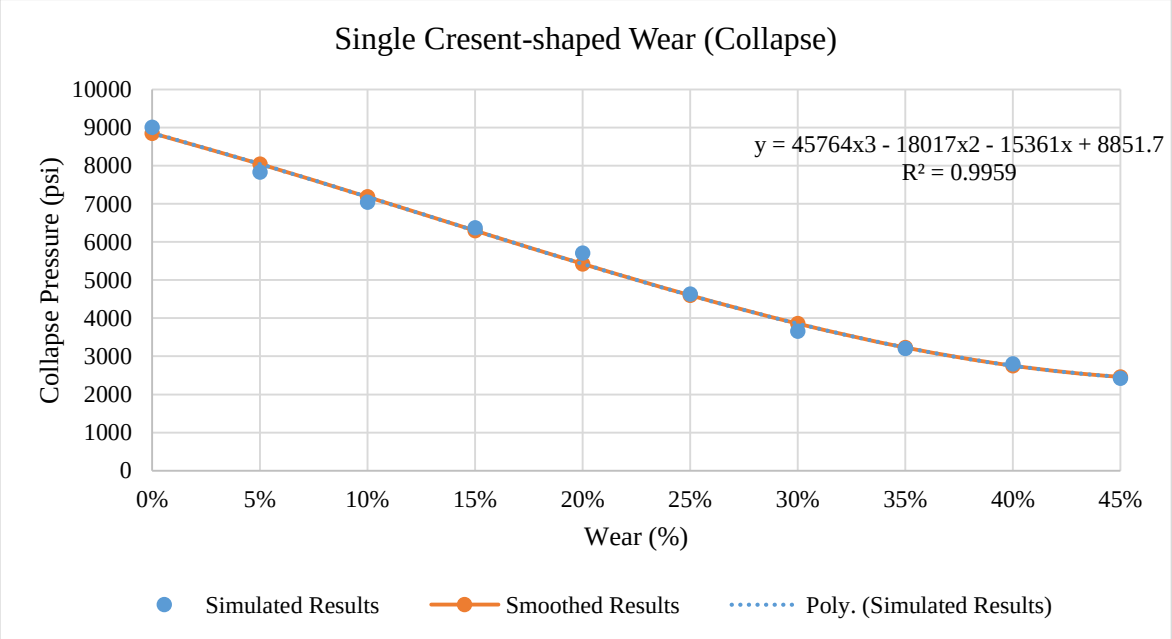

Figure 78. Safe and failure zones for maximum external pressure on single crescent-shaped wear

The collapse pressure model from the simulation is:

$$P_{collapse} = -45764\ x\ Wear^3 + 18017\ x\ Wear^{\,2} - 15361\ x\ Wear + 8851.7 \qquad (53)$$

The coefficient of determination of this model (R^2) is 0.9959. This value suggests that the data from the simulation fit the statistical model. This simulated model already includes the safety factor. Figure 79 shows the comparison between the simulated model and the triaxial collapse model (Equation (33)).

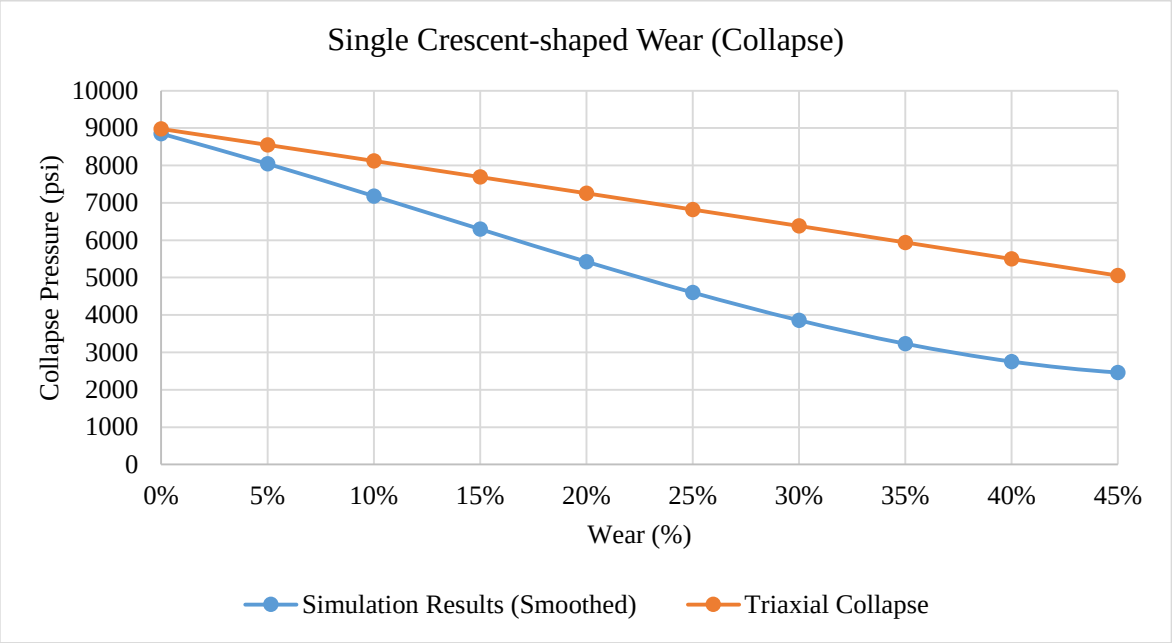

Figure 79. Comparison between triaxial collapse model and the simulation results

5.2.2.2 Wedge-shaped

The simulation scenarios for the wedge-shaped wear in production casing are divided based on three different wear width: 0.2, 0.25, and 0.3 unit width.

5.2.2.2.1 Wedge-shaped 0.2 Width Wear

5.2.2.2.1.1 Wedge-shaped 0.2 Width Wear (10% Wear Model)

The result from 10% wedge-shaped wear model shows that the maximum external yield pressure for the production casing is 6531 psi. This simulated result is a 27% reduction from the reference model (0% wear).

5.2.2.2.1.2 Wedge-shaped 0.2 Width Wear (30% Wear Model)

For the 30% wedge-shaped wear model, the maximum external pressure before the production casing started to yield is 4750 psi. Compared to the reference model (0% wear), there is a reduction by 47% of the maximum external pressure in the production casing.

5.2.2.2.1.3 Wedge-shaped 0.2 Width Wear (45% Wear Model)

In the 45% wedge-shaped wear model, the maximum external pressure before the production casing material yielded is 2997 psi. The simulated result is a reduction of 67% from the undamaged reference model (0% wear).

5.2.2.2.1.4 Collapse Pressure Limits Results

Figure 80 shows the linear slopes for the wear percentages of the different external pressures for all wedge-shaped 0.2 width scenarios. The maximum external yield pressure for the production casing decreases as the wear percentage increases. Table 26 shows the maximum external yield pressure of the production casing for all simulated wear percentage scenarios, from 0% to 45%. The maximum external yield pressure is obtained by solving the linear interpolation.

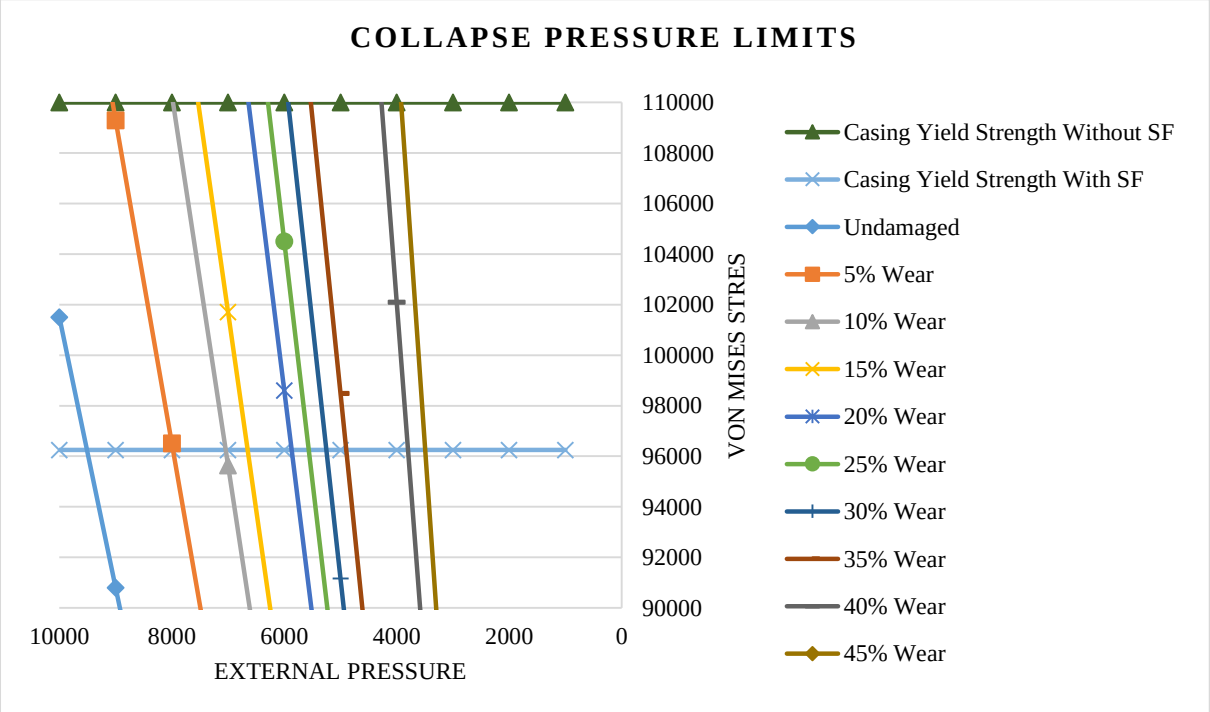

Figure 80. External pressure with respective Von Mises stress for different wear depths (0.2 width single wedge-shaped wear model)

Table 26. Linear Interpolation for Maximum External Pressure

Wear (%)	Collapse Pressure (psi)
0%	9505
5%	7988
10%	7031
15%	6651
20%	5857
25%	5553
30%	5250
35%	4892
40%	3802
45%	3497

Figure 81 presents the safe and failure zones for the maximum operating external yield pressure for the 0.2 width wedge-shaped scenario. The area below the curve represents the safe zone, while the area above the curve is the failure zone. The collapse pressure model buildt from the simulation is also shown.

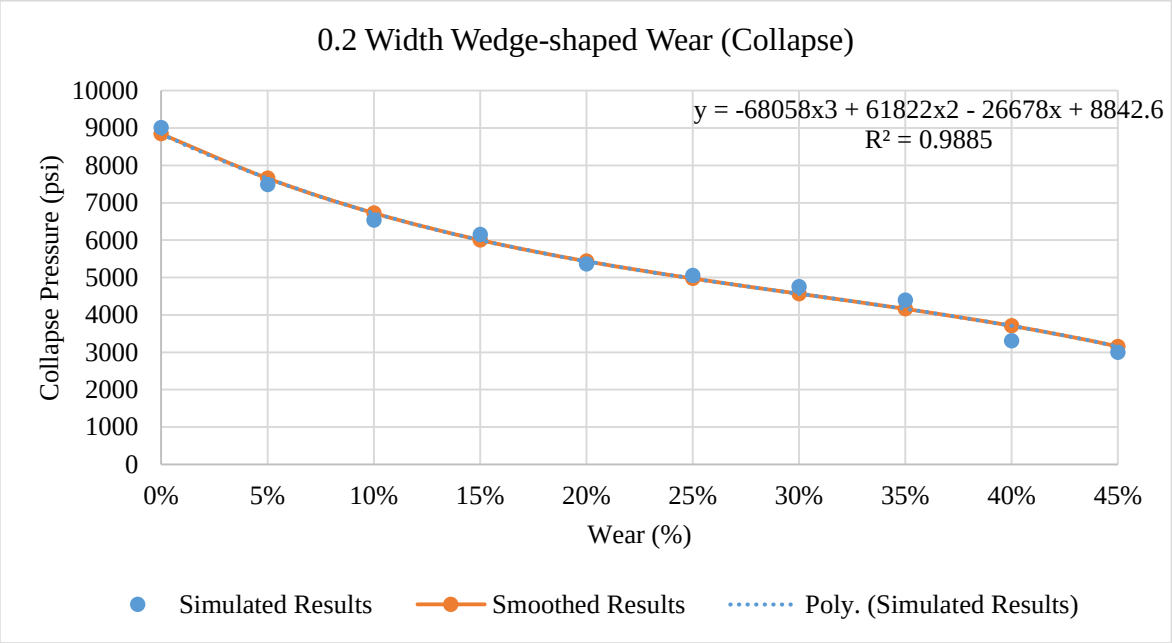

Figure 81. Safe and failure zones for maximum external pressure on 0.2 width single wedge-shaped wear

The collapse pressure model from the simulation is:

$$P_{collapse} = -68058\ x\ Wear^3 + 61822\ x\ Wear^2 - 26678\ x\ Wear + 8842.6 \qquad (54)$$

The coefficient of determination of this model (R^2) is 0.9885. This value suggests that the data from the simulation fit the statistical model. This simulated model already includes safety factor. The comparison between the simulated model and the triaxial collapse results is shown in Figure 82.

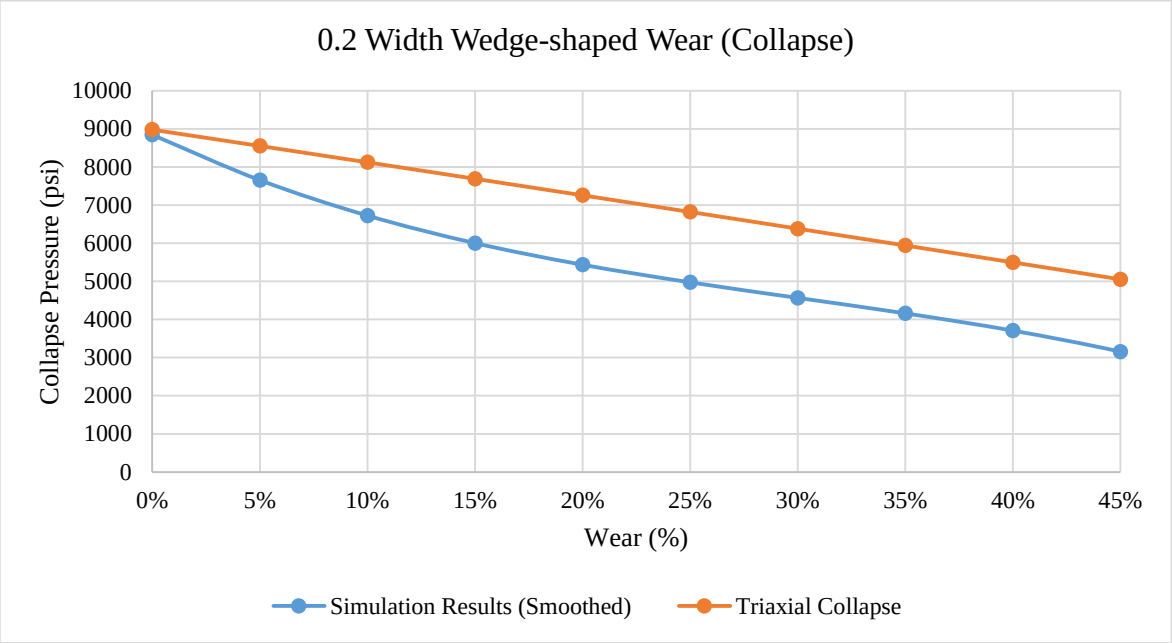

Figure 82. Comparison between triaxial collapse model and the simulation results

5.2.2.2.2 Wedge-shaped 0.25 Width Wear

5.2.2.2.2.1 Wedge-shaped 0.25 Width Wear (10% Wear Model)

The result of the 10% wedge-shaped 0.25 width model shows that the maximum external yield pressure for the production casing is 6187 psi. This simulated result is a 31% reduction from the reference model (0% wear).

5.2.2.2.2.2 Wedge-shaped 0.25 Width Wear (30% Wear Model)

For the 30% wedge-shaped wear model, the maximum external pressure before the production casing started to yield is 4059 psi. Compared to the reference model (0% wear), there is a reduction by 55% of the maximum external pressure in the production casing.

5.2.2.2.2.3 Wedge-shaped 0.25 Width Wear (45% Wear Model)

In the 45% wedge-shaped wear model, the maximum external pressure before the production casing material yielded is 2812 psi. The simulated result is a reduction of 69% from the undamaged reference model (0% wear).

5.2.2.2.2.4 Collapse Pressure Limits Results

Figure 83 represents the linear slopes for the wear percentages of the different external pressures for all wedge-shaped 0.25 width scenarios. The maximum external yield pressure for the production casing decreases as the wear percentage increases. Table 27 presents the maximum external yield pressure of the production casing for all simulated wear percentage scenarios, from 0% to 45%. The maximum external yield pressure is obtained by solving the linear interpolation.

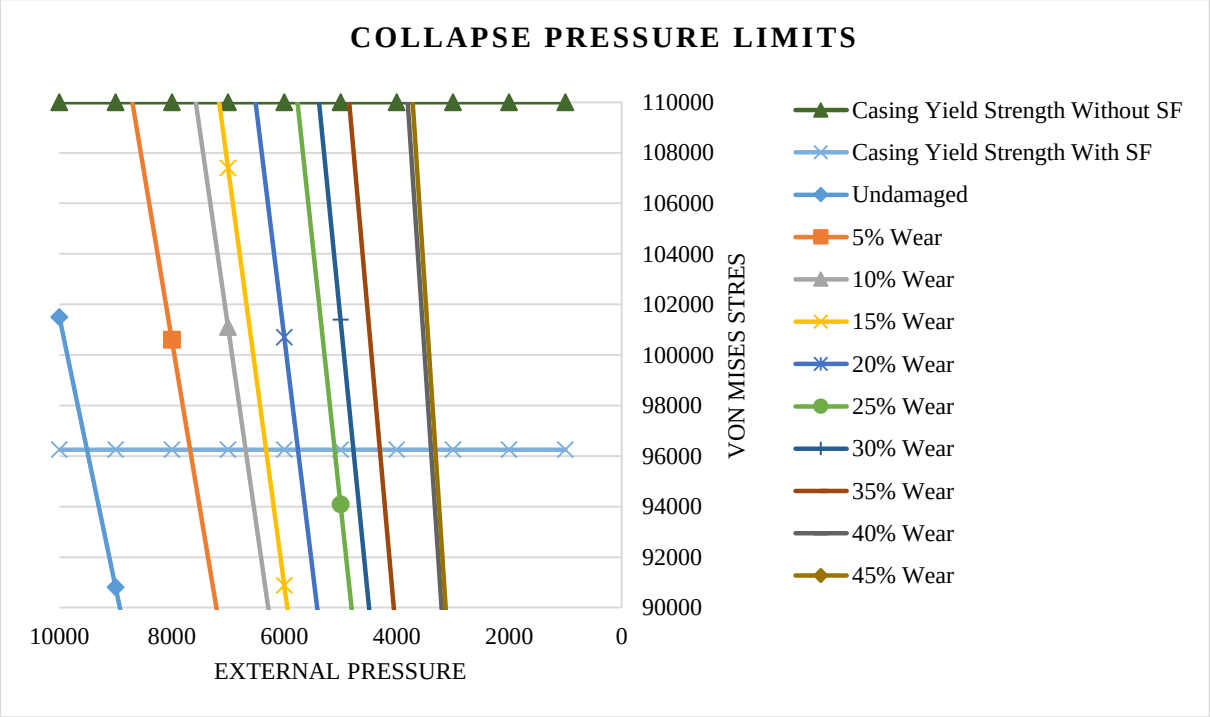

Figure 83. External pressure with respective Von Mises stress for different wear depths (0.25 width single wedge-shaped wear model)

Table 27. Linear Interpolation for Maximum External Pressure

Wear (%)	Collapse Pressure (psi)
0%	9005
5%	7175
10%	6187
15%	5830
20%	5262
25%	4599
30%	4059
35%	3796
40%	2893
45%	2812

Figure 84 presents the safe and failure zones for the maximum operating external yield pressure for the 0.25 width wedge-shaped scenario. The area below the curve represents the safe zone, while the area above the curve is the failure zone. The collapse pressure model developed from the simulation is also shown.

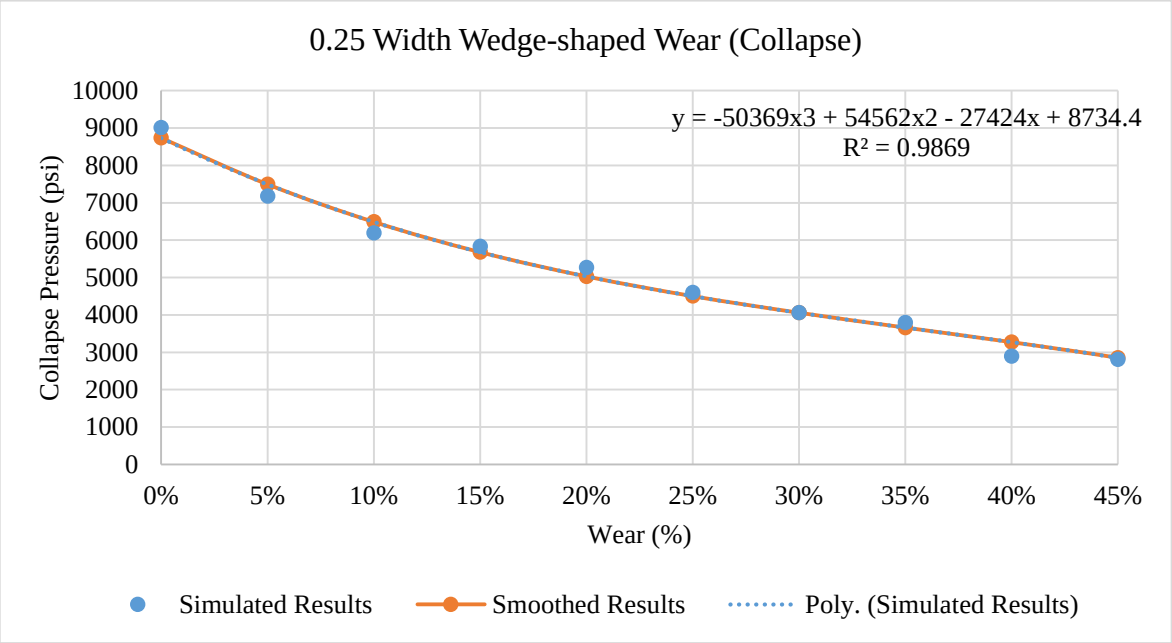

Figure 84. Safe and failure zones for maximum external pressure on 0.25 width single wedge-shaped wear

The collapse pressure model from the simulation is:

$$P_{collapse} = -50369\ x\ Wear^3 + 54562\ x\ Wear^{\ 2} - 27424\ x\ Wear + 8734.4 \qquad (55)$$

The coefficient of determination of this model (R^2) is 0.9869. This value suggests that the data from the simulation fit the statistical model. This simulated model already includes the safety factor. Figure 85 shows a comparison between the simulated model and the triaxial collapse model.

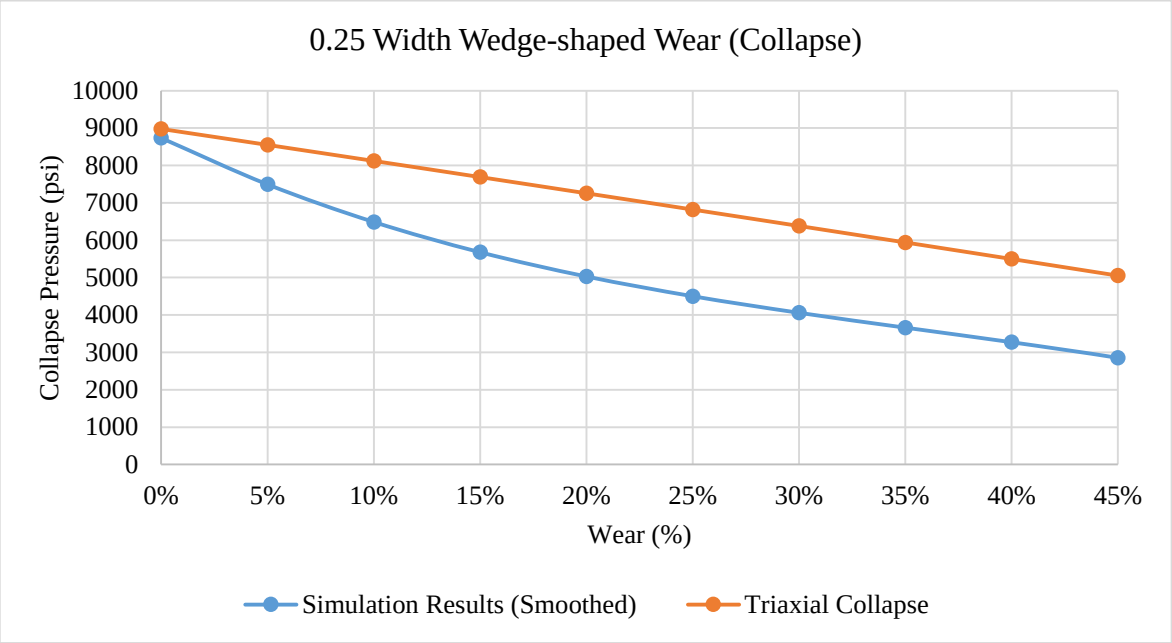

Figure 85. Comparison between triaxial collapse model and the simulation results

5.2.2.2.3 Wedge-shaped 0.3 Width Wear

5.2.2.2.3.1 Wedge-shaped 0.3 Width Wear (10% Wear Model)

The result from the 10% wedge-shaped 0.3 width model shows that the maximum external yield pressure for the production casing is 6146 psi. This simulated result is a 32% reduction from the reference model (0% wear).

5.2.2.2.3.2 Wedge-shaped 0.3 Width Wear (30% Wear Model)

There is a reduction by 58% from the reference model for the 30% wear wedge-shaped wear model. The maximum external pressure before the production casing is started to yield is 3809 psi.

5.2.2.2.3.3 Wedge-shaped 0.3 Width Wear (45% Wear Model)

In the 45% wedge-shaped wear model, the maximum external pressure before the production casing material yielded is 2536 psi. The simulated result is a reduction of 72% from the undamaged reference model (0% wear).

5.2.2.2.3.4 Collapse Pressure Limits Results

Figure 86 represents the linear slopes for the wear percentages of the different external pressures for all wedge-shaped 0.3 width scenarios. The maximum external yield pressure for the production casing decreases as the wear percentage increases. Table 28 presents the maximum external yield pressure of the production casing for all simulated wear percentage scenarios, from 0% to 45%. The maximum external yield pressure is obtained by solving the linear interpolation.

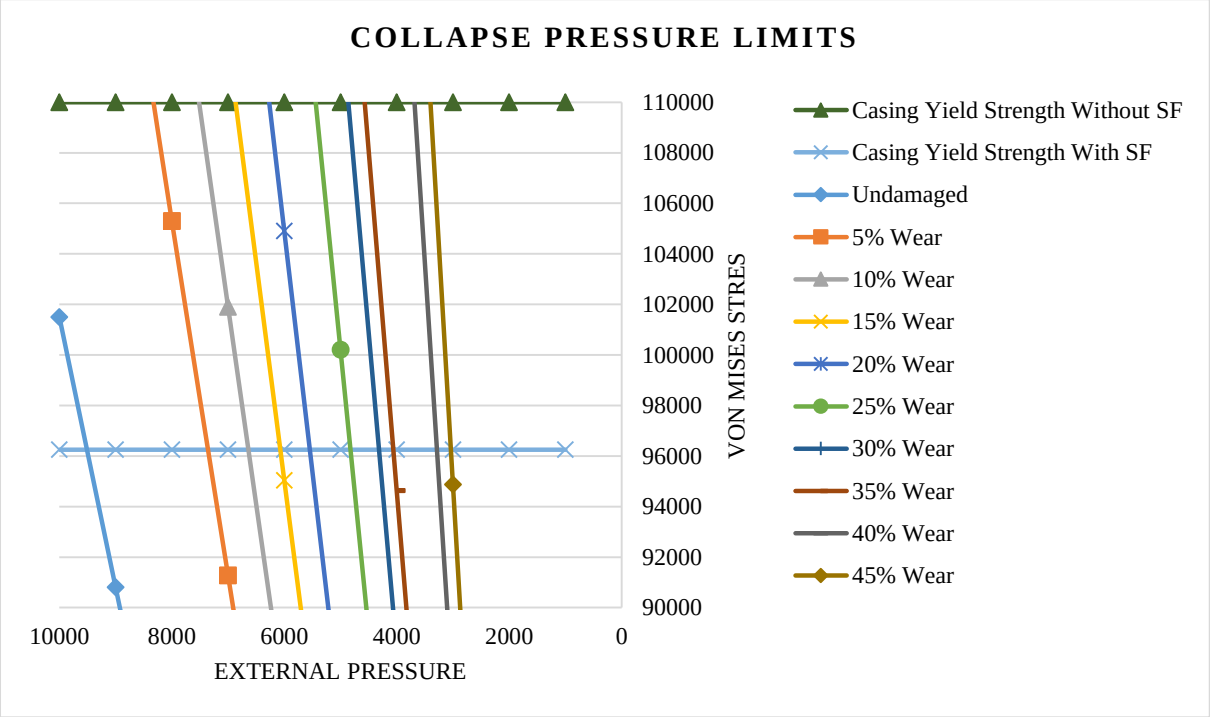

Figure 86. External pressure with respective Von Mises stress for different wear depths (0.3 width single wedge-shaped wear model)

Table 28. Linear Interpolation for Maximum External Pressure

Wear (%)	Collapse Pressure (psi)
0%	9005
5%	6776
10%	6146
15%	5567
20%	5045
25%	4322
30%	3809
35%	3554
40%	2781
45%	2536

Figure 87 shows the safe and failure zones for the maximum operating external yield pressure for the 0.3 width wedge-shaped scenario. The area below the curve represents the safe zone while the area above the curve is the failure zone. The collapse pressure model developed from the simulation is also shown.

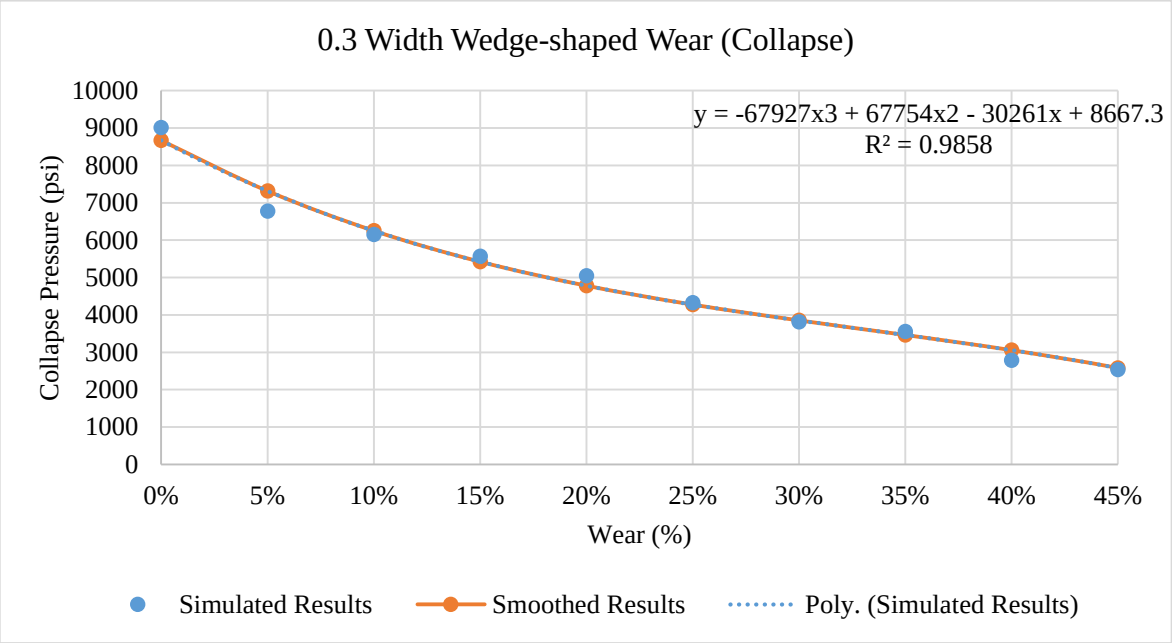

Figure 87. Safe and failure zones for maximum external pressure on 0.3 width single wedge-shaped wear

The collapse pressure model from the simulation is:

$$P_{collapse} = -67927\ x\ Wear^3 + 67754\ x\ Wear^2 - 30261\ x\ Wear + 8667.3 \qquad (56)$$

The coefficient of determination of this model (R^2) is 0.9858. This value suggests that the data from the simulation fit the statistical model. This simulated model already includes the safety factor. Figure 88 presents a comparison between the simulated model and the triaxial collapse model.

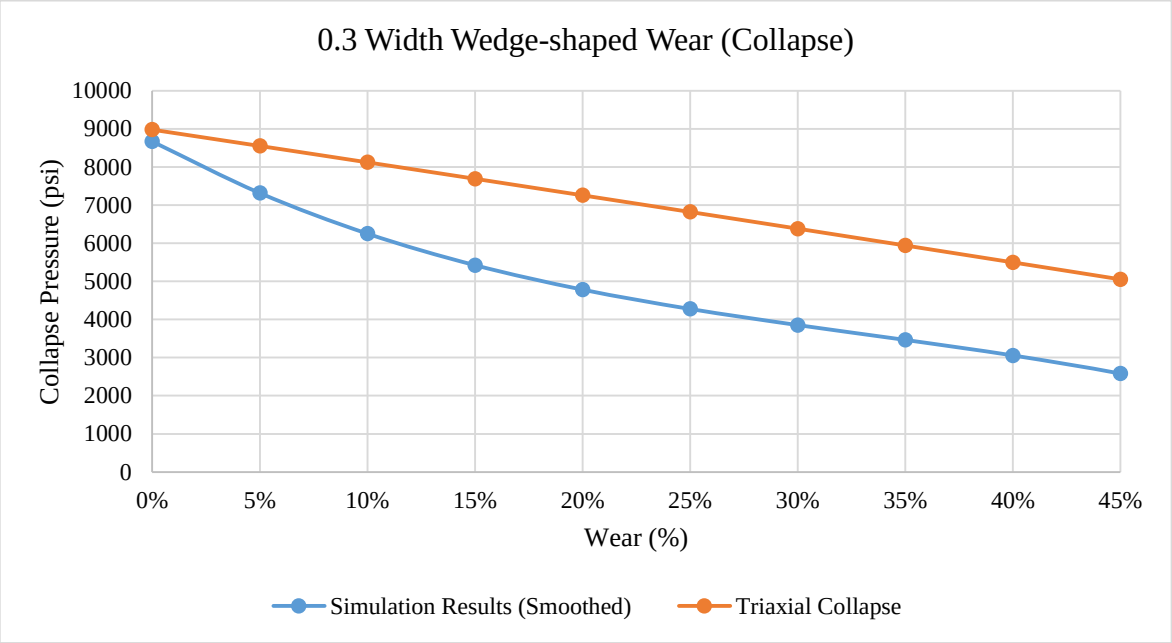

Figure 88. Comparison between triaxial collapse model and the simulation results

5.2.3 Double Scars Scenario

The study of the effect of double scars on the maximum collapse pressure limit of the production casing is presented in Appendix 1. The results are not presented in this section due to the fact that the production casing no longer has the thick-walled cylinder characteristic due to increasing wear that leads to significant decrease in wall thickness. Therefore, the results from the double scars scenarios cannot be compared to the triaxial collapse result.

6. Discussion of Results

Well integrity is the paramount aspect during the whole life cycle of a well. To eliminate the risk of loss of well integrity, the well should be planned and constructed in a safe manner according to well integrity principles and practice in the industry. The realistic loads during the life cycle of the well should be carried by the casing and material for casing must be carefully selected to resist and tolerate a corrosive environment [3].

The results of a field investigation in the Gullfaks Field showed that the casing there experienced wear up to 35% [2]. In reference [1], it is reported that the production tubing in the North Sea experience about 47% local wear.

In industry practice, the current API model for burst and the triaxial model for collapse are used to determine the strength of the casing and tubing. These models are derived based on thin-walled and thick-walled cylinder theory, respectively. In this thesis, a Finite Element Method (FEM) study is conducted to assess the applicability of the current API Burst/Barlow and triaxial models to non-uniform wear on the casing.

An undamaged FEM reference production casing model was built and compared with several models of local wear on the production casing. The simulation results revealed that the damaged part of the casing has the highest stress concentration, while the undamaged part of the casing has a lower stress concentration in all local wear model scenarios for both burst and collapse cases.

From the interpolation of Von Mises stress results, the maximum burst and collapse pressures for each production casing wear case from 0% to 45% wear are obtained. Comparison of the FEM simulation results and the API Burst/Barlow and triaxial collapse models shows that the calculation of the maximum burst and collapse strength of the locally damaged production casing by using FEM analysis have lower results than calculation of casing using API Burst/Barlow and triaxial models. The following section presents a detailed analysis of the difference between the FEM simulation results and the API Burst/Barlow and triaxial collapse models in terms of deviation percentage on the production casing for 0% production casing wear case until 45% production casing wear case.

6.1 Burst Case Analysis

In this section, the simulation results presented in chapter 5 will be analyzed in terms of percentage of deviation, which is between the FEM and API modelling. The percentage of deviation is calculated as:

$$\%\, Deviation = \frac{(FEM - API)}{API} * 100 \tag{57}$$

where, *FEM* is the de-rated pressure for casing with local wear calculated based on FEM model and *API* is the de-rated pressure for casing with local wear calculated based on API model.

6.1.1 Single Scar Scenario

The modelling results of single scar case scenario is presented in section 5.1.2. Figure 89 illustrates the percentage of deviation in the burst strength of the production casing. For the 0.3 unit width, single wedge-shaped wear shows a maximum deviation of 49%. Similarly, the single wedge-shaped wear with 0.25 unit shows a maximum deviation of 43%, while single wedge-shaped wear with 0.2 unit width shows a maximum deviation up to 38%. All of the deviations show the same trend in which the deviation percentage is higher as the wear percentage increases. Therefore, all of the maximum deviations for the single wedge-shaped wear are observed in the 45% wear scenario.

In crescent-shaped wear, a different deviation percentage trend is observed as shown in Figure 89. The single crescent-shaped wear has the maximum deviation of 52% on the 45% production casing wear scenario. The trend of deviation percentage for the crescent-shaped wear is somewhat different in that it has a lower deviation than all three wedge-shaped wear scenarios in the 5% to 15% wear scenario and surpasses the maximum deviation percentage of the three types of wedge-shaped scenario in the 20% to 30% wear scenario. In the 35% to 45% wear scenario, the maximum deviation percentage of crescent-shaped wear is higher than for all of the three types of wedge-shaped wear. The maximum deviation percentage for the single crescent-shaped wear increases when the wear percentage increases, with the highest maximum deviation percentage observed in the 45% wear scenario. All of the single-scar shape FEM simulations show lower de-rated burst strength compared to the API Burst/Barlow model. Therefore, the API Burst/Barlow model overestimates the maximum burst strength for locally damaged production casing.

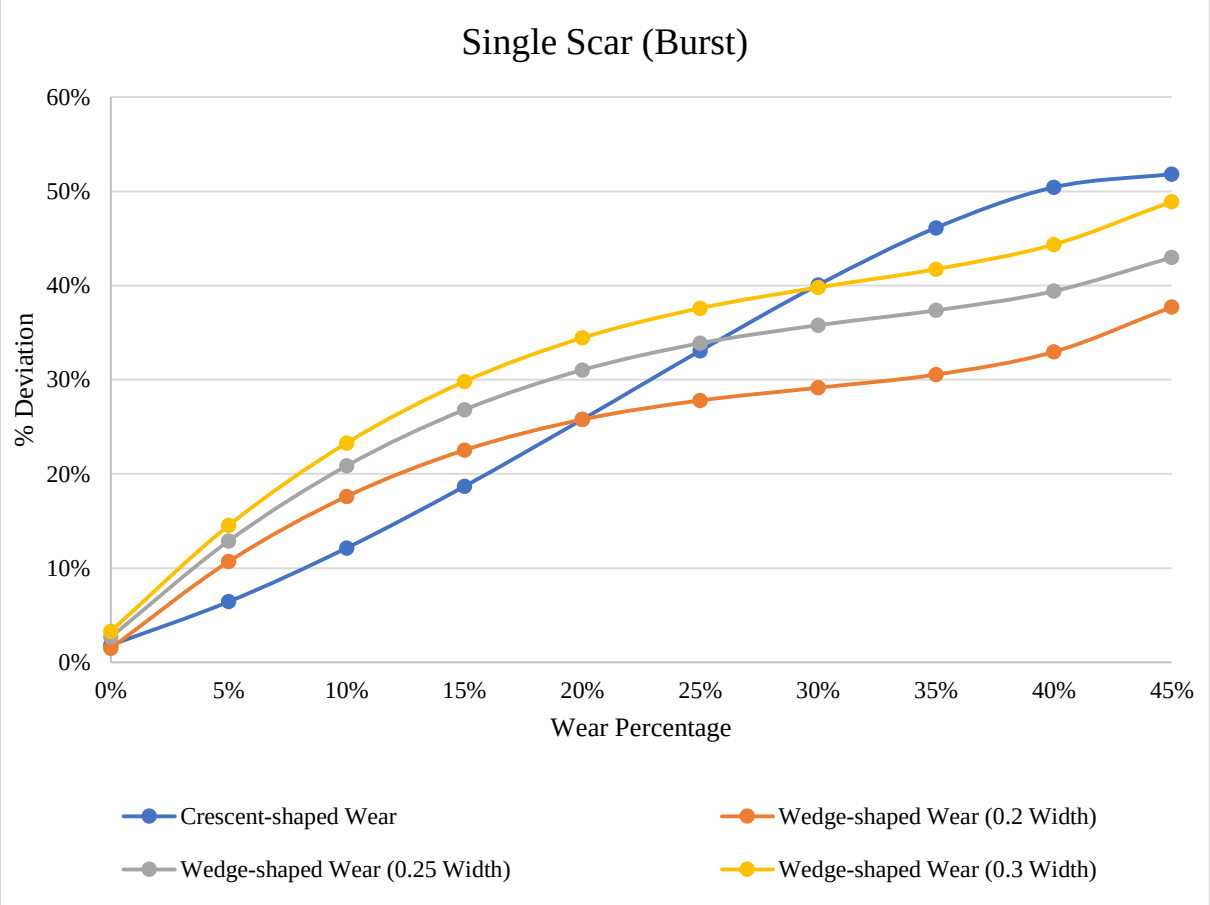

Figure 89. Deviation Percentage between API Burst/Barlow model and FEM simulation results for different single scar scenarios

6.1.2 Double Scars Scenario (Model 1)

The modelling results of double scars case scenario (model 1) is presented in section 5.1.3. The deviation percentage result analysis for the model 1 case in which the production casing has double scars located on the internal part of the production casing is shown in Figure 90. The deviation percentage in both curves increases as the wear percentage on the casing increases. However, the trend for the double crescent-shaped wear and double wedge-shaped wear are considerably different. The double crescent-shaped wear has lower deviation compared to double wedge-shaped wear in the 5% to 25% wear scenario and has a higher deviation in the 30% to 45% wear scenario. On the other hand, the double wedge-shaped wear has a significant increase in deviation percentage from 5% to 25% wear and a smaller increase in the deviation percentage from 30% to 45%. The calculation results show that double crescent-shaped wear has a 55% maximum deviation, and a maximum deviation of 51% is observed for the double wedge-shaped wear. The maximum deviation for both double scars models is observed in the

maximum production casing wear scenario (45% casing wear). All of the simulation results show significant deviation from the API Burst/Barlow model. It can be concluded that API Burst/Barlow model overestimates the maximum burst strength of locally damaged production casing.

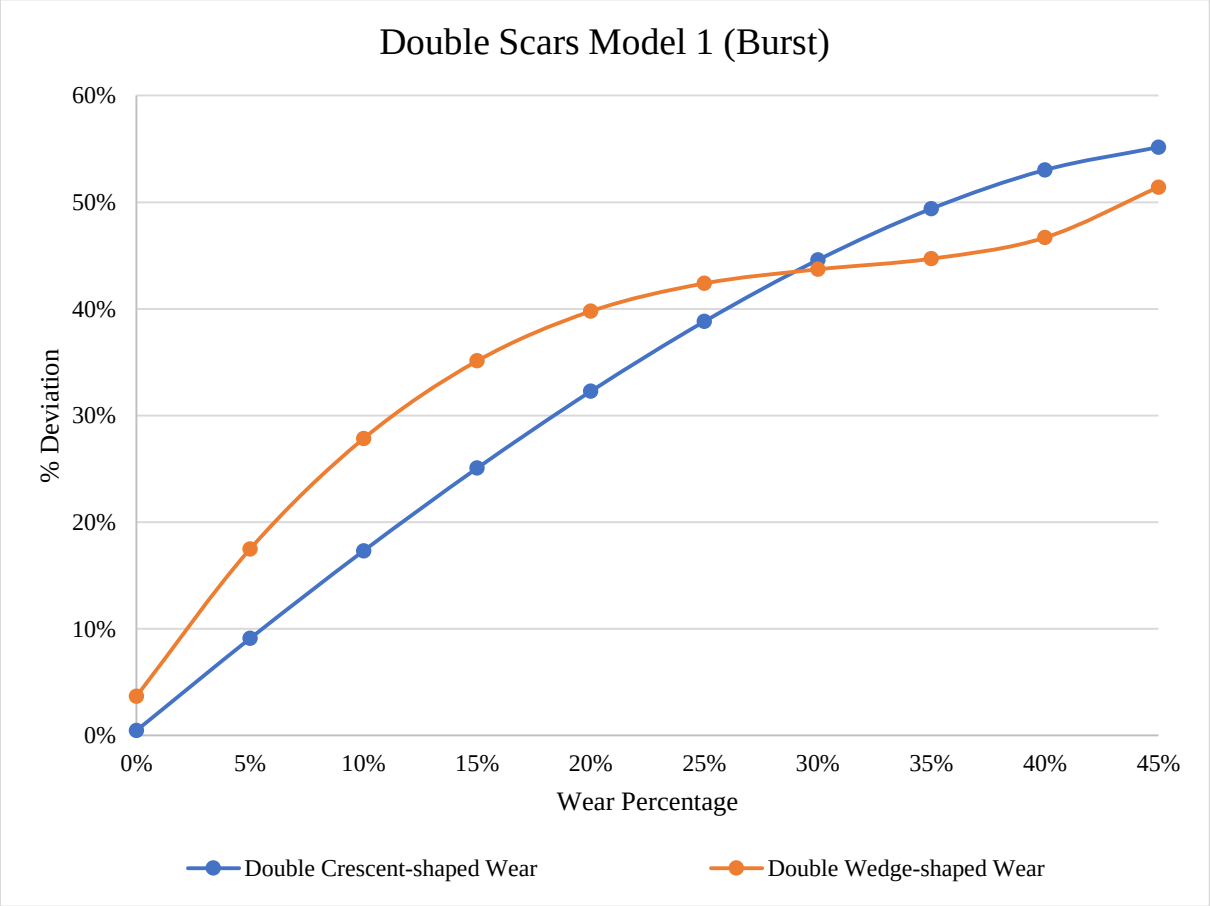

Figure 90. Deviation Percentage between API Burst/Barlow model and FEM simulation results for different double scars scenarios (model 1)

6.1.3 Double Scars Scenario (Model 2)

The modelling results of double scars case scenario (model 2) is presented in section 5.1.4. The model 2 scenarios in which the production casing has wear on the internal and external parts are analyzed on this section. Figure 91 presents the FEM simulation for three types of mixed-shape wear in which the first model has crescent-shaped wear on the external part of the casing and wedge-shaped wear on the internal part of the casing, the second model has wedge-shaped wear on the external part of the casing and crescent-shaped wear on the internal part of the casing, and the third model has rectangle-shaped wear on the external part of the casing and crescent-shaped wear on the internal part of the casing. The maximum deviation of the first,

second, and third model are 50%, 59%, and 56% respectively. All results from the three models show that as the wear percentage increases, the deviation percentage also increases. Three curves generated from the deviation percentage result and the production casing wear percentage show similar trends from 5% to 40%. However, there is a significant deviation increase in the second model when the second model curve surpasses the third model in the 45% casing wear case and becomes the largest deviation percentage in the double scars scenario for model 2. All of the results show significant deviation percentages from the API Burst/Barlow model. Thus, this indicates that the API Burst/Barlow model overestimates the maximum burst capacity of production casing with local wear.

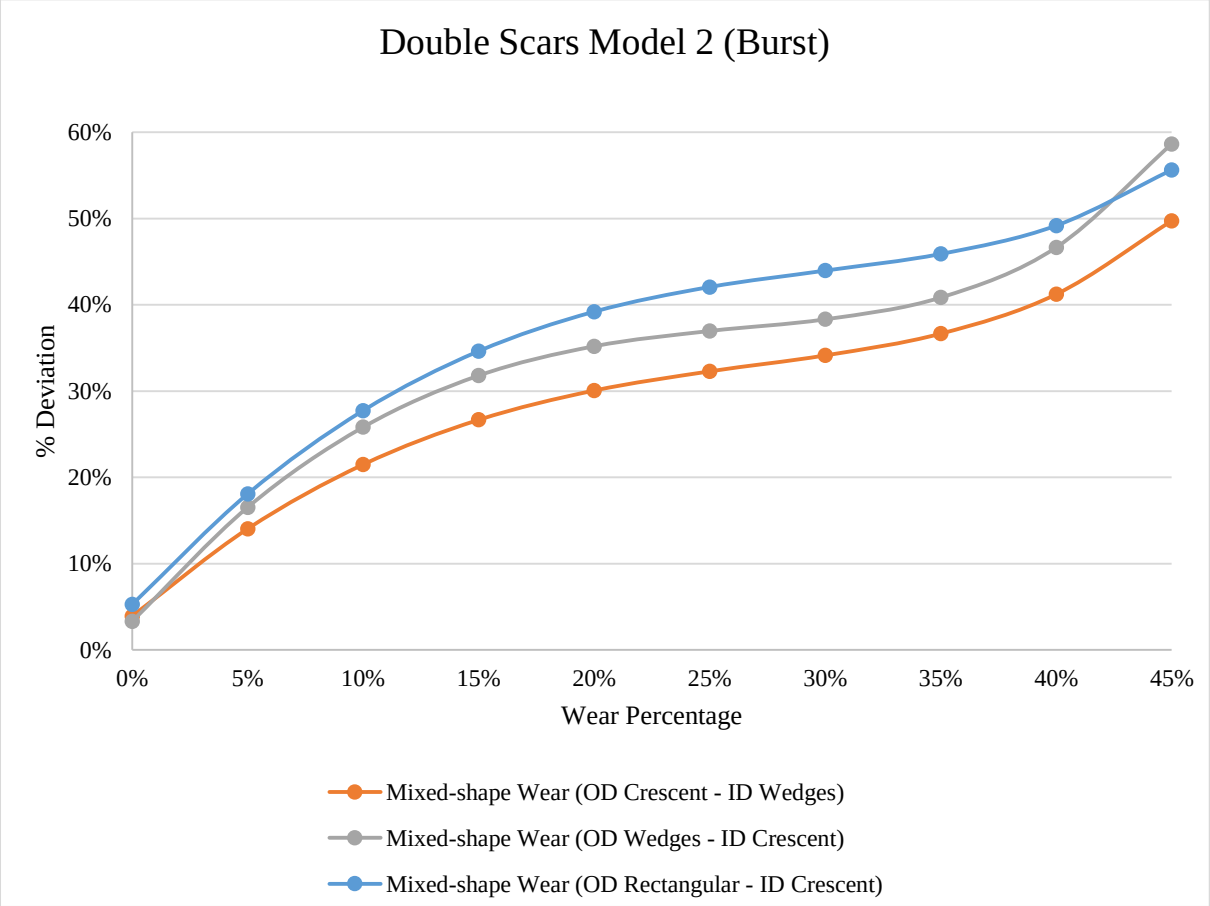

Figure 91. Deviation Percentage between API Burst/Barlow model and FEM simulation results for different double scars scenarios (model 2)

6.2 Collapse Case Analysis

As previously mentioned on the Result section 5.2.3, the result of the study of the effect of double scars on maximum collapse pressure limit of the production casing are presented in Appendix 1. The results are not presented in the Results section because the production casing

no longer has the thick-walled characteristic due to increasing wear that significantly reduces the wall thickness of the casing. Therefore, the results from the double scars scenarios cannot be compared to the triaxial collapse result. However, the discussion of the collapse case analysis included double scars scenarios in order to give the reader comprehensive information regarding the maximum deviation percentage which occurs in all the scenarios of FEM simulation for the locally worn production casing.

Similarly, the percentage of deviation for collapse analysis is calculated as:

$$\%\ Deviation = \frac{(FEM - Triaxial\ collapse)}{Triaxial\ collapse} * 100 \qquad (58)$$

where, *FEM* is the de-rated pressure for casing with local wear calculated based on FEM model and *Triaxial collapse* is the de-rated pressure for casing with local wear calculated based on triaxial collapse model.

6.2.1 Single Scar Scenario

The modelling results of single scar case scenario is presented in section 5.2.2. Figure 90 illustrates the deviation in the percentages of collapse strength of production casing. Single wedge-shaped wear with 0.3 unit width has the maximum deviation of 49%. The single wedge-shaped wear with 0.25 unit shows a maximum deviation of 44 % and the 0.2 unit width single wedge-shaped wear deviated up to 38%. All of the deviations show same trend in which the deviation percentage is higher as the wear depth increases. Therefore, all of the maximum deviations in the single wedge-shaped wear are observed in the 45% wear scenario.

For the crescent-shaped wear, a different deviation percentage trend is observed as shown in Figure 92. The single crescent-shaped wear has the maximum deviation of 51% in the 45% production casing wear scenario. To some extent, the curve trend of the deviation percentage for crescent-shaped wear is different compared to the single wedge-shaped wear curve. The maximum deviation percentage for crescent-shaped wear has a lower deviation than all three of the wedge-shaped wear scenarios in the 5% to 15% wear scenario and surpasses the maximum deviation percentage of the three types of wedge-shaped scenarios in the case of 20% to 30% wear. A higher maximum deviation percentage for crescent-shaped wear compared to wedge-shaped wear is discovered in the 35% to 45% wear scenario. In a similar way, the maximum deviation percentage for the single crescent-shaped wear also increases when the wear depth increases, and the maximum deviation percentage for single crescent-

shaped wear is in the 45% wear scenario. All of the types of single scar shape FEM simulations show lower de-rated collapse strength compared to the triaxial collapse model. Therefore, the triaxial collapse model overestimates the maximum collapse strength for locally damaged production casing.

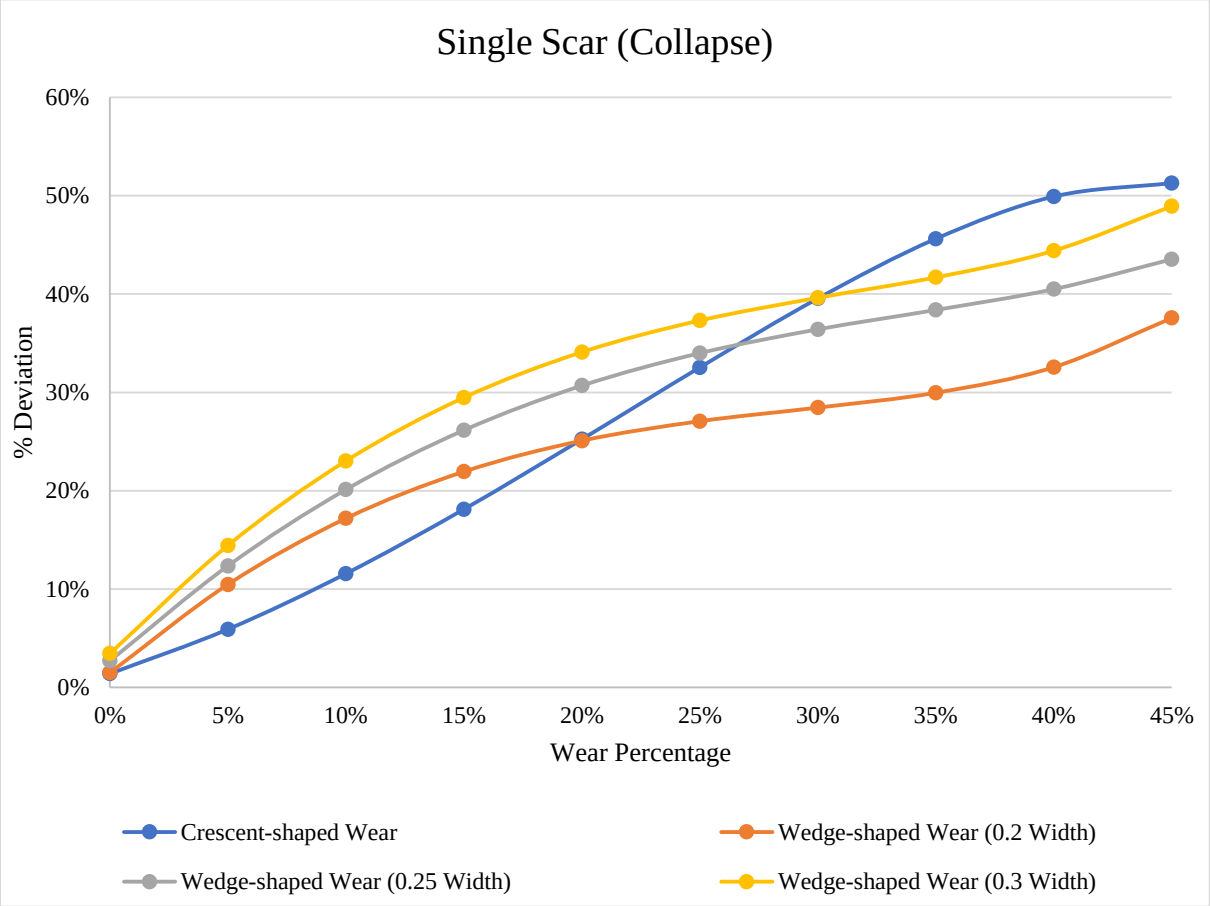

Figure 92. Deviation Percentage between triaxial collapse model and FEM simulation results for different single scar scenarios

6.2.2 Double Scars Scenario (Model 1)

The modelling results of double scars case scenario (model 1) is presented in section 5.2.3. The deviation percentage result analysis for the model 1 double scars scenario in which the model has both scars located on the internal part the production casing is shown on the Figure 93. The deviation percentage in both curves increases as the wear percentage on the casing increases. However, the trends for the double crescent-shaped wear and double wedge-shaped wear are considerably different. The double crescent-shaped has a lower deviation compared to the double wedge-shaped wear in the 5% to 25% wear scenario and a higher deviation in the 30% to 45% wear scenario. On the other hand, the double wedges wear shows a significant increase

in deviation percentage in the 5% to 25% wear and a smaller increase in the deviation percentage from 30% to 45%. The calculation results show that double crescent-shaped wear has a 55% maximum deviation, and a maximum deviation of 51% is observed in the double wedge-shaped wear case. The maximum deviations for both double scars models are observed in the maximum production casing wear scenario (45% casing wear). It can be concluded that the triaxial collapse model overestimates the maximum collapse strength of locally damaged production casing due to fact that the FEM simulation results for all scenarios have a significant deviation in percentage from the triaxial collapse model.

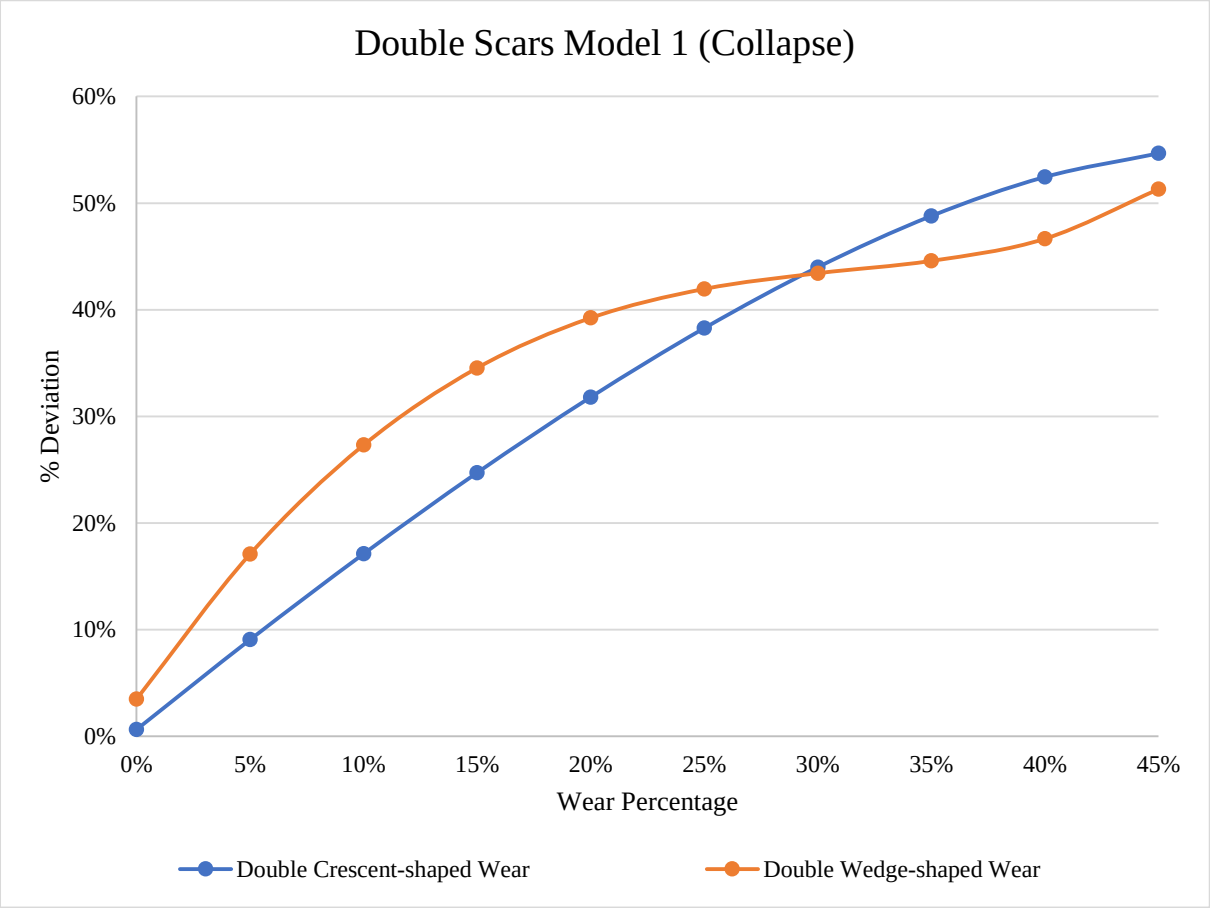

Figure 93. Deviation Percentage between triaxial collapse model and FEM simulation results for different double scars scenarios (model 1)

6.2.3 Double Scars Scenario (Model 2)

The modelling results of double scars case scenario (model 2) is presented in Appendix 1. The model 2 scenarios in which the production casing has wear on the internal part and external parts are analyzed on this section. Figure 94 presents the FEM simulation of the three types of mixed-shaped wear in which the first model has crescent-shaped wear on the external part of

the casing and wedge-shaped wear on the internal part of the casing, second model where it has wedge-shaped wear on the external part of the casing and crescent-shaped wear on the internal part of the casing, and third model has the rectangle-shaped wear on the internal part of the casing and crescent-shaped wear on the internal part of the casing. The maximum deviations from the triaxial collapse model of the first, second, and third model are 49%, 58%, and 55% respectively. All results from the three models show that as the wear percentage increases, the deviation percentage also increases. Three curves generated from the deviation percentage result and production casing wear percentage show similar trends from 5% to 40%. However, there is a significant increase in the deviation of the second model when the second model curve passes the third model in the 45% casing wear case and becomes the largest deviation percentage on the double scars scenario for model 2. All of the results show a significant deviation percentage from the triaxial collapse model. This clearly indicates that the triaxial collapse model overestimates the maximum collapse capacity of locally worn production casing.

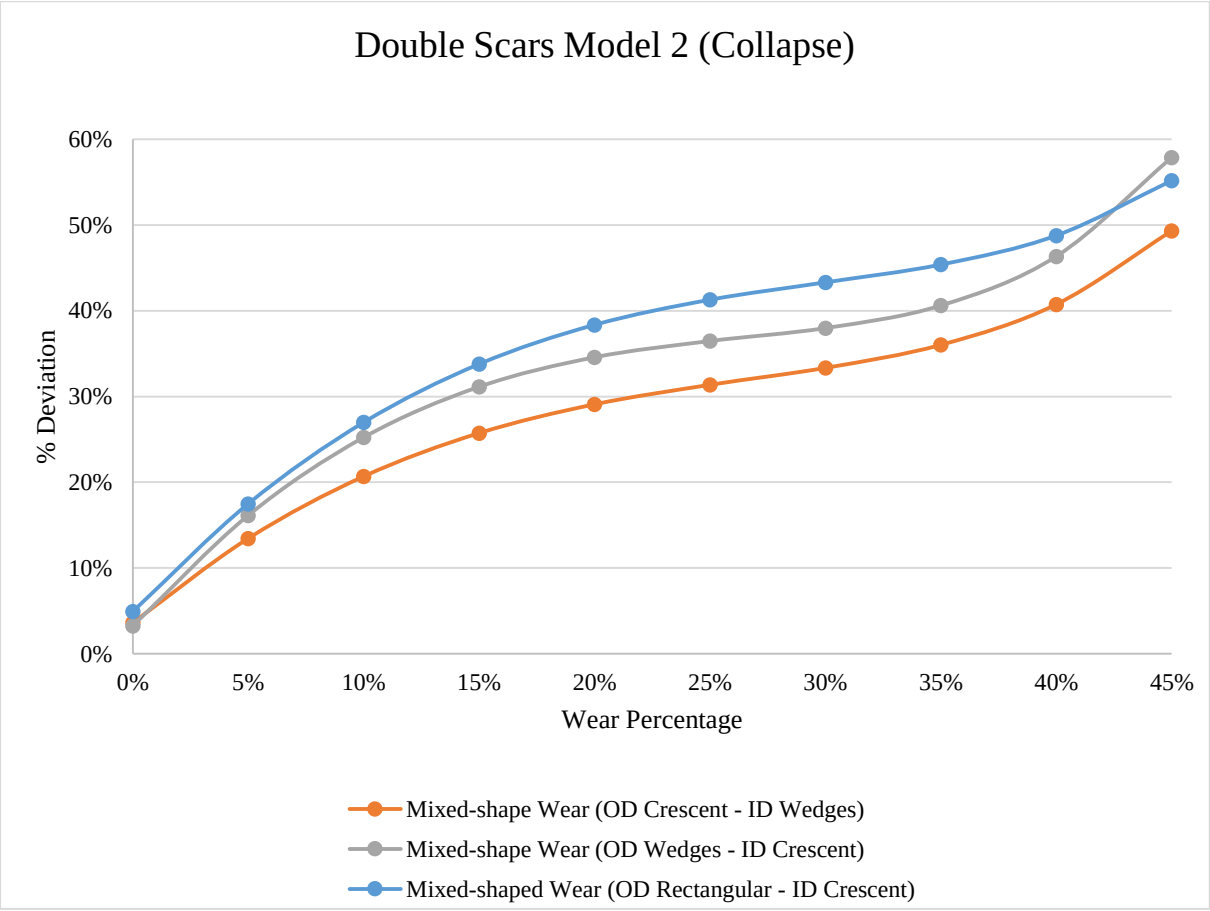

Figure 94. Deviation Percentage between triaxial model and FEM simulation results for different double scars scenarios (model 2)

The FEM models for simulations are generated based on the assumption of a symmetrical-shaped wear model, and bending stress on the production casing is neglected. A total of nine wear models are simulated using FEM analysis to investigate the effect of local wear on production casing. The FEM analysis simulation produces the maximum Von Mises stress due to the hoop, radial, and axial stresses which occur on the casing wall for each wear scenario. Furthermore, the maximum Von Mises stress results for each scenario from the FEM simulations are compared to the material yield strength after including the safety factor. Using the results of the data comparisons, the trend lines of the de-rated burst and collapse strengths of the production casing are generated by implementing linear interpolation. It should be noted that the FEM modelling and simulation results are only accurate for the specific parameter used in this particular study.

7. Summary and Conclusion

The prediction of maximum burst and collapse limit for production casing are very critical for well integrity. Wear on the tubing and casing contribute to reducing the maximum burst and pressure limits. In previous studies [1, 4, 5, 9], it was found that wear on the tubing and casing is dominated by local wear type. The common practice in the industry for the local wear damage tubular is by removing the damaged part to reduce the wall thickness uniformly and apply analytical models (API /Triaxial), which are derived based on uniform wall thickness [8]. By contrast, the FEM approach considers local wear as part of the analysis. This thesis analyses the locally worn production casing by implementing the FEM approximation concept using Abaqus software. The FEM simulation results are then compared to the results of the API Burst/Barlow and triaxial collapse models.

Based on the FEM simulation work carried out using the Abaqus software, the conclusions drawn from the results in this thesis are:

- The wear shape and wear location on the production casing have a considerable impact on the reduction of the burst and collapse pressure limits of production casing. The local wear model which gives the highest reduction of both burst and collapse limits is the model that has crescent-shaped wear on the internal part of the casing and wedge-shaped wear on the external part in the 45% wear scenario.
- Overall, all model 2 types that have wear on the external and internal parts of the casing have higher burst and collapse pressure limit reduction compared to the model 1 wear type (model 1 has both scars located on the internal part of the production casing).
- In the single wear scenario, the crescent-shaped wear has a higher burst and collapse pressure limit compared to the wedge-shaped wear model.
- Based on the FEM simulation results, there should be more awareness regarding not only local wear occurrence on the internal part of the casing but also local occurrence on the external part of the casing due to scratching and pitting corrosion when computing the de-rated burst and collapse pressure limit estimation for the production casing.
- The API Burst/Barlow model which is often used in the industry is found to be incompatible with locally worn production casing in both the single and double scars scenarios. The API Burst/Barlow results to predict the maximum safe operational

window are significantly higher than the result from FEM simulation for locally worn production casing.

- The triaxial collapse model is used to predict the maximum collapse pressure limit in this study. This model is chosen because the computation of the undamaged casing scenario using it is similar to the result of the maximum collapse pressure limit of the undamaged casing scenario in the FEM simulation.
- The triaxial collapse model results for collapse limit computation are only applicable for the single wear scenario. This limitation occurs due to the fact that the production casing no longer has the thick-walled characteristic due to increasing wear that significantly reduces the wall thickness of the casing in the double scars scenario. Therefore, the results from the double scars scenarios cannot be compared to the triaxial collapse model results.
- In the locally worn production casing scenario, the maximum collapse pressure limit computed by the using triaxial collapse model is higher than the FEM simulation result for locally worn production casing in the single wear scenario.
- Different deviation percentage curve trend lines are observed between crescent-shaped wear and wedge-shaped wear in both the single scar and double scars scenarios.
- The results from the API Burst/Barlow model for computing maximum burst limit and the triaxial model for computing maximum collapse limit for production casing are over-predicted compared to the FEM simulation results. It can be concluded that the current models which are often used in industry practice are not applicable when calculating burst and collapse limits for locally worn production casing.

8. References

1. Vu, T., *Finite Element Method Simulation and Modeling of Tubing Wear*. 2015, University of Stavanger, Norway.
2. Wu, J. and M. Zhang. *Casing Burst Strength after Casing Wear*. in *SPE Production Operations Symposium*. 2005. Society of Petroleum Engineers.
3. Standard, N., *Well Integrity in Drilling and Well Operations.* D-010, rev, 2004. **3**.
4. Shen, Z., F.E. Beck, and K. Ling, *The Mechanism of Wellbore Weakening in Worn Casing-Cement-Formation System.* Journal of Petroleum Engineering, 2014. **2014**.
5. Eriksen, J.V., *Analysis of the de-rated Burst and Collapse Resistance of a Locally Worn Tubing by using the Finite Element Method and API models*. 2017, University of Stavanger, Norway.
6. Vignes, B. and B.S. Aadnoy. *Well-Integrity Issues Offshore Norway*. in *IADC/SPE Drilling Conference*. 2008. Society of Petroleum Engineers.
7. Watson, T.L. and S. Bachu. *Identification of Wells with High CO2-Leakage Potential in Mature Oil Fields Developed for CO2-Enhanced Oil Recovery*. in *SPE Symposium on Improved Oil Recovery*. 2008. Society of Petroleum Engineers.
8. Bellarby, J., *Well Completion Design*. Vol. 56. 2009: Elsevier.
9. Kaldal, G.S., et al. *Collapse Analysis of the Casing in High Temperature Geothermal Wells*. in *Proceedings, 38th Workshop on Geothermal Reservoir Engineering, Stanford University, Stanford, CA*. 2013.
10. Nagy, M. *Casing Wear evaluation through simulation*. 2013 [cited 2018 30 May]; Available from: http://connect.spe.org/HigherLogic/System/DownloadDocumentFile.ashx?DocumentFileKey=02de3cd3-8384-4ba6-9b83-fd9be93a3743.
11. Bradley, W.B. and J.E. Fontenot, *The Prediction and Control of Casing Wear (includes associated papers 6398 and 6399).* Journal of Petroleum Technology, 1975. **27**(02): p. 233-245.
12. Haning, M., A.P.J. Doherty, and A. House. *3D Non-Linear FEA to Determine Burst and Collapse Capacity of Eccentrically Worn Casing*. in *CEED Seminar Proceedings*. 2012.
13. Irawan, S., et al. *Effect of Wear on The Burst Strength of L-80 Steel Casing*. in *IOP Conference Series: Materials Science and Engineering*. 2015. IOP Publishing.

14. Agonafir, M.B., *Corrosion and Prevention (Control) Methods*. 2017, University of Stavanger: Norway.
15. Puspitarini, N., *Uniform Corrosion and Its Effect on Tubing Simulation Study*. 2017, University of Stavanger, Norway.
16. Ebbing, D. and S.D. Gammon, *General Chemistry*. 2016: Cengage Learning.
17. Rothwell, N. and M. Tullmin, *The Corrosion Monitoring Handbook*. 2000: Coxmoor.
18. Corrosion Doctors. *Crevice Corrosion*. 2018 [cited 2018 2 June]; Available from: https://corrosion-doctors.org/Forms-crevice/Crevice.html.
19. Corrosion Clinic. *Intergranular Corrosion (Cracking)*. 2018 [cited 2018 30 May]; Available from: http://www.corrosionclinic.com/types_of_corrosion/intergranular_corrosion_cracking.html.
20. Koteeswaran, M., *CO2 and H2S Corrosion in Oil Pipelines*. 2010, University of Stavanger, Norway.
21. Goodnight, R. and J. Barret. *Oil-well Casing Corrosion*. in *Drilling and Production Practice*. 1956. American Petroleum Institute.
22. Agonafir, M.B., *Grading, Tube stress and Failure analysis*. 2017, University of Stavanger: Norway. p. 77.
23. Boresi, A.P., R.J. Schmidt, and O.M. Sidebottom, *Advanced Mechanics of Materials*. Vol. 6. 1993: Wiley New York.
24. Aadnøy, B.S., K. Larsen, and P.C. Berg, *Analysis of Stuck Pipe in Deviated Boreholes.* Journal of Petroleum Science and Engineering, 2003. **37**(3-4): p. 195-212.
25. Josh Parker. *Normal Stress, Bending Stress, & Shear Stress*. 2018 [cited 2018 30 May]; Available from: http://www.strucalc.com/normal-stress-bending-stress-shear-stress/.
26. Aasen, J.A. and B.S. Aadnoy, *Three-Dimensional Well Tubular Design Improves Margins in Critical Wells.* Journal of Petroleum Science and Engineering, 2007. **56**(4): p. 232-240.
27. Aadnoy, B.S., *Modern Well Design*. 2010: CRC Press.
28. International, S. *Strength of Casing and Tubing*. 2018 [cited 2018 30 May]; Available from: http://petrowiki.org/Strength_of_casing_and_tubing.
29. API, T., *5C3*. 2008, Technical Report on Equations and Calculations for Casing, Tubing, and Line Pipe Used as Casing or Tubing.

30. Roylance, D., *Introduction to Fracture Mechanics.* Massachusetts Institute of Technology, Cambridge, 2001. **1**.
31. de Weck, O. and I.Y. Kim, *Finite Element Method.* Engineering Design and Rapid Prototyping, 2004.
32. Felippa, C.A., *Introduction to Finite Element Methods.* University of Colorado, USA, 2001.
33. Morgan, E.F. and M.L. Bouxsein, *Use of Finite Element Analysis to Assess Bone Strength.* BoneKEy-Osteovision, 2005. **2**(12): p. 8-19.

Appendix 1

Double Scars Collapse Scenarios

The modelling of two scars scenarios in the production casing is divided into two types. In model 1, both scars occur on the internal part of the production casing and in model 2 where one scar located on the internal part of the production casing and other scar located on the external part the production casing.

Model 1

Double Crescent-shaped Wear

Double Crescent-shaped Wear (10% Wear Model)

For the 10% double crescent-shaped wear model, the maximum external pressure before the production casing started to yield is 6801 psi. Compared to the reference model (0% wear), there is a reduction by 24% of the maximum external pressure in the production casing.

Double Crescent-shaped Wear (30% Wear Model)

In the 30% double crescent-shaped wear model, the maximum external pressure before the production casing material yielded is 3348 psi. The simulated result has a reduction of 63% from the undamaged reference model (0% wear).

Double Crescent-shaped Wear (45% Wear Model)

The result of the 45% double crescent-shaped wear model shows that the maximum external yield pressure for the production casing is 2308 psi. This simulated result is a 74% reduction from the reference model (0% wear).

Collapse Pressure Limits Results

Figure 95 presents the linear slopes for the wear percentages of the different external pressures for all simulated scenarios. The maximum external yield pressure for the production casing decreases as the wear percentage increases. Table 29 shows the maximum external yield pressure of the production casing for all simulated wear percentage scenarios, from 0% to 45%. The maximum external yield pressure is obtained by solving the linear interpolation.

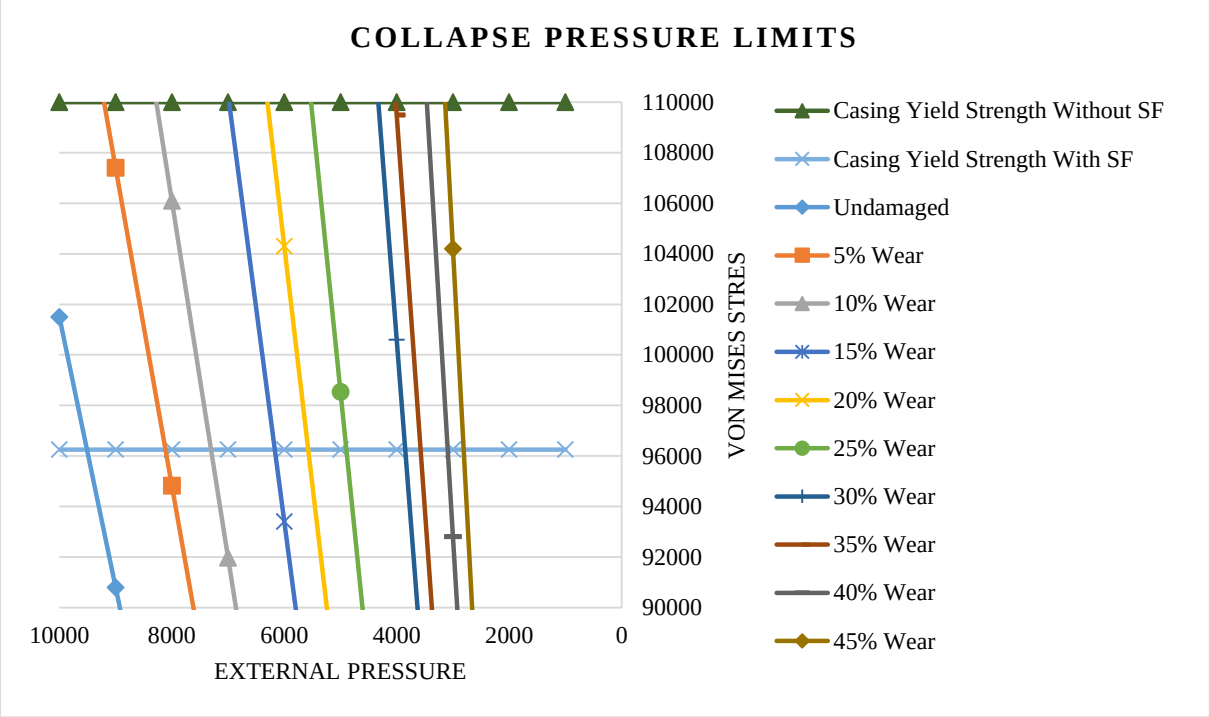

Figure 95. External pressure with respective Von Mises stress for different wear depths (double crescent-shaped wear model)

Table 29. Linear Interpolation for Maximum External Pressure

Wear (%)	Collapse Pressure (psi)
0%	9005
5%	7615
10%	6801
15%	5668
20%	5076
25%	4396
30%	3348
35%	3075
40%	2593
45%	2308

Figure 96 presents the safe and failure zones for the maximum operating external yield pressure. The area below the curve represents the safe zone, while the area above the curve is the failure zone. The collapse pressure model developed from the simulation is also shown.

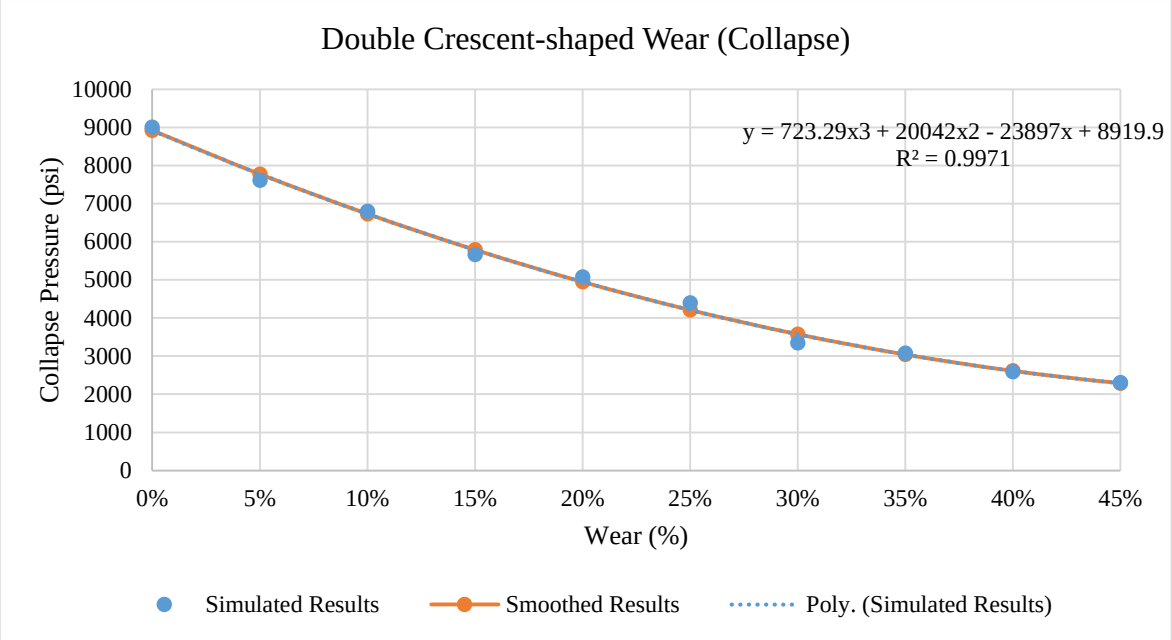

Figure 96. Safe and failure zones for maximum external pressure on double crescent-shaped wear

The collapse pressure model from the simulation is:

$$P_{collapse} = -723.29\ x\ Wear^3 + 20042\ x\ Wear^{\ 2} - 23897\ x\ Wear + 8919.9 \qquad (59)$$

The coefficient of determination of this model (R^2) is 0.9971. This value suggests that the data from the simulation fit the statistical model. This simulated model already includes the safety factor.

Double Wedge-shaped Wear

Double Wedge-shaped Wear (10% Wear Model)

For the 10% double wedge-shaped wear model, the maximum external pressure before the production casing started to yield is 5407 psi. Compared to the reference model (0% wear), there is a reduction by 40% of the maximum external pressure in the production casing.

Double Wedge-shaped Wear (30% Wear Model)

In the 30%, double wedge-shaped wear model, the maximum external pressure before the production casing material yielded is 3385 psi. The simulated result is a reduction of 62% from the undamaged reference model (0% wear).

Double Wedge-shaped Wear (45% Wear Model)

The result of the 45% double wedge-shaped wear model shows that the maximum external yield pressure for the production casing is 2251 psi. This simulated result shows a 75% reduction from the reference model (0% wear).

Collapse Pressure Limits Results

Figure 97 shows the linear slopes for the wear percentages of different external pressures for all simulated scenarios. The maximum external yield pressure for the production casing decreases as the wear percentage increases. Table 30 presents the maximum external yield pressure of the production casing for all simulated wear percentage scenarios, from 0% to 45%. The maximum external yield pressure is obtained by solving the linear interpolation.

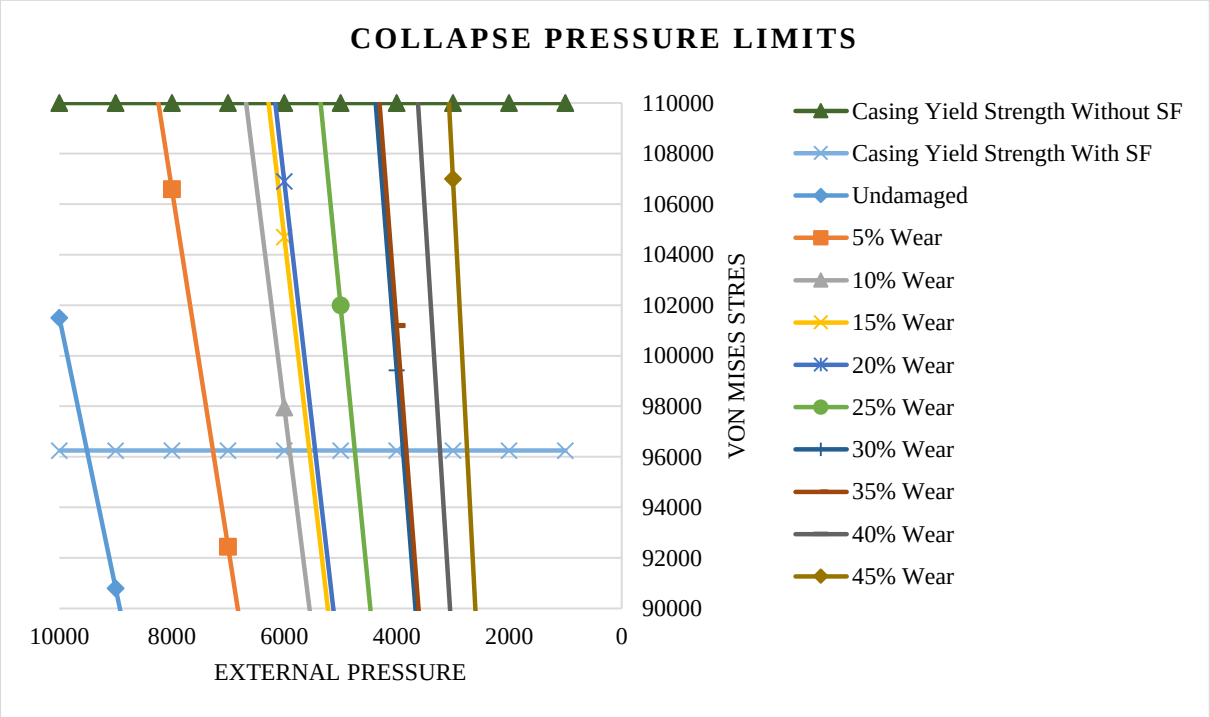

Figure 97. External pressure with respective Von Mises stress for different wear depths (double wedge-shaped wear model)

Table 30. Linear Interpolation for Maximum External Pressure

Wear (%)	Collapse Pressure (psi)
0%	9005
5%	6771
10%	5407
15%	5055
20%	4951
25%	4246
30%	3385
35%	3328
40%	2726
45%	2251

Figure 98 presents the safe and failure zones for the maximum operating external pressure. The area below the curve represents the safe zone, while the area above the curve is the failure zone. The collapse pressure model developed from the simulation is also shown.

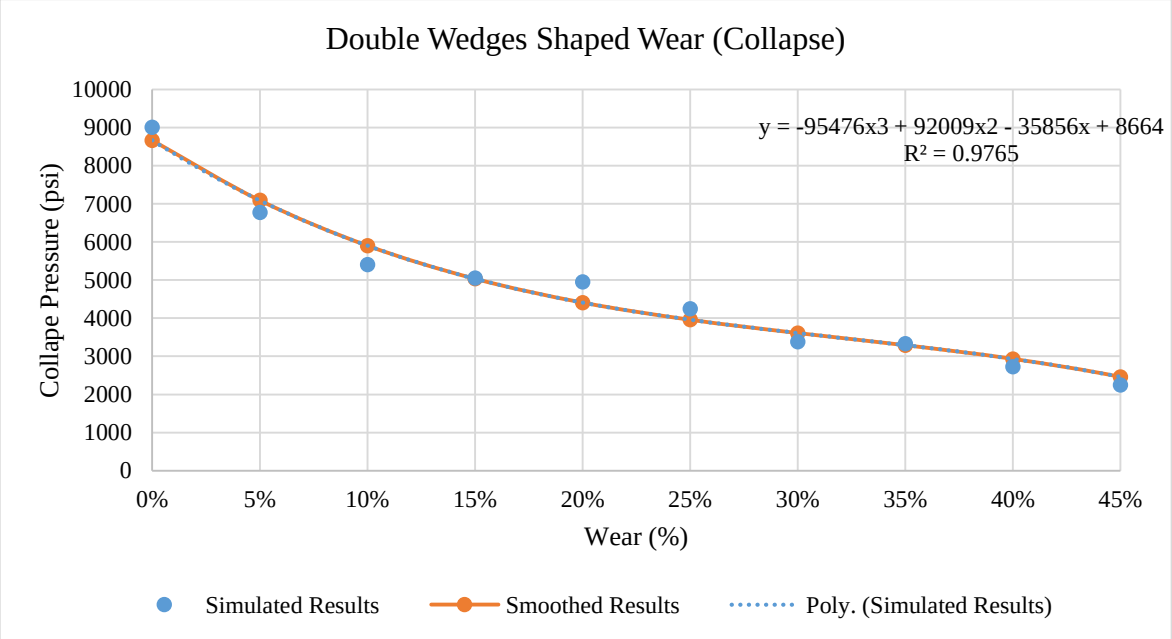

Figure 98. Safe and failure zones for maximum external pressure on double wedge-shaped wear

The collapse pressure model from the simulation is:

$$P_{collapse} = -95476\ x\ Wear^3 + 92009\ x\ Wear^2 - 35856\ x\ Wear + 8664 \qquad (60)$$

The coefficient of determination of this model (R^2) is 0.9765. This value suggests that the data from the simulation fit the statistical model. This simulated model already includes the safety factor.

Model 2

Wedge-shaped Wear (inside) and Crescent-shaped Wear (outside)

Wedge-shaped Wear (inside) and Crescent-shaped Wear (outside) (10% Wear Model)

The result from the 10% wear model shows that the maximum external yield pressure for the production casing is 6050 psi. This simulated result has a 33% reduction from the reference model (0% wear).

Wedge-shaped Wear (inside) and Crescent-shaped Wear (outside) (30% Wear Model)

For the 30% wear model, the maximum external pressure before the production casing started to yield is 4116 psi. Compared to the reference model (0% wear), there is a reduction by 54% of the maximum external pressure in the production casing.

Wedge-shaped Wear (inside) and Crescent-shaped Wear (outside) (45% Wear Model)

In the 45% wear model, the maximum external pressure before the production casing material yielded is 2399 psi. The simulated result has a reduction of 73% from the undamaged reference model (0% wear).

Collapse Pressure Limits Results

Figure 99 represents the linear slopes for the wear percentages of different external pressures for all simulated scenarios. The maximum external yield pressure for the production casing decreases as the wear percentage increases. Table 31 shows the maximum external yield pressure of the production casing for all simulated wear percentage scenarios, from 0% to 45%. The maximum external yield pressure is obtained by solving the linear interpolation.

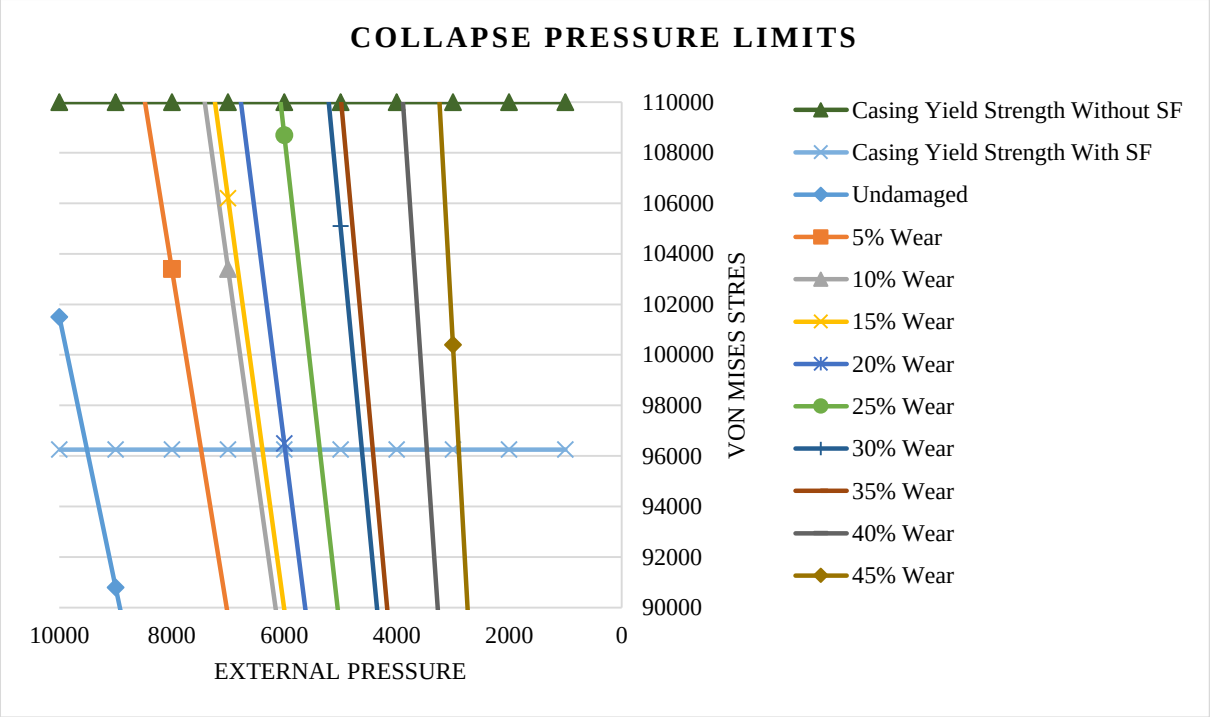

Figure 99. External pressure with respective Von Mises stress for different wear depths (mixed-shape wear model)

Table 31. Linear Interpolation for Maximum External Pressure

Wear (%)	Collapse Pressure (psi)
0%	9005
5%	6982
10%	6050
15%	5890
20%	5486
25%	4881
30%	4116
35%	3920
40%	2965
45%	2399

Figure 100 presents the safe and failure zones for the maximum operating external yield pressure. The area below the curve represents the safe zone, while the area above the curve is the failure zone. The collapse pressure model developed from the simulation is also shown.

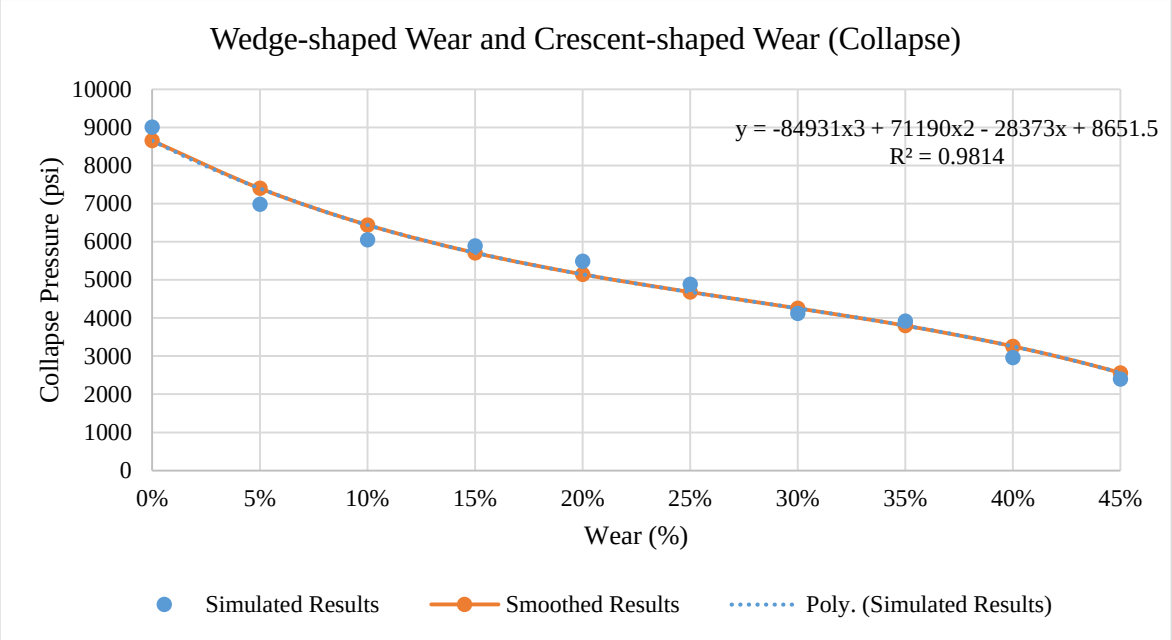

Figure 100. Safe and failure zones for maximum external pressure on mixed-shape wear

The collapse pressure model from the simulation is:

$$P_{collapse} = -84931\ x\ Wear^3 + 71190\ x\ Wear^{\ 2} - 28373\ x\ Wear + 8651.5 \qquad (61)$$

The coefficient of determination of this model (R^2) is 0.9814. This value suggests that the data from the simulation fit the statistical model. This simulated model already includes the safety factor.

Crescent-shaped Wear (inside) and Wedge-shaped Wear (outside)

Crescent-shaped Wear (inside) and Wedge-shaped Wear (outside) (10% Wear Model)

The result from the 10% wear model shows that the maximum external yield pressure for the production casing is 5723 psi. This simulated result has a 36% reduction from the reference model (0% wear).

Crescent-shaped Wear (inside) and Wedge-shaped Wear (outside) (30% Wear Model)

For the 30% wear model, the maximum external pressure before the production casing started to yield is 3662 psi. Compared to the reference model (0% wear), there is a reduction by 59% of the maximum external pressure in the production casing.

Crescent-shaped Wear (inside) and Wedge-shaped Wear (outside) (45% Wear Model)

In the 45% wear model, the maximum external pressure before the production casing material yielded is 2384 psi. The simulated result has a reduction of 74% from the undamaged reference model (0% wear).

Collapse Pressure Limits Results

Figure 101 represents the linear slopes for the wear percentages of the different external pressures for all simulated scenarios. The maximum external yield pressure for the production casing decreases as the wear percentage increases. Table 32 presents the maximum external yield pressure of the production casing for all simulated wear percentages scenario, from 0% to 45%. The maximum external yield pressure is obtained by solving the linear interpolation.

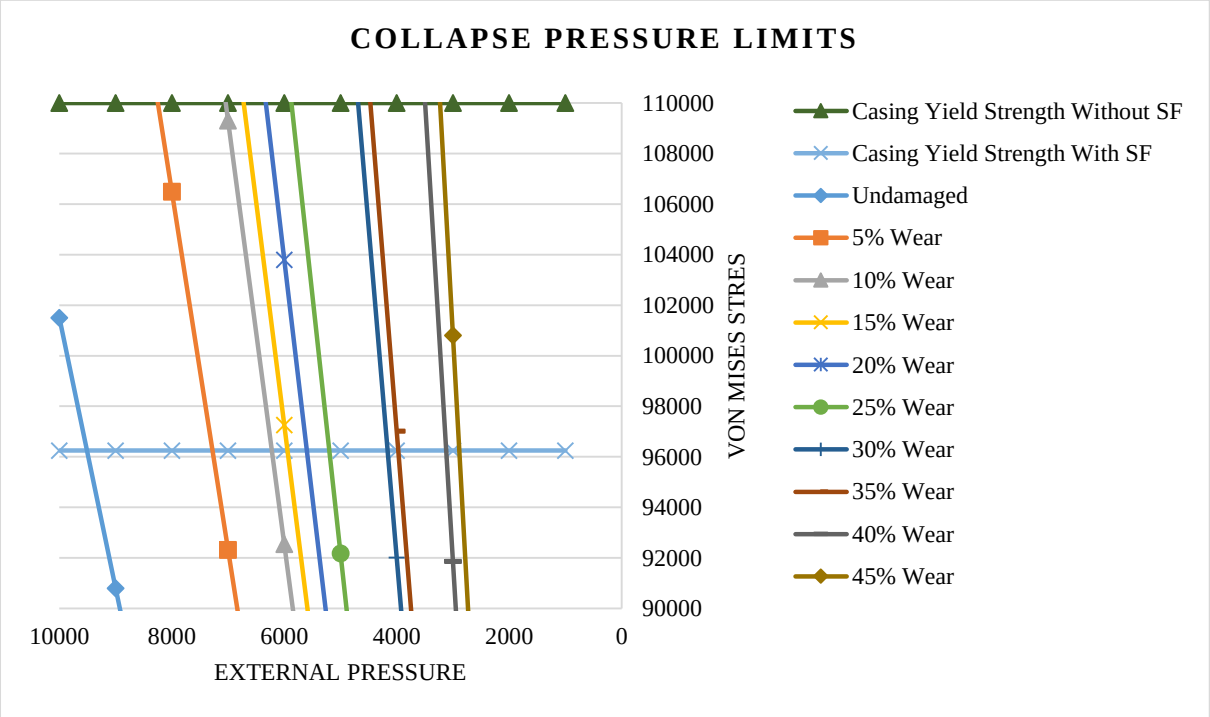

Figure 101. External pressure with respective Von Mises stress for different wear depths (mixed-shape wear model)

Table 32. Linear Interpolation for Maximum External Pressure

Wear (%)	Collapse Pressure (psi)
0%	9005
5%	6773
10%	5723
15%	5440
20%	5101
25%	4694
30%	3662
35%	3466
40%	2616
45%	2384

Figure 102 shows the safe and failure zones for the maximum operating external yield pressure. The area below the curve represents the safe zone, while the area above the curve is the failure zone. The collapse pressure model developed from the simulation is also shown.

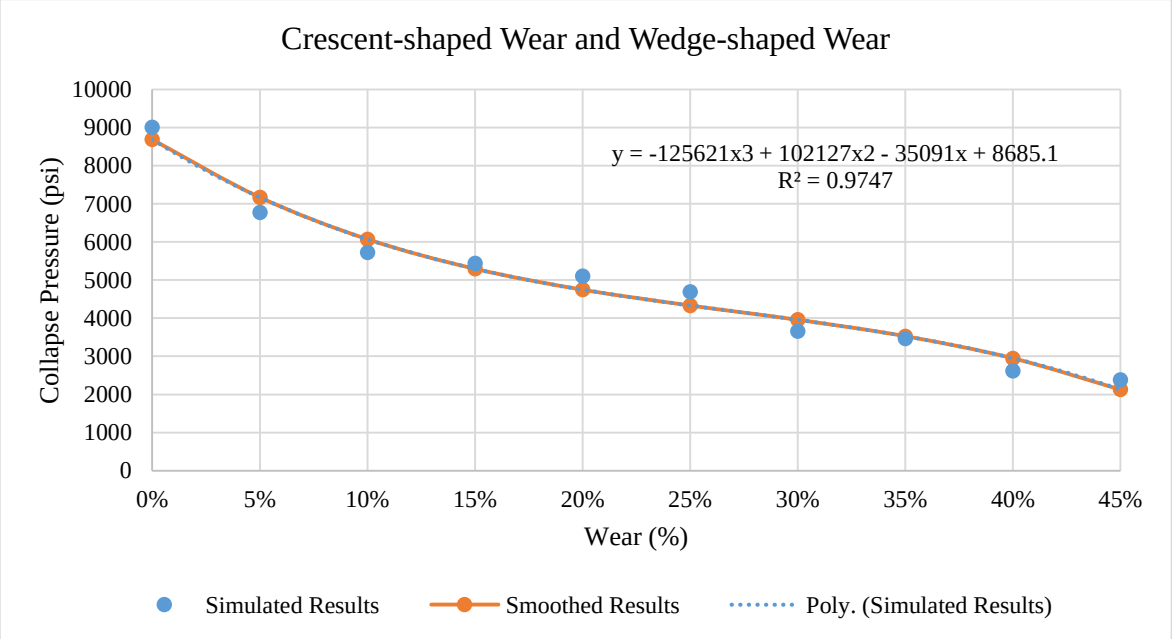

Figure 102. Safe and failure zones for maximum external pressure on mixed-shape wear

The collapse pressure model from the simulation is:

$$P_{collapse} = -125621\ x\ Wear^3 + 102127\ x\ Wear^2 - 35091\ x\ Wear + 8685.1 \quad (62)$$

The coefficient of determination of this model (R^2) is 0.9747. This value suggests that the data from the simulation fit the statistical model. This simulated model already includes the safety factor.

Crescent-shaped Wear (inside) and Rectangle-shaped Wear (outside)

Crescent-shaped Wear (inside) and Rectangle-shaped Wear (outside) (10% Wear Model)

For the 10% wear model, the maximum external pressure before the production casing started to yield is 5680 psi. Compared to the reference model (0% wear), there is a reduction by 37% of the maximum external pressure in the production casing.

Crescent-shaped Wear (inside) and Rectangle-shaped Wear (outside) (30% Wear Model)

In the 30% wear model, the maximum external pressure before the production casing material yielded is 3495 psi. The simulated result has a reduction of 61% from the undamaged reference model (0% wear).

Crescent-shaped Wear (inside) and Rectangle-shaped Wear (outside) (45% Wear Model)

The result from the 45% wear model shows that the maximum external yield pressure for the production casing is 2197 psi. This simulated result is a 76% reduction from the reference model (0% wear).

Collapse Pressure Limits Results

Figure 103 represents the linear slopes for the wear percentages of different external pressures for all simulated scenarios. The maximum external yield pressure for the production casing decreases as the wear percentage increases. Table 33 shows the maximum external yield pressure of the production casing for all simulated wear percentage scenarios, from 0% to 45%. The maximum external yield pressure is obtained by solving the linear interpolation.

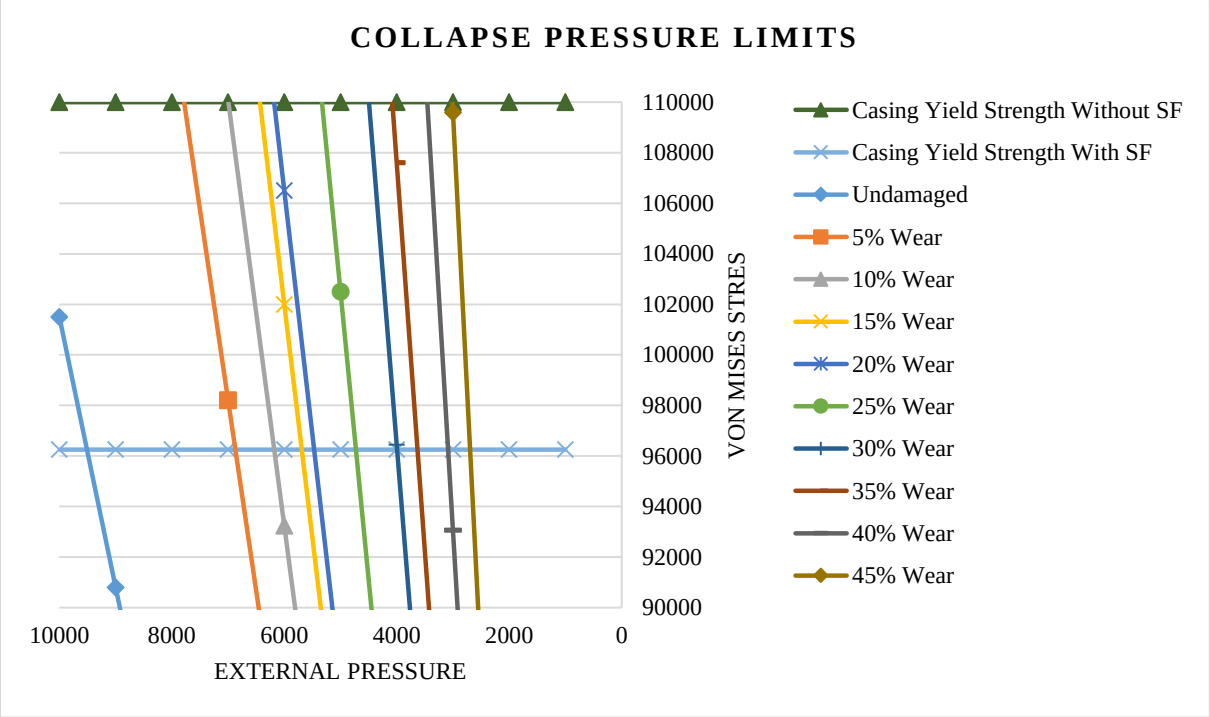

Figure 103. External pressure with respective Von Mises stress for different wear depths (mixed-shape wear model)

Table 33. Linear Interpolation for Maximum External Pressure

Wear (%)	Collapse Pressure (psi)
0%	9005
5%	6371
10%	5680
15%	5189
20%	4969
25%	4225
30%	3495
35%	3137
40%	2593
45%	2197

Figure 104 presents the safe and failure zones for the maximum operating external pressure. The area below the curve represents the safe zone, while the area above the curve is the failure zone. The collapse pressure model developed from the simulation is also shown.

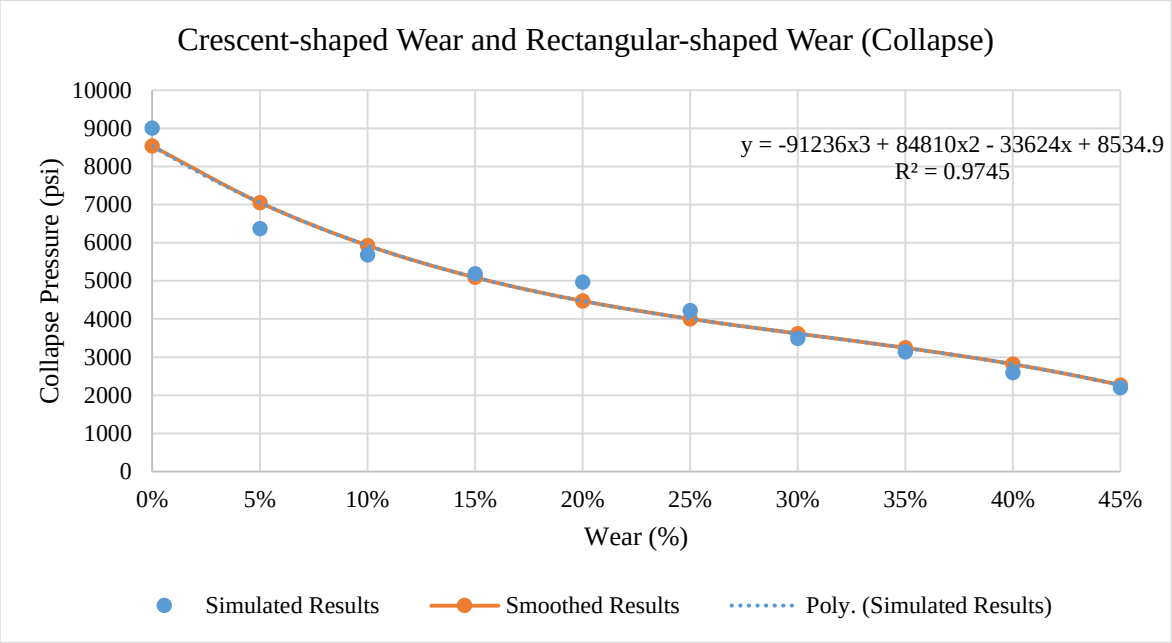

Figure 104. Safe and failure zones for maximum external pressure on mixed-shape wear

The collapse pressure model from the simulation is:

$$P_{collapse} = -91236\ x\ Wear^3 + 84810\ x\ Wear^{\,2} - 33624\ x\ Wear + 8534.9 \qquad (63)$$

The coefficient of determination of this model (R^2) is 0.9745. This value suggests that the data from the simulation fit the statistical model. This simulated model already includes the safety factor.

Appendix 2

A. API Burst/Barlow Model and FEM Simulation Results for All Wear Models

1. Single Scar Scenario

Table 34. API Burst/Barlow Model and FEM Simulation Data for Single Crescent-shaped Wear Model

Wear (%)	Simulated Results (psi)	Smoothed Results (psi)	API Burst/Barlow (psi)
0%	9470	9267	9440
5%	8067	8391	8968
10%	7344	7465	8496
15%	6662	6525	8024
20%	5869	5605	7552
25%	4775	4738	7080
30%	3749	3961	6608
35%	3275	3306	6136
40%	2858	2808	5664
45%	2463	2501	5192

Table 35. API Burst/Barlow Model and FEM Simulation Data for 0.2 Width Single Wedge-shaped Wear Model

Wear (%)	Simulated Results (psi)	Smoothed Results (psi)	API Burst/Barlow (psi)
0%	9470	9298	9440
5%	7821	8009	8968
10%	6823	7000	8496
15%	6332	6217	8024
20%	5572	5605	7552
25%	5180	5112	7080
30%	4859	4682	6608
35%	4488	4262	6136
40%	3396	3797	5664
45%	3075	3234	5192

Table 36. API Burst/Barlow Model and FEM Simulation Data for 0.25 Width Single Wedge-shaped Wear Model

Wear (%)	Simulated Results (psi)	Smoothed Results (psi)	API Burst/Barlow (psi)
0%	9470	9187	9440
5%	7481	7812	8968
10%	6446	6724	8496
15%	5988	5872	8024
20%	5388	5208	7552
25%	4770	4682	7080
30%	4429	4243	6608
35%	3941	3843	6136
40%	2972	3432	5664
45%	2888	2961	5192

Table 37. API Burst/Barlow Model and FEM Simulation Data for 0.3 Width Single Wedge-shaped Wear Model

Wear (%)	Simulated Results (psi)	Smoothed Results (psi)	API Burst/Barlow (psi)
0%	9470	9128	9440
5%	7133	7665	8968
10%	6383	6518	8496
15%	5778	5632	8024
20%	5231	4951	7552
25%	4460	4418	7080
30%	3945	3978	6608
35%	3673	3575	6136
40%	2859	3152	5664
45%	2596	2653	5192

2. Double Scars Scenario (Model 1)

Table 38. API Burst/Barlow Model and FEM Simulation Data for Double Crescent-shaped Wear Model

Wear (%)	Simulated Results (psi)	Smoothed Results (psi)	API Burst/Barlow (psi)
0%	9470	9396	9440
5%	8013	8153	8968
10%	7092	7025	8496
15%	5890	6013	8024
20%	5236	5115	7552
25%	4515	4332	7080
30%	3434	3662	6608
35%	3157	3105	6136
40%	2635	2661	5664
45%	2339	2328	5192

Table 39. API Burst/Barlow Model and FEM Simulation Data for Double Wedge-shaped Wear Model

Wear (%)	Simulated Results (psi)	Smoothed Results (psi)	API Burst/Barlow (psi)
0%	9470	9093	9440
5%	7044	7400	8968
10%	5590	6131	8496
15%	5227	5206	8024
20%	5150	4548	7552
25%	4389	4079	7080
30%	3476	3720	6608
35%	3431	3393	6136
40%	2797	3020	5664
45%	2286	2523	5192

3. Double Scars Scenario (Model 2)

Table 40. API Burst/Barlow Model and FEM Simulation Data for Mixed-shape Wear Model (ID Wedge-shaped Wear and OD Crescent-shaped Wear)

Wear (%)	Simulated Results (psi)	Smoothed Results (psi)	API Burst/Barlow (psi)
0%	9470	9070	9440
5%	7203	7709	8968
10%	6283	6670	8496
15%	6073	5884	8024
20%	5687	5281	7552
25%	4969	4794	7080
30%	4198	4352	6608
35%	4021	3887	6136
40%	3022	3329	5664
45%	2436	2609	5192

Table 41. API Burst/Barlow Model and FEM Simulation Data for Mixed-shape Wear Model (ID Crescent-shaped Wear and OD Wedge-shaped Wear)

Wear (%)	Simulated Results (psi)	Smoothed Results (psi)	API Burst/Barlow (psi)
0%	9470	9126	9440
5%	7058	7485	8968
10%	5920	6302	8496
15%	5637	5472	8024
20%	5273	4894	7552
25%	4839	4462	7080
30%	3778	4076	6608
35%	3542	3629	6136
40%	2673	3021	5664
45%	2421	2147	5192

Table 42. API Burst/Barlow Model and FEM Simulation Data for Mixed-shape Wear Model (ID Crescent-shaped Wear and OD Rectangle-shaped Wear)

Wear (%)	Simulated Results (psi)	Smoothed Results (psi)	API Burst/Barlow (psi)
0%	9470	8942	9440
5%	6565	7346	8968
10%	5881	6138	8496
15%	5364	5245	8024
20%	5127	4591	7552
25%	4336	4101	7080
30%	3580	3703	6608
35%	3204	3320	6136
40%	2630	2878	5664
45%	2223	2303	5192

B. Triaxial Model and FEM Simulation Data for All Wear Models

1. Single Scar Scenario

Table 43. Triaxial Collapse Model and FEM Simulation Data for Single Crescent-shaped Wear Model

Wear (%)	Simulated Results (psi)	Smoothed Results (psi)	Triaxial Collapse (psi)
0%	9005	8852	8977
5%	7829	8044	8550
10%	7040	7181	8121
15%	6368	6297	7690
20%	5705	5425	7256
25%	4632	4600	6820
30%	3660	3857	6381
35%	3204	3230	5940
40%	2806	2753	5497
45%	2422	2461	5052

Table 44. Triaxial Collapse Model and FEM Simulation Data for 0.2 Width Single Wedge-shaped Wear Model

Wear (%)	Simulated Results (psi)	Smoothed Results (psi)	Triaxial Collapse (psi)
0%	9005	8843	8977
5%	7488	7655	8550
10%	6531	6725	8121
15%	6151	6002	7690
20%	5357	5435	7256
25%	5053	4974	6820
30%	4750	4566	6381
35%	4392	4161	5940
40%	3302	3707	5497
45%	2997	3155	5052

Table 45. Triaxial Collapse Model and FEM Simulation Data for 0.25 Width Single Wedge-shaped Wear Model

Wear (%)	Simulated Results (psi)	Smoothed Results (psi)	Triaxial Collapse (psi)
0%	9005	8734	8977
5%	7175	7493	8550
10%	6187	6487	8121
15%	5830	5678	7690
20%	5262	5029	7256
25%	4599	4502	6820
30%	4059	4058	6381
35%	3796	3660	5940
40%	2893	3271	5497
45%	2812	2853	5052

Table 46. Triaxial Collapse Model and FEM Simulation Data for 0.3 Width Single Wedge-shaped Wear Model

Wear (%)	Simulated Results (psi)	Smoothed Results (psi)	Triaxial Collapse (psi)
0%	9005	8667	8977
5%	6776	7315	8550
10%	6146	6251	8121
15%	5567	5423	7690
20%	5045	4782	7256
25%	4322	4275	6820
30%	3809	3853	6381
35%	3554	3463	5940
40%	2781	3056	5497
45%	2536	2580	5052

Note: The results of FEM simulation on the double scars scenarios cannot be compared to the triaxial collapse results because the production casing no longer has the thick-walled cylinder characteristic due to increasing wear that leads to a significant decrease in its wall thickness.

Appendix 3

Empirical Data for API Collapse Formula [29]

A. Empirical Data for Yield Collapse Pressure

Table 47. Yield Collapse Pressure Formula Range [29]

Grade*	Maximum *D/t**
H–40	16.40
–50	15.24
J–K–55	14.81
–60	14.44
–70	13.85
C–75 & E	13.60
L–N–80	13.38
C–90	13.01
C–T–95 & X	12.85
–100	12.70
P–105 & G	12.57
P–110	12.44
–120	12.21
Q–125	12.11
–130	12.02
S–135	11.92
–140	11.84
–150	11.67
–155	11.59
–160	11.52
–170	11.37
–180	11.23

*Grades indicated without a letter designation are not API grades but are grades in use or grades being considered for use. They are shown for information purposes.

B. Empirical Data for Plastic Collapse Pressure

Table 48. Formula Factors and D/t Range for Plastic Collapse [29]

Grade*	Formula Factor A	Formula Factor B	Formula Factor C	*D/t* Range
H–40	2.950	0.0465	754	16.40–27.01
–50	2.976	0.0515	1,056	15.24–25.63
J–K–55	2.991	0.0541	1,206	14.81–25.01
–60	3.005	0.0566	1,356	14.44–24.42
–70	3.037	0.0617	1,656	13.85–23.38
C–75 & E	3.054	0.0642	1,806	13.60–22.91
L–N–80	3.071	0.0667	1,955	13.38–22.47
C–90	3.106	0.0718	2,254	13.01–21.69
C–T–95 & X	3.124	0.0743	2,404	12.85–21.33
–100	3.143	0.0768	2,553	12.70–21.00
P–105 & G	3.162	0.0794	2,702	12.57–20.70
P–110	3.181	0.0819	2,852	12.44–20.41
–120	3.219	0.0870	3,151	12.21–19.88
Q–125	3.239	0.0895	3,301	12.11–19.63
–130	3.258	0.0920	3,451	12.02–19.40
S–135	3.278	0.0946	3,601	11.92–19.18
–140	3.297	0.0971	3,751	11.84–18.97
–150	3.336	0.1021	4,053	11.67–18.57
–155	3.356	0.1047	4,204	11.59–18.37
–160	3.375	0.1072	4,356	11.52–18.19
–170	3.412	0.1123	4,660	11.37–17.82
–180	3.449	0.1173	4,966	11.23–17.47

*Grades indicated without a letter designation are not API grades but are grades in use or grades being considered for use. They are shown for information purposes.

C. Empirical Data for Plastic and Transition Collapse Pressure

Table 49. Formula Factors and D/t Range for Plastic and Transition Collapse [29]

Grade*	Empirical Coefficients				
	F_1	F_2	F_3	F_4	F_5
H-40	2.950	0.0465	754	2.063	0.0325
-50	2.976	0.0515	1,056	2.003	0.0347
J-K 55 & D	2.991	0.0541	1,206	1.989	0.0360
-60	3.005	0.0566	1,356	1.983	0.0373
-70	3.037	0.0617	1,656	1.984	0.0403
C-75 & E	3.054	0.0642	1,806	1.990	0.0418
L-80 & N-80	3.071	0.0667	1,955	1.998	0.0434
C-90	3.106	0.0718	2,254	2.017	0.0466
C-95	3.124	0.0743	2,404	2.029	0.0482
-100	3.143	0.0768	2,553	2.040	0.0499
P-105	3.162	0.0794	2,702	2.053	0.0515
P-110	3.181	0.0819	2,852	2.066	0.0532
-120	3.219	0.0870	3,151	2.092	0.0565
-125	3.239	0.0895	3,301	2.106	0.0582
-130	3.258	0.0920	3,451	2.119	0.0599
-135	3.278	0.0946	3,601	2.133	0.0615
-140	3.297	0.0971	3,751	2.146	0.0632
-150	3.336	0.1021	4,053	2.174	0.0666
-155	3.356	0.1047	4,204	2.188	0.0683
-160	3.375	0.1072	4,356	2.202	0.0700
-170	3.412	0.1123	4,660	2.231	0.0734
-180	3.449	0.1173	4,966	2.261	0.0769

D. Empirical Data for Elastic Collapse Pressure

Table 50. D/t Range for Elastic Collapse [29]

Grade*	Minimum *D/t* Range
H–40	42.64
–50	38.83
J–K–55	37.21
–60	35.73
–70	33.17
C–75 & E	32.05
L–N–80	31.02
C–90	29.18
C–T–95 & X	28.36
–100	27.60
P–105 & G	26.89
P–110	26.22
–120	25.01
Q–125	24.46
–130	23.94
S–135	23.44
–140	22.98
–150	22.11
–155	21.70
–160	21.32
–170	20.60
–180	19.93

*Grades indicated without a letter designation are not API grades but are grades in use or grades being considered for use. They are shown for information purposes.

Appendix 4

Comparison of Von Mises Stress Results between Uniform Wear and Local Wear Type

A. Burst Scenario

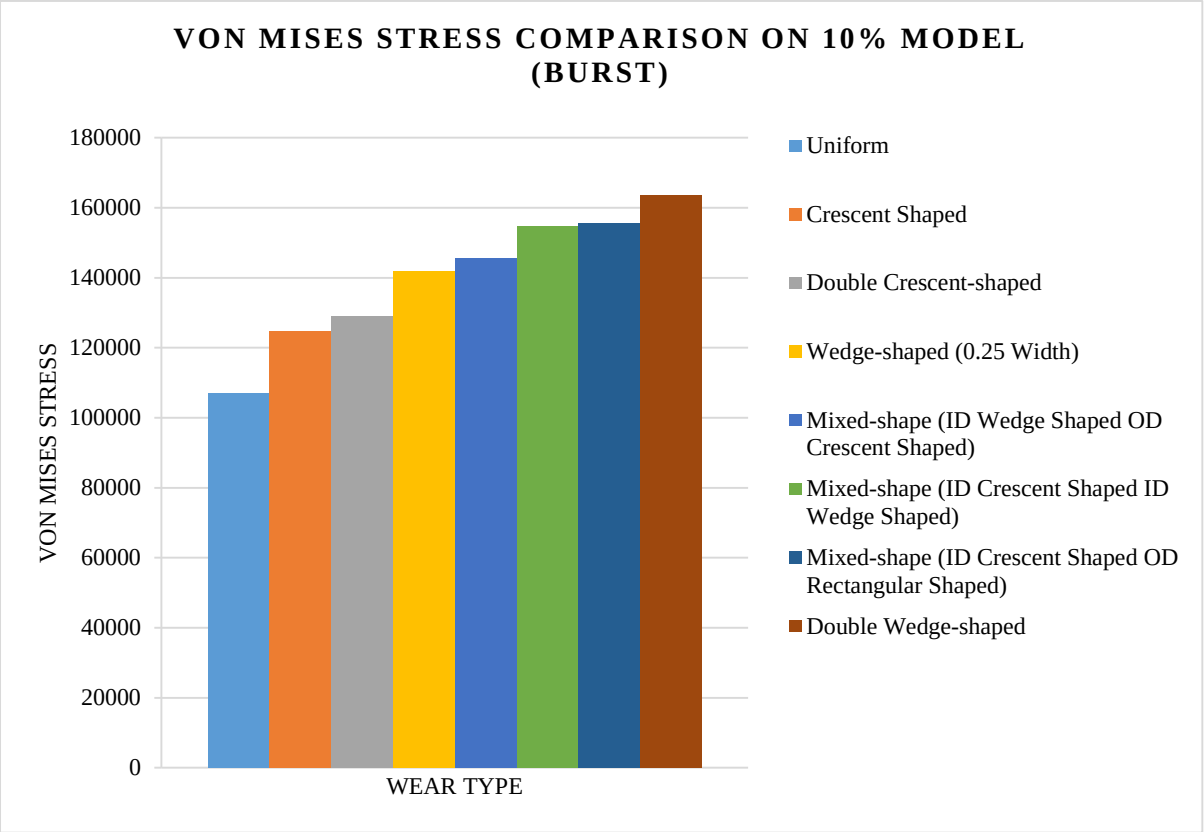

Figure 105. Von Mises stress comparison on 10% wear model when loaded by internal pressure 10000 psi

B. Collapse Scenario

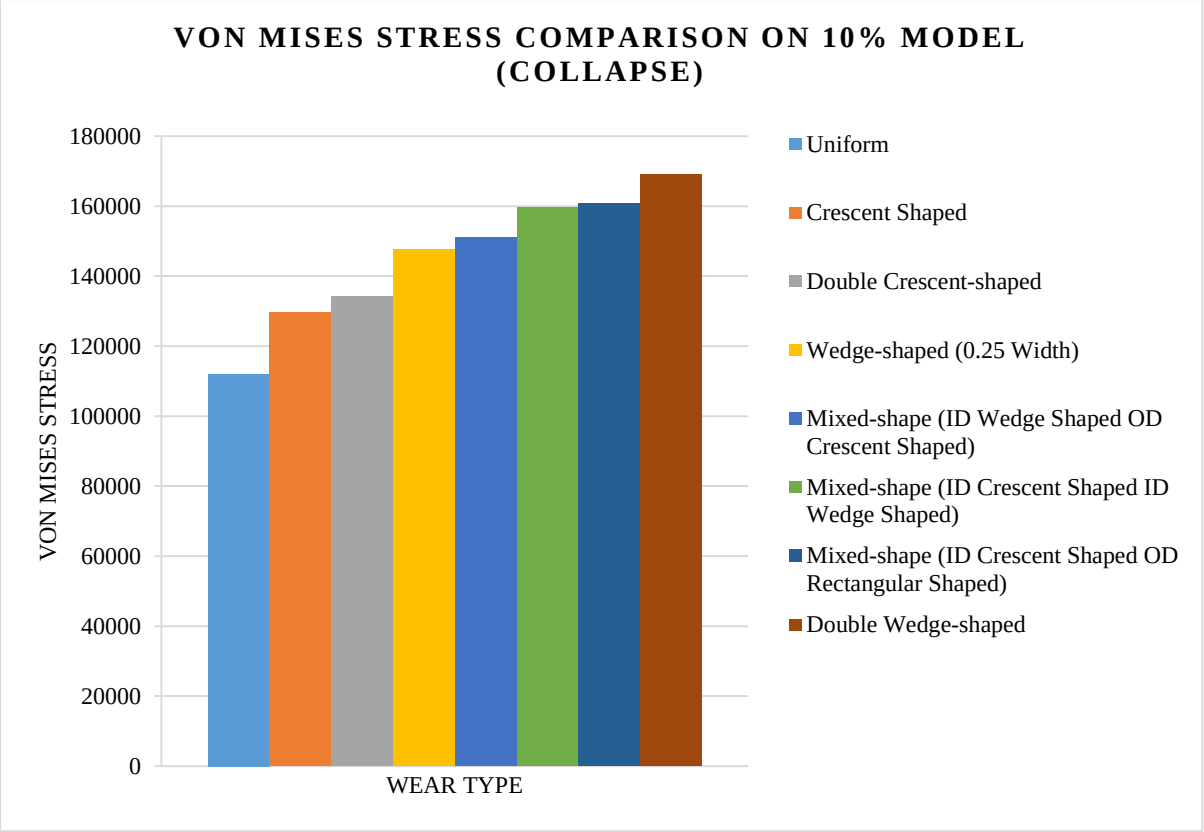

Figure 106. Von Mises stress comparison on 10% wear model when loaded by external pressure 10000 psi